

Uncertainties in measuring and modelling erosion-induced soil organic carbon dynamics in arable landscapes

Florian Wilken

Angaben zur Veröffentlichung / Publication details:

Wilken, Florian. 2018. "Uncertainties in measuring and modelling erosion-induced soil organic carbon dynamics in arable landscapes." Augsburg: Universität Augsburg.

Nutzungsbedingungen / Terms of use:

licgercopyright

Dieses Dokument wird unter folgenden Bedingungen zur Verfügung gestellt: / This document is made available under the following conditions:

Deutsches Urheberrecht

Weitere Informationen finden Sie unter: / For more information see:

<https://www.uni-augsburg.de/de/organisation/bibliothek/publizieren-zitieren-archivieren/publizieren>



**Uncertainties in measuring and modelling
erosion-induced soil organic carbon dynamics
in arable landscapes**

Kumulative Dissertation zur Erlangung des
naturwissenschaftlichen Doktorgrades (Dr. rer. nat.) der
Universität Augsburg (Fakultät für Angewandte Informatik)

Vorgelegt von
Florian Wilken

aus
Bonn

Augsburg 2017

First Reviewer: Prof. Dr. Peter Fiener, University Augsburg
Second Reviewer: Prof. Dr. Karl Wetzels, University Augsburg
Third Reviewer: Prof. Dr. Michael Sommer, University Potsdam

Date of oral exam: December 18th, 2017

Foreword

Based on a passion for rivers, I wanted to understand more about hydrological processes. As a student assistant, I found interest in environmental measuring techniques that raised my interest in data analysis and modelling. From this point onwards, applying measurements to numerical models that are able to explain and predict environmental processes has deeply fascinated me. I had the luck of working in a project doing both environmental measuring and modelling. This PhD-project was supported by the Terrestrial Environmental Observatory TERENO-Northeast of the Helmholtz Association and is part of the TEROS (Tereno EROsion Observation System) that focusses on a comprehensive assessment of C redistribution processes and corresponding changes in C fluxes against the background of the landscape erosion history.

A large number of people supported this project whom I want to thank. In particular, I would like to sincerely thank my promotor Peter Fiener for all the passionate discussions, his persistent support and keeping me enthusiastic for science. For his valuable feedback and providing the infrastructural framework of this study, I greatly thank Michael Sommer. For sharing his models and support, I truly like to thank Kristof van Oost. For the support and initiating this project, I would like to thank Oliver Bens. For opening the scientific world for me, the support of Karl Schneider is highly acknowledged. I like to thank Sebastian Doetterl for constantly encouraging me during the time of my PhD and the nice office atmosphere (this also goes to Buddy the dachshund). Within many good years in Cologne, I learned a lot from Paul Wagner, which is highly appreciated. I would like to thank Tim Reichenau and Verena Dlugoß for support and sharing their knowledge. I like to thank my project colleague Christoph Kappler for good times and support during field work. I like to thank Heather Mc Lean for editing parts of this thesis. During numerous field trips, I stayed at the ZALF research farm in Dedelow, which provided a nice home and support in many ways. The highly valuable technical support of Peter Rakowski and Nico Zindler is greatly appreciated. Thanks also go to Alexander Graf and Ferdinand Engels who partly provided disdrometer data, which was of great value. Special thanks also go to the farm owners Bernd Sohn and Dietrich von Wedel for his permission to carry out various types of measurements on their field in the Uckermark. For giving the “Prussian” a chance to feel home in Bavaria, I would like to thank the Institute for Geography of the University Augsburg. For their endless support, I want to convey my deepest

appreciation to my parents Ingeborg and Karl-Heinz Wilken and family Markus, Petra and Lars Kral and Olaf, Alexandra, Max and Mara Naumann. For walking along the way of PhD with me and never losing contact, I would like to express my deep appreciation to Matthias Behrend, Till Krewer, Helge Behm, Christoph Burow and Wolfgang Merkel. Finally, I want to offer my heartfelt thanks to Anne Wilken for encouraging me half of my life.

Abstract

Soil organic carbon (SOC) is the largest terrestrial carbon (C) pool and has been identified as a cornerstone for the global C cycle. Alterations in the soil-atmosphere flux have substantial implications for climate change and can be an atmospheric C sink or source. Over the past decades, global estimates on the role of soil erosion on SOC dynamics have shown conflicting results. Some studies showed that soil erosion leads to a global atmospheric C source, where other studies indicated an erosion-induced C sink. These conflicting results are partly caused by insufficient input data and oversimplifications on process-level in soil erosion modelling.

This study aims at detecting and assessing potential uncertainties for soil erosion and SOC redistribution modelling based on input data and missing processes. Therefore, rainfall kinetic energy (KE), as the main driver initiating interrill erosion, was investigated by state-of-the-art optical disdrometers. A water erosion model was used to compare deviations in sediment delivery between directly measured and derived rainfall KE based on 32 theoretical rainfall kinetic energy-intensity (KE-I) relationships. To understand the role of event size on SOC delivery by water erosion, the process-based multi-class sediment transport model and C dynamics (MCST-C) model was applied on a long-term (100-yr) high temporal resolution (10-min) rainfall series in an arable catchment of the Belgian loess belt. To analyse the effect of single processes on SOC dynamics, the MCST-C model was applied in two arable catchments of different characteristics. The study assesses variations induced by the implementation and variation of different water and tillage erosion processes to the model. As tillage erosion is an important process in soil and SOC redistribution, a plot experiment to determine the uncertainty of different measuring techniques for tillage erosion was finally carried out.

The results of this PhD-project suggest that modelling soil erosion-induced SOC dynamics are subject to large uncertainties originating from input data limitations and missing representation of process-level control mechanisms. (i) Substantial variations in simulated sediment delivery were shown for different KE-I relations. Furthermore, a distinct overestimation of the KE-I relations compared to directly measured KE was detected, which is not systematic for high KE events. Hence, especially KE predictions of extreme events are subject to large uncertainties. (ii) The majority of delivered sediments and associated SOC is mostly driven by rare extreme events, which was also shown by the measurements used in this study. However, small events need to be taken into account due to the preferential transport of SOC and corresponding SOC enrichment processes in

delivered sediments. (iii) Soil aggregation reduces interrill erosion and transport distances of SOC due to the encapsulation of highly mobile SOC-rich fine particles into rather immobile soil aggregates. (iv) Tillage erosion substantially alters vertical C fluxes with a large SOC sequestration potential. (v) The intra-field catchment connectivity controls sediment delivery and corresponding SOC enrichment processes. Catchments with reduced sedimentological connectivity show enhanced SOC enrichment in delivered sediments due to depositional processes. (vi) Large uncertainties were found for different tillage erosion measurement techniques that may largely influence model parametrizations.

Zusammenfassung

Organischer Bodenkohlenstoff (SOC) stellt den größten terrestrischen Kohlenstoffspeicher dar und wurde als bedeutsamer Bestandteil des globalen Kohlenstoffkreislaufes erkannt. Hierbei haben Änderungen in den Austauschraten zwischen Pedosphäre und Atmosphäre direkten Einfluss auf den CO₂-Gehalt der Atmosphäre. Während der vergangenen Jahrzehnte wurden gegensätzliche Abschätzungen zur Rolle der Bodenerosion auf die Bodenkohlenstoffdynamik veröffentlicht, welche sowohl auf eine erosionsinduzierte Kohlenstoffsinke als auch Quelle hingewiesen haben. Die gegensätzlichen Ergebnisse resultieren unter anderem aus unzureichenden Eingangsdaten und Vereinfachungen von Erosionsprozessen in den verwendeten Modellansätzen.

Ziel des Promotionsprojektes ist es potenzielle Unsicherheiten in der Bodenerosions- und SOC-Umsatzmodellierung, welche auf Schwächen in den Eingangsdaten und Prozessvereinfachungen basieren, zu erfassen und analysieren. Hierfür wurde die kinetische Energie (KE) des Niederschlags, welcher der Hauptantrieb der flächenhaften Erosion ist, mittels optischer Distrometer analysiert. Um die Unterschiede zwischen der direkt gemessenen und der aus 32 unterschiedlichen kinetischer Energie-Intensitäts (KE-I) Gleichungen auf den simulierten Sedimentaustrag miteinander zu vergleichen, wurde die gemessene und abgeleitete KE in einem Wassererosionsmodell angewendet und gegenübergestellt. Für ein tiefergehendes Verständnis der Bedeutung der Erosionsereignisgröße auf den SOC-Austrag, wurde das prozessbasierte Wassererosionsmodell multi-class sediment transport and carbon dynamics model MCST-C mit einer 100-jährigen, zeitlich hochauflösenden (10 Minuten) Niederschlagszeitreihe in einem Ackerlandeinzugsgebiet angewendet. Zudem wurde das MCST-C Modell mit einem Bearbeitungserosions- und Kohlenstoffumsatzmodell gekoppelt und auf zwei Ackerlandeinzugsgebiete unterschiedlicher

hydrologischer und sedimentologischer Konnektivität angewendet. Die Studie analysiert dabei gezielt einzelne Erosionsprozesse und deren Auswirkungen auf die Einzugsgebietskohlenstoffdynamik. Messunsicherheiten unterschiedlicher Messverfahren der wichtigen aber unterrepräsentierten Bearbeitungserosion wurden in einem Versuch gegenübergestellt und analysiert.

Die Ergebnisse weisen auf große Modellunsicherheiten der erosionsbedingten Kohlenstoffdynamiken hin, welche sich aus Eingangsdatenlimitationen und fehlender Prozessimplementierung ergeben. (i) Es wurden substantielle Unterschiede des simulierten Sedimentexports für verschiedene KE-I Gleichungen festgestellt. Es konnte gezeigt werden, dass die KE-I Gleichungen die KE Direktmessungen deutlich überschätzen, was jedoch nicht ausnahmslos auf große Ereignisse zutrifft. Daher sind insbesondere große Erosionsereignisse Gegenstand von hohen Unsicherheiten. (ii) Die Modellierung konnte zeigen, dass der Großteil des SOC Exports durch wenige starke Erosionsereignisse verursacht wird, jedoch führen Anreicherungsprozesse des präferentiellen SOC-Transports zu einer deutlichen Bedeutungszunahme von kleinen Erosionsereignissen für den Kohlenstoffexport und damit die Einzugsgebietskohlenstoffbilanz. (iii) Die Bodenaggregation bedingt eine Reduzierung der flächenhaften Erosion sowie der Transportdistanzen von SOC-reichem Sediment. Dies ist bedingt durch den physischen Zusammenschluss der mobilen SOC-reichen Feinkornfraktion zu Aggregaten geringerer Erodier- und Transportierbarkeit. (iv) Die Bearbeitungserosion bewirkt eine deutliche Änderung der vertikalen Kohlenstoffflüsse und weist ein hohes Kohlenstoffsequestrierungspotenzial auf. (v) Die Einzugsgebietsdurchgängigkeit ist ein wichtiger Steuerungsmechanismus für die Kohlenstoffanreicherungsprozesse im ausgetragenen Sediment. Eine geringere sedimentologische Konnektivität führt durch Depositionsprozesse zu einer höheren SOC-Anreicherung im ausgetragenen Sediment. (vi) Die Bestimmung der Bearbeitungserosion unterliegt großen Unsicherheiten und kann einen bedeutenden Einfluss auf Modellparametrisierungen haben.

Contents

Foreword	i
Abstract	iii
Zusammenfassung	iv
1. Introduction	1
2. Uncertainties in rainfall kinetic energy-intensity relations	9
3. Modelling a century of soil redistribution processes and carbon delivery	28
4. Modelling to identify main drivers of erosion-induced carbon fluxes	47
5. Measurement uncertainties of tillage erosion	65
6. Summary and general discussion	87
7. Conclusion and outlook	91
References	93
List of tables	106
List of figures	106
Contribution of the author to the articles	108

1 Introduction

The role of soil erosion on the carbon cycle

Soil organic carbon (SOC) is the largest terrestrial carbon (C) pool with approx. 1400 Pg C stored in the upper soil meter and approx. 700 Pg C in the upper 0.3 m (Hiederer and Köchy, 2011). Hence, it exceeds the atmospheric and living biomass pools by far (Houghton, 2007; Jobbágy and Jackson, 2000; Schlesinger, 1990). SOC has been identified to be a cornerstone for the global C cycle (Amundson et al., 2015; Sanderman and Berhe, 2017) as the soil-atmosphere exchange rates are highly sensitive to anthropogenic manipulations such as land use change and agricultural management. Therefore, adjustments in agricultural management strategies (e.g. no-till farming) allow for the sequestration of atmospheric C in soils (Franzluebbers, 2010) and has received great political attention (e.g. Lima Paris Action Agenda: 4‰ initiative; Kyoto protocol: Article 3.4; IPCC, 2013) due to its climate change mitigation potential (Chabbi et al., 2017; Lal, 2007). To understand and quantify the efficiency of management strategies for SOC sequestration, global model projections are needed. However, global projections of the C cycle, particularly the component of anthropogenic land cover change, are subject to large uncertainties (Wang et al., 2017). The anthropogenic land cover change is highly related to accelerated soil erosion and corresponding feedback processes on SOC dynamics. Soil erosion has been recognized as an important process for the C cycle (Chappell et al., 2016; Quinton et al., 2010; Wang et al., 2017), but is not represented in current C cycle-climate models. Hence, C dynamics of the terrestrial pool are still not sufficiently represented in global projections and their uncertainties are likely to increase if erosion-induced SOC dynamics are taken into account.

Soil systems under natural conditions are usually in a sustainable equilibrium that equals soil loss by lateral redistribution and soil production by weathering (Montgomery, 2007; Verheijen et al., 2009). Due to land use conversion from natural soil cover to agricultural land, soil erosion substantially increases and disturbs this equilibrium (Montgomery, 2007). In erosion-affected landscapes, soil redistribution can lead to pronounced spatial patterns in soil nutrients such as SOC (Dlugoß et al., 2010; Gregorich et al., 1998; Nadeu et al., 2012; Wang et al., 2010). SOC dynamics show substantial response to soil erosion and have been identified as a controlling process for the soil-atmosphere C flux (Sanderman and Berhe, 2017). However, studies on the global role of soil erosion on the C cycle showed conflicting results of a global erosion-induced C sink or source in the

same order of magnitude ($\pm 1 \text{ Pg yr}^{-1}$; for recent reviews see Doetterl et al., 2016; Kirkels et al., 2014). These large variations are caused by different data sources and/or modelling approaches used to derive global estimates. Global estimates of erosion-induced C dynamics are commonly based on sediment delivery measurements of river systems or model simulations driven by plot experiments. Extrapolations that are based on the sediment delivery of mayor river systems (Lal, 2003; Smith et al., 2005) miss on-site redistribution processes, which cause high uncertainties as large quantities of eroded topsoil are deposited within the terrestrial system (De Vente et al., 2007) or mineralized during transport within river systems before entering lakes or oceans (Aufdenkampe et al., 2011; Battin et al., 2009; Tranvik et al., 2009; Walling and Webb, 1996). In contrast, spatially distributed soil erosion and C dynamics modelling of the terrestrial C cycle enables the representation of on-site redistribution processes. However, input data (e.g. rainfall, land use, yield, soil management and properties) with an appropriately high spatio-temporal resolution is not available on global scale. In consequence, global soil erosion models are mostly parameterized based on experimental plot extrapolations (Doetterl et al., 2012b). These small-scale studies are to some extent biased as these experiments are mostly carried out in eroding landscape positions and underrepresent depositional processes (Auerswald et al., 2009; Doetterl et al., 2016). Hence, even on field scale the feedbacks between redistribution processes and their effect on C dynamics are still not sufficiently understood (Doetterl et al., 2016).

A comprehensive landscape analysis to strengthen the understanding of erosion-induced C dynamics on arable land is in the focus of the TERENO northeast subproject TEROS (Tereno ERosion Observation System; Fig. 1). To understand the anthropogenic impact on soil erosion over the course of increasing mechanization, a chronostratigraphical analysis of colluvial deposits and corresponding C stocks is part of the landscape analysis. Vertical fluxes of dissolved organic carbon (DOC) can be an important component of the C balance on arable land (Kindler et al., 2011) that interacts with the erosion-induced changes in soil physical properties and crop yield (Herbrich et al., 2017), which are continuously monitored by lysimeter monoliths. This PhD-project deals with the role of episodic short-term processes of lateral soil redistribution on long-term C dynamics. Therefore, lateral redistribution and export of sediment and SOC by water and tillage erosion is monitored and modelled in four highly erosion affected field scale catchments of northeast Germany. The new insight given by the monitoring has the goal to improve

soil erosion and C dynamics models for a better representation of the erosion-induced impact on the C cycle.

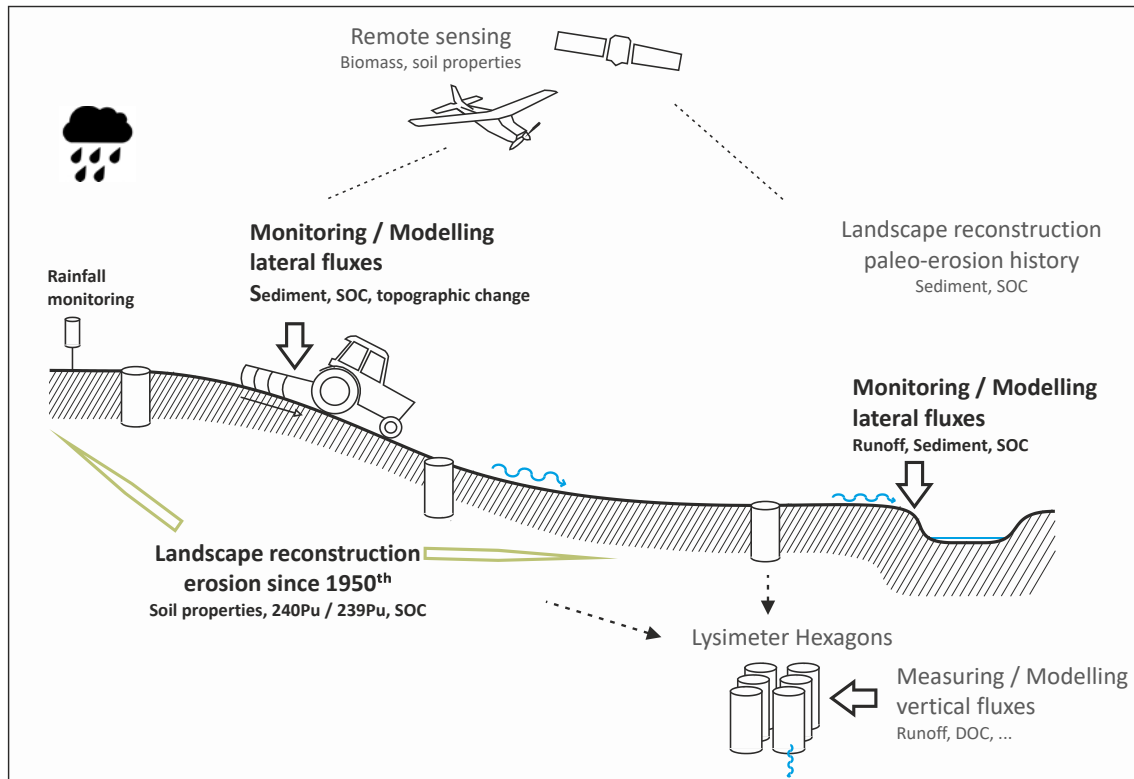


Figure 1: TEROS project schematic overview for vertical and lateral fluxes of sediment and soil organic carbon against the background of the landscape erosion history. The subjects of this PhD-project are highlighted in black.

Relevant processes in soil erosion and C dynamics modelling

Event size and the conflict of temporal scales

A major challenge for process-oriented SOC redistribution and turnover models is the conflict of different temporal scales (Doetterl et al., 2016) as short-term erosion events have long-term effects on C dynamics. To account for these long-term effects, most erosion models that were coupled to C turnover models are based on USLE-type long-term mean annual erosion rates (e.g. CENTURY/EDCM: Liu et al., 2003b; SPEROS-C: Van Oost et al., 2005b). However, catchment monitoring studies have shown that water erosion and sediment delivery are largely controlled by rare extreme events (Fiener and Auerswald, 2007b; Fiener et al., 2008; Steegen et al., 2000). A number of processes are largely controlled by event size and are associated to high uncertainties such as dynamics in rainfall kinetic energy (Angulo-Martinez et al., 2016; Montero-Martinez and Garcia-Garcia, 2016), SOC enrichment in delivered sediments (Fiener et al., 2015; Quinton et

al., 2001; Wang et al., 2010) and deep burial of SOC by deposition (Fiener et al., 2015; Van Hemelryck et al., 2011; Wang et al., 2014b).

SOC enrichment in delivered sediments

The assumption of most coupled water erosion and C turnover models is that the C concentration of delivered sediments equals the mean C concentration of the parent soil. However, this assumption leads to biased estimates of lateral SOC delivery and redistribution and its effect on vertical C fluxes (Fiener et al., 2015). Experimental and modelling studies have pointed out that erosion preferentially removes and delivers SOC (Kuhn et al., 2010; Polyakov and Lal, 2004b; Schiettecatte et al., 2008a b). The preferential transport originates from a heterogeneous SOC distribution throughout the soil structure, consisting of several fractions, characterized by differences in particle density and size (Doetterl et al., 2015). The major proportion of SOC is associated to the fractions of (i) silt and clay primary particles, (ii) soil aggregates and (iii) a mineral-free particulate organic matter (POM) fraction of a much lower density (John et al., 2005; Von Lützow et al., 2007). SOC-rich fine and low density particles are preferentially transported due to selective interrill erosion and cause enriched SOC concentrations in delivered sediments compared to the parent soil (Kuhn et al., 2010). Rill erosion, driven by concentrated flow with much higher transport capacities is able to detach and transport the entire soil matrix. Therefore, extreme events, which are dominated by rill erosion, show similar SOC concentrations of delivered sediments compared to the parent soil (Kuhn et al., 2010; Polyakov and Lal, 2004b; Quinton et al., 2001; Schiettecatte et al., 2008b). The depositional properties of fines and POM are mainly different from water stable aggregates as SOC associated to water stable aggregates deposits faster compared to their encapsulated primary and POM particles (Hu and Kuhn, 2014). Hence, soil aggregation is an important soil property that can control SOC enrichment processes. Recent research has pointed out that neglecting event based C enrichment processes leads to a substantial underestimation of delivered SOC (Fiener et al., 2015; Quinton et al., 2001; Wang et al., 2010).

SOC burial and dynamic replacement

Just 10-30% of eroded soil is subsequently delivered to lakes or oceans via major river systems (De Vente et al., 2007; Walling and Webb, 1996). Hence, large quantities of SOC-rich topsoil redistribution is not exported from catchments and is deposited in the terrestrial system (Stallard, 1998). As decomposition rates typically decrease with depth,

topsoil deposition buries SOC-rich sediments into slow C turnover environments (Doetterl et al., 2016). Thus, the C stocks of depositional soil profiles are higher compared to undisturbed sites (Doetterl et al., 2016; Gregorich et al., 1998; Smith et al., 2001; Smith et al., 2005). Numerous studies have shown that SOC burial can act as an important C sink function (Polyakov and Lal, 2004a b; Van Hemelryck et al., 2011; VandenBygaart et al., 2015; Wang et al., 2014a b).

At erosional sites, subsoil of low SOC concentration is uplifted to the rhizosphere and the plough layer. Therefore, new reactive mineral surfaces are exposed to C input from roots and litter, which leads to higher C sequestration rates compared to undisturbed sites (Berhe et al., 2008; Doetterl et al., 2016; Harden et al., 1999; Quine and Van Oost, 2007). The studies of Rosenbloom et al. (2001) and Doetterl et al. (2012a) showed for moderate eroded soil profiles (2–4 m soil loss since start of agriculture) that the topsoil SOC content does not substantially differ between eroded and undisturbed profiles. This indicates that C sequestration can have the same rate as SOC removal by erosion and is dynamically replaced (Doetterl et al., 2016). However, dynamic C replacement is largely controlled by environmental feedbacks and conditions that go back to erosion-induced yield reductions and physicochemical properties of newly exposed subsoil (Doetterl et al., 2016).

SOC protection by soil aggregation

SOC can be physically protected from mineralization by soil aggregation. The formation and stability of soil aggregates is complex due to interacting processes. Water stable aggregates that resist disruption during detachment and transport of erosion processes are hierarchically formed within clusters of labile aggregates (Tisdall and Oades, 1982). The breakdown of labile soil aggregate clusters is driven by erosion-induced splash and transport processes (Lal, 2003; Van Hemelryck et al., 2010) and furthermore shows a distinct annual seasonality due to freeze-thaw and dry-wet cycles (Angers and Mehuys, 1988; Coote et al., 1988; Six et al., 2004; Wang et al., 2010). Furthermore, soil aggregation is subject to pronounced spatial patterns related to soil nutrients, moisture, grain size distribution, management practices, erosion and soil biota (Denef et al., 2002). Soil aggregates encapsulate SOC-rich fines (clay and silt particles) and POM, which physically separates SOC from decomposers (Doetterl et al., 2016; Tisdall and Oades, 1982) and encapsulates SOC in oxygen limited environments (Sexstone et al., 1985). Furthermore, soil aggregation alters the grain size distribution of the soil and reduces the transport dis-

tance of aggregated SOC fractions (Hu and Kuhn, 2014; Hu and Kuhn, 2016). Fine particles and POM have slow settling velocities and show longer transport distances compared to coarser particles. Soil aggregation encapsulates these highly mobile SOC fractions into larger particles, consisting of faster settling velocities, which substantially reduces the transport distance. Soil aggregation leads to large uncertainties concerning the general soil erodibility and transport distances of SOC.

On-field redistribution by tillage

Compared to rapid landscape changes by event driven water erosion, tillage erosion takes place on a regular basis and continuously levels the landscape topography. Therefore, tillage erosion is not as visible as linear water erosion and it may take decades until environmental (e.g. soil texture and nutrients, and crop yields) or topographical (e.g. tillage banks at field borders, hilltop levelling) patterns become visible. Tillage erosion leads to different redistribution patterns compared to water erosion. While water erosion is most effective along areas of high flow accumulation (e.g. thalwegs), tillage erosion is strongest at convex hilltops and deposits in concave structures such as thalwegs (Govers et al., 1999; Van Oost et al., 2006). Therefore, tillage erosion mobilizes soil from landform positions of minimum water erosion to regions of highest water erosion (Govers et al., 1999; Van Oost et al., 2006). Under mechanized agriculture, tillage erosion is at least in the same order of magnitude compared to water erosion (Van Oost et al., 2006). Nevertheless, the effect of tillage erosion on C dynamics has not yet received great attention, although a representation has been accounted for in few modelling studies (Dlugoß et al., 2012; Fiener et al., 2015; Lacoste et al., 2015; Van Oost et al., 2005b). Tillage erosion is an on-field process that is limited to field borders without sediment and SOC delivery. Hence, dynamic C replacement at erosional sites and stabilisation by deep burial at depositional sites may lead to a high SOC sequestration potential of tillage erosion.

Objectives and structure of the thesis

The overall aim of this thesis is to detect and assess potential uncertainties related to soil erosion and corresponding SOC dynamics modelling on arable land. The main aims of this study are

- To improve the understanding of uncertainties related to erosion processes and their corresponding measurement techniques.
- To implement relevant processes in a coupled water and tillage erosion and C turnover model to assess the role of short-term erosion processes on long-term C dynamics.

This PhD-thesis consists of four articles addressing uncertainties related to input data and missing processes in soil erosion and C dynamics modelling.

Article I, deals with rainfall kinetic energy (KE), which is a widely used input data for soil erosion modelling. As direct measurements of KE are mostly not available, numerous relationships between rainfall KE and intensity (KE-I relations) were developed for different meteorological regions. However, recent research indicates that KE-I relations are not well represented by meteorological regions due to large dynamics between and during rainfall events (Angulo-Martinez et al., 2016). To assess these dynamics, five optical disdrometers were used to compare direct measurements against derived rainfall KE based on 32 published KE-I relations. The analysis compares measured drop size and fall velocity distributions against traditional models of Marshall and Palmer (1948) and Gunn and Kinzer (1949). Furthermore, the deviation between measured and derived KE was assessed on different temporal resolutions (minute, event and year). Subsequently, deviations in sediment delivery between measured and derived KE were quantified using a RUSLE based water erosion model. The article provides novel insight on the direct effect of different KE-I relations for soil erosion modelling and inter and intra event dynamics of drop size distributions.

Article II addresses the long-term effect of event-size on sediment and C delivery. Therefore, the grain size specific sediment and associated SOC delivery was modelled, using the process-oriented MCST water erosion model. The model was driven by a unique 100-yr high-resolution rainfall data set in a field scale catchment of the Belgian loess belt. The novelty of the study is the long-term simulation of C enrichment processes with

a process-oriented model that takes the grain size selective transport on a physical basis into account.

Article III is a follow-up modelling study that implements additional erosion processes to strengthen the understanding of relevant processes for different catchment characteristics. The MCST model was enhanced for the representation of tillage erosion, different soil physical properties (soil aggregation, interrill vs. rill erosion) and coupled to a C turnover model. Subsequently, the model was used to exclude and alter processes to understand and quantify the effect of sediment redistribution on C dynamics in two catchments of different hydrological and sedimentological connectivity. The study gives novel insight on the relevance of distinct soil erosion processes on SOC dynamics against the background of catchment properties.

Article IV deals with uncertainties in determining tillage erosion as Article III has shown a high sensitivity to varying tillage transport coefficients on simulated C fluxes. Therefore, various tracer and topographical measuring techniques were applied in a plot experiment and compared to each other. The study provides new insight on uncertainties that are related to different tillage erosion measuring techniques.

Article I

Uncertainties in rainfall kinetic energy-intensity relations for soil erosion modelling

Florian Wilken^{1,2}, Martin Baur¹, Michael Sommer^{2,3}, Detlef Deumlich², Oliver Bens⁴ and Peter Fiener¹: Uncertainties in rainfall kinetic energy-intensity relations for soil erosion modelling, *Catena* (in review).

¹Institute for Geography, Universität Augsburg, Germany

²Institute of Soil Landscape Research, Leibniz-Centre for Agricultural Landscape Research ZALF e.V., Germany

³University of Potsdam, Institute of Earth and Environmental Sciences, Germany

⁴Helmholtz Centre Potsdam GFZ German Research Centre for Geosciences, Germany

In review at the Journal CATENA as is, except for minor formatting changes.

Article abstract

For bare soil conditions, the most important process initiating interrill erosion is the detachment of soil particles via raindrop impact. Splash erosion is mainly controlled by rainfall characteristics, which are essentially determined by the drop size and fall velocity, leading to a specific kinetic energy of rainfall. In consequence, the kinetic energy of rainfall is often directly or indirectly included in erosion models to calculate detachment via splash erosion. Therefore, numerous theoretical functions have been developed for the estimation of rainfall kinetic energy from available rainfall intensity measurements. The aim of this study is to analyze the uncertainties inherent in these theoretical rainfall kinetic energy-intensity (KE-I) relationships and their implications for soil erosion modelling. We compare 32 KE-I relations against measured rainfall energies based on optical disdrometer measurements carried out at five stations. These allow for the direct measurement of rainfall kinetic energy from a detailed spectrum of measured drop sizes and corresponding fall velocities. To quantify the effect of different KE-I relations on sediment delivery, we apply the erosion model WATEM/SEDEM (as implemented in SPEROS-C) to four catchments of NE-Germany. We found a distinct overestimation of the KE-I relations compared to the measured kinetic energy. However, for events of high kinetic energy the estimations are highly dynamic and do not show a systematic offset. This implies that estimating soil erosion of rare extreme events is subject to high uncertainties when estimating rainfall kinetic energy from rainfall intensity.

2.1 Introduction

Soil erosion on arable land is one of the major threats for a sustainable use of soil resources (Morgan, 2005). Therefore, measuring and modelling soil erosion processes has, for a long time, been an important element in several scientific disciplines including soil science, agronomy, hydrology, geomorphology etc. The process of water erosion is traditionally subdivided into a number of sub-processes, ranging from splash induced interrill erosion to surface runoff based rill erosion processes. The initial process of interrill erosion is closely related to the kinetic energy (KE) of raindrops destroying soil aggregates and leading to splash erosion. The associated change in soil surface (soil sealing and crusting) generally reduces infiltration capacity and hence indirectly governs surface runoff generation and initiation of rill erosion (Morgan, 2005).

Due to these direct and indirect implications of the KE of raindrops on several erosion processes KE is widely used as an important input parameter in erosion models. It is implemented in conceptual models, especially the USLE (Wischmeier and Smith, 1960) and its derivatives (RUSLE: Renard et al., 1996; WaTEM/SEDEM: Van Oost et al., 2000a) as well as in physically-oriented models (LISEM: De Roo et al., 1996; EUROSEM: Morgan et al., 1998).

The assessment of rainfall KE started more than a century ago with the pioneer work of Wiesner (1895) and Bentley (1904) who introduced the filter-paper and fleur pellet method to measure drop size distributions. Later, Laws and Parsons (1943) and Marshall and Palmer (1948) found an exponential relation between drop size distribution (DSD) and rainfall intensity and furthermore Laws (1941) and Gunn and Kinzer (1949) developed a model for the terminal velocity of different drop sizes used to calculate drop size specific fall velocities. Linking the models of DSD and terminal velocity provided the necessary information to calculate KE as a function of rainfall intensity. The most prominent KE-I relation in erosion research was published by Wischmeier and Smith (1958). The authors used a relation between DSD and intensity from Laws and Parsons (1943) with a combined approach of Laws (1941) and Gunn and Kinzer (1949) of drop size specific fall velocities to calculate rainfall KE. Based on the calculated KE, a regression equation between KE and intensity was derived and used as the basis for the first erosivity index of the Universal Soil Loss Equation (USLE; Wischmeier and Smith, 1960). Later, other combinations of DSD and drop size specific fall velocities were used to calculate rainfall kinetic energy, whereas the DSD of Marshall and Palmer (1948) is the most fre-

quently used (Renard et al., 1997). Based on new rainfall measuring techniques that enable the continuous and simultaneous recording of drop sizes and fall velocities (e.g. optical disdrometer), it was shown that drop size and fall velocity distributions can have complex patterns between different storm events (Sempere-Torres et al., 2000), and also vary during different phases within a rainfall event (Angulo-Martinez et al., 2016). To date, a few KE-I relations are based on continuous measurements of drop size distributions (e.g. Cerro et al., 1998; Petan et al., 2010; Sanchez-Moreno et al., 2012), but almost no KE-I relation is based on both continuously measured drops size and fall velocity distributions. Instead, continuous DSD measurements are linked to terminal velocity models (except for Lim et al., 2015). Nonetheless, recent research shows that a large amount of drops is not well represented by terminal velocity models, which might have large implications for deriving rainfall KE from intensity (Angulo-Martinez et al., 2016; Larsen et al., 2014; Montero-Martinez and Garcia-Garcia, 2016).

The aim of this study is (i) to use state of the art measuring techniques to directly calculate/measure KE from measured drop sizes and fall velocities, (ii) to analyze the potential differences between measured and theoretically derived KE from a large number of existing KE-I relations and (iii) to use the different KE results as inputs in a RUSLE based water erosion model to quantify the ‘erosion-uncertainty’ associated with different KE approaches.

2.2 Materials and Methods

2.2.1 Rainfall, drop size distribution and fall velocity data

Rainfall intensity, drop size distribution and drop size specific fall velocity are available at five stations equipped with optical laser disdrometers (Laser Precipitation Monitor: Thies-Clima, Germany). The disdrometers are mounted at a height of one meter and record the full spectrum of drop size and fall velocity distributions. Technically, the shade of a falling hydrometeor passing a flat laser beam (228 x 20 mm) is measured. The corresponding amplitude of signal reduction is used to measure the drop diameter, whereas the duration of signal reduction determines the fall velocity of the drop (Thies-Clima, 2011). Each raindrop is measured individually and classified into 22 particle size classes ranging from 0.125 to 8 mm (largest class ranges from 8 mm to infinity) and 20 fall velocity classes from 0 to 20 m s⁻¹, respectively. Therefore, all the required information is available to directly calculate the rainfall KE (in Joule) as

$$KE = \frac{1}{2}mv^2 \quad (2.1)$$

where m is the drop mass (kg) and v is the fall velocity (m s^{-1}). The device corrects for the drag force induced deformation of a falling drop and returns the corresponding drop diameter for a perfectly round spheroid. Therefore, m can be calculated as

$$m = \frac{4}{3}\pi\rho r^3 \quad (2.2)$$

where r is the radius in meter and water density (ρ) is assumed to be 1 Mg m^{-3} . KE calculated from drop size and fall velocity based on measurements of the optical disdrometer are subsequently referred to as measured KE.

For comparison against the measured KE we used 32 published KE-I relations (Fig. 2.1; Table 2.1) to derive rainfall KE from intensity (subsequently referred to as derived KE). The selection of equations cover the most common KE-I relations representing all equation types published (linear, logarithmic, exponential and power functions; reference see Table 2.1). Both measured and derived KE are calculated based on optical disdrometer measurements of the same devices. For full comparability of the measured rainfall

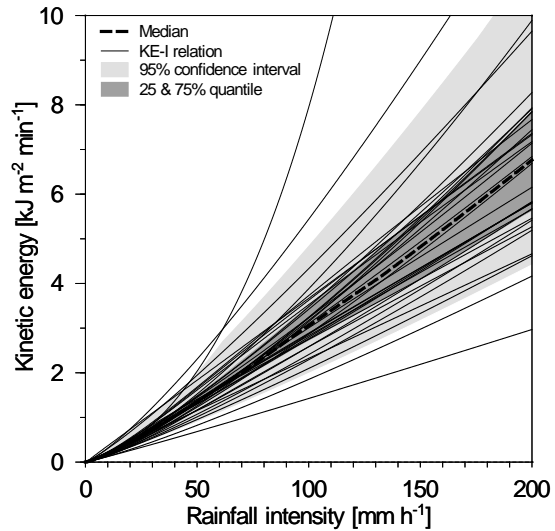


Figure 2.1: Rainfall kinetic energy-intensity (KE-I) relations based on the equations given in Table 2.1.

amount, the rainfall intensity, which is the input for the KE-I relations, is based on the corresponding drop volume that is also used for the direct measurements of the KE. All KE-I relations are validated against the reference, which is based on measured KE that is directly calculated from drop size and fall velocity values.

Table 2.1: Table of theoretical relationships for rainfall kinetic energy ($\text{J m}^{-2} \text{h}^{-1}$) and rainfall intensity (I : mm h^{-1} ; see Figure 2.1). Equations based on measured drop size distributions (DSD) are indicated by a geographical region. Majority of equations are harmonized according to Salles et al. (2002).

Original reference	Equation	Data base
<i>Logarithmic</i>		
Wischmeier & Smith 1958	$I(11.9 + 8.73 \log_{10}I)$ if $I \leq 76 \text{ mm h}^{-1}$	Theoretical DSD
Zanchi & Torri 1980	$I(9.81 + 11.25 \log_{10}I)$	Italy
Kinnell 1981 ^a	$I(17.124 + 5.229 \log_{10}I)$	USA (Florida)
Onaga et al. 1988	$I(9.81 + 10.6 \log_{10}I)$	Japan (Okinawa)
Brandt 1990	$I(8.95 + 8.44 \log_{10}I)$	Theoretical DSD
<i>Exponential</i>		
McGregor & Mutchler 1976	$I(27.3 + 21.68 e^{-0.048I} - 41.26 e^{-0.072I})$	USA
Kinnell 1981 ^b	$29.31 I(1 - 0.281 e^{-0.018I})$	USA (Florida)
Rosewell 1986 ^a	$29 I(1 - 0.596 e^{-0.0404I})$	Australia (NSW)
Rosewell 1986 ^b	$26.35 I(1 - 0.669 e^{-0.0349I})$	Australia (Queensland)
Brown & Foster 1987	$29 I(1 - 0.72 e^{-0.05I})$	USA
Coutinho & Tomás 1995	$35.9 I(1 - 0.559 e^{-0.034I})$	Portugal
Cerro et al. 1998	$38.4 I(1 - 0.538 e^{-0.029I})$	Spain
Jayawardena & Rezaur 2000	$36.8 I(1 - 0.691 e^{-0.038I})$	China (Hong Kong)
Fornis et al. 2005	$30.8 I(1 - 0.550 e^{-0.031I})$	Philippines
<i>Intensity power</i>		
Park et al. 1980	$21.1069 I^{1.156}$	USA
Smith & De Veaux 1992 ^a	$13 I^{1.21}$	USA (Oregon)
Smith & De Veaux 1992 ^b	$11 I^{1.23}$	USA (Alaska)
Smith & De Veaux 1992 ^c	$18 I^{1.24}$	USA (Arizona)
Smith & De Veaux 1992 ^d	$11 I^{1.17}$	USA (New Jersey)
Smith & De Veaux 1992 ^e	$10 I^{1.18}$	USA (North Carolina)
Smith & De Veaux 1992 ^f	$11 I^{1.14}$	USA (Florida)
Uijlenhoet & Stricker 1999 ^a	$7.20 I^{1.32}$	Theoretical DSD
Uijlenhoet & Stricker 1999 ^b	$8.53 I^{1.29}$	Theoretical DSD
Uijlenhoet & Stricker 1999 ^c	$8.46 I^{1.17}$	Theoretical DSD
Uijlenhoet & Stricker 1999 ^d	$8.89 I^{1.28}$	Theoretical DSD
Uijlenhoet & Stricker 1999 ^e	$10.8 I^{1.06}$	Theoretical DSD
Uijlenhoet & Stricker 1999 ^f	$7.74 I^{1.35}$	Theoretical DSD
Steiner & Smith 2000	$11 I^{1.25}$	USA (Mississippi)
Shin et al. 2016	$10.3 I^{1.19}$	Theoretical DSD
<i>Others</i>		
Carter et al. 1974	$11.32I + 0.5546 I^2 - 0.5009 * 10^{-2} I^3 + 0.126 * 10^{-4} I^4$	USA (south central)
Usón & Ramos 2001	$23.4 I - 18$	Spain
Nyssen et al. 2005	$36.65 (I - 0.6/I)$	Ethiopia

The data set covers disdrometer measurements over 13 yrs. and 1.9×10^5 min of measurements during erosive events (Table 2.2). Two stations are located in the Uckermark in the Northeast of Germany (Fig. 2.2), representing a relatively dry and continental climate (mean annual precipitation 483 mm and temperature 8.7 °C; Aldana-Jague et al., 2016). The stations are mounted both in close proximity (300 m distance between stations) to the small catchments that are modelled (see section 2.2.2). Furthermore, three stations are

located in the Rur catchment in Western Germany (Fig. 2.2), representing a relatively wet and oceanic climate. The distances between the stations are much larger compared to the Uckermark stations (13 km minimum distance), where two stations are located in the hilly Eifel region (Rur1 and Rur2: mean annual precipitation up to 1300 mm, Graf et al., 2014, and temperature 8 °C) and the third station is located in flat and intensively used arable land close to the village of Selhausen (Rur3: mean annual precipitation 700 mm and temperature 10 °C; Reichenau et al., 2016).

Table 2.2: Descriptive statistics of observed annual rainfall data. Following Schwertmann et al. (1990), an erosive rainfall event was classified according to the exceedance of 10 mm total rainfall or 5 mm rainfall within 30 min. Individual events are separated by 6 h without observed rainfall (Max I_{30} : maximum 30-min rainfall intensity).

Station	Year	Sum of erosive events [mm]	Erosive events [n]	Max event sum [mm]	Max I_{30}
Uck1	2015	173	15	28.2	15.4
	2016	203	12	38.0	73.7
Uck2	2015	199	15	35.8	19.6
	2016	238	12	47.7	92.5
Rur1	2015	578	20	91.5	22.3
	2016	545	16	46.6	39.9
Rur2	2013	396	19	49.0	22.5
	2015	461	16	67.0	40.9
	2016	193	10	38.9	50.1
Rur3	2013	328	19	34.9	52.1
	2014	95	6	39.1	78.1
	2015	357	21	51.3	20.5
	2016	219	12	36.2	21.6

For general differences between the meteorological stations in the Uckermark and the Rur region see Table 2.2. The heaviest precipitation event (maximum 30-min rainfall intensities: I_{30}) of the dataset occurred at the Uckermark stations in June 2016 (Uck1 I_{30} : 73.7 mm h⁻¹; Uck2 I_{30} : 92.5 mm h⁻¹; Table 2.2). However, the Rur stations recorded higher rainfall amounts and larger numbers of erosive rainfall events per year, whereas I_{30} are higher at the Uckermark stations.

2.2.2 Erosion modelling

Test site

The modelling test site consists of four small catchments (0.3 to 1.5 ha) located in the proximity of the disdrometer stations in the Uckermark (Fig. 2.2). The small catchments surround and drain in a closed depression (kettle hole), which represents a typical situation for the young, hummocky ground moraine landscape of Northeast Germany. Due to different sizes and slope characteristics, these catchments possess heterogeneous sediment delivery ratios into the kettle hole. The typical crop rotation is rape (*Brassica napus* L.) – winter wheat (*Triticum aestivum* L.) - winter barley (*Hordeum vulgare* L.) – winter barley, cultivated without cover crops. The soils are developed from glacial till and vary with respect to their location in the

landscape. Extremely eroded Calcaric Regosols (IUSS, 2015) are located at the summit due to high tillage erosion, moderately to strongly eroded Luvisols can be found along the slopes and Colluvic Regosols, partly influenced by groundwater, at concave downslope areas (Gerke et al., 2010; Sommer et al., 2008). The closed depression itself is built up by degraded Histosols and covered by a thin colluvial layer of mineral soil (10-40cm). Between 7 and 11 erosive rainfall events per year take place (Deumlich, 1999). In the region, maximum intensities up to 103 mm h^{-1} (per 30-min interval) were recorded during an extreme event in June 2007 (Vogel et al., 2016).

WaTEM/SEDEM

We utilized the water erosion module WaTEM/SEDEM (Van Oost et al., 2000a; Van Rompaey et al., 2001) as implemented in SPEROS-C (Fiener et al., 2015; Nadeu et al., 2015; Van Oost et al., 2005c) model. WaTEM/SEDEM is a widely used grid based water erosion model, which spatially implements the Revised Universal Soil Loss Equation

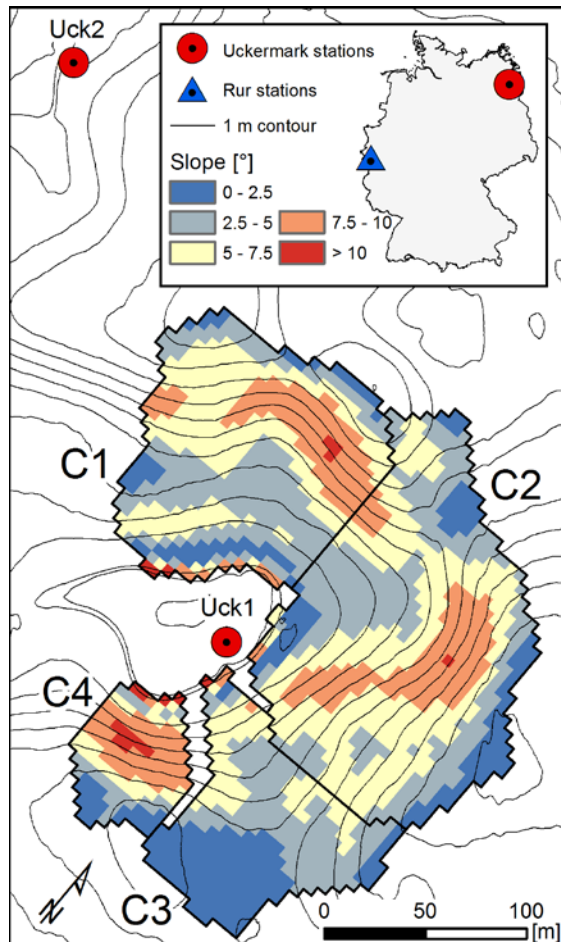


Figure 2.2: Location of rainfall stations in the Uckermark and Rur region and topography of the modelled kettle hole catchments (C1 – C4).

(RUSLE: Renard et al., 1996). Where erosion is calculated according to a slightly modified RUSLE approach, transport and deposition is based on the grid cell specific local transport capacity TC ($\text{kg m}^{-1} \text{a}^{-1}$), which multiplies the RUSLE equation by the transport capacity coefficient (ktc ; in meter)

$$TC = ktc R C K L S \quad (2.3)$$

where R , C , K , L and S are the RUSLE factors (see Renard et al., 1996): The model input rainfall-runoff erosivity (R) factor and cover-management (C) factor are directly or indirectly related to the rainfall KE. The annual R factor is calculated following Renard et al. (1996)

$$R = \sum_{i=1}^j (EI_{30})_i \quad (2.4)$$

where E is the rainfall KE of event i (kJ m^{-2}). As the product of EI_{30} is the event based rainfall erosivity. The C factor is calculated from daily rainfall erosivity proportions (based on 1-min KE values) and the average daily soil cover of the applied crop rotation. The average soil cover is derived from Schwertmann et al. (1990).

Model implementation

The model applies 13 years of rainfall measurements from the different stations individually to a generalized four year crop rotation (rape – winter wheat - winter barley – winter barley; see section 2.2.1) in the four catchments (Fig. 2.2). This results in 52 yrs of reference model runs driven by measured KE. In the next step, the 32 KE-I relations (Table 2.1) are used as model input, which leads to a total number of 1664 model runs.

All model parameters except for the R and C factor remain constant throughout all model runs to isolate the effect of different KE-I relations upon sediment delivery. The model operates on a 5×5 m grid resolution. Topographic information is based on an airborne laser scanning digital elevation model aggregated to 5×5 m resolution. With respect to a detected optimum transport capacity of 150 m under arable land and similar resolution, we followed Van Oost et al. (2003). According to measurements of Gerke and Hierold (2012) at a nearby (9 km east) located study area, the topsoil bulk density was set to 1550 kg m^{-3} . According to BGR (2014) a RUSLE K factor of $0.25 (\text{Mg h}) (\text{ha N})^{-1}$ was applied. The P factor was set to 1 as no soil conservation measures are applied at the test site.

2.3 Results

2.3.1 Drop size and terminal velocity distributions

Comparing the measured DSD against the theoretical DSD model of Marshall and Palmer (1948; MP) indicates rainfall intensity specific differences (Fig. 2.3). (i) For minutes of low rainfall intensities ($4\text{--}6\text{ mm h}^{-1}$, Fig. 2.3a), the MP-DSD substantially overestimates the proportion of small drops ($< 0.25\text{ mm}$), but underestimates the amount of all other drop size classes. (ii) For moderate rainfall intensities ($20\text{--}30\text{ mm h}^{-1}$) the MP distribution predicts the proportion of the smallest drops size class and furthermore large drops appropriately ($> 1\text{ mm}$, Fig. 2.3b). (iii) However, the proportions of large drops are systematically overestimated by the MP distribution for high intensities ($40\text{--}60$ and $100\text{--}150\text{ mm h}^{-1}$, Fig. 2.3c and 2.3b).

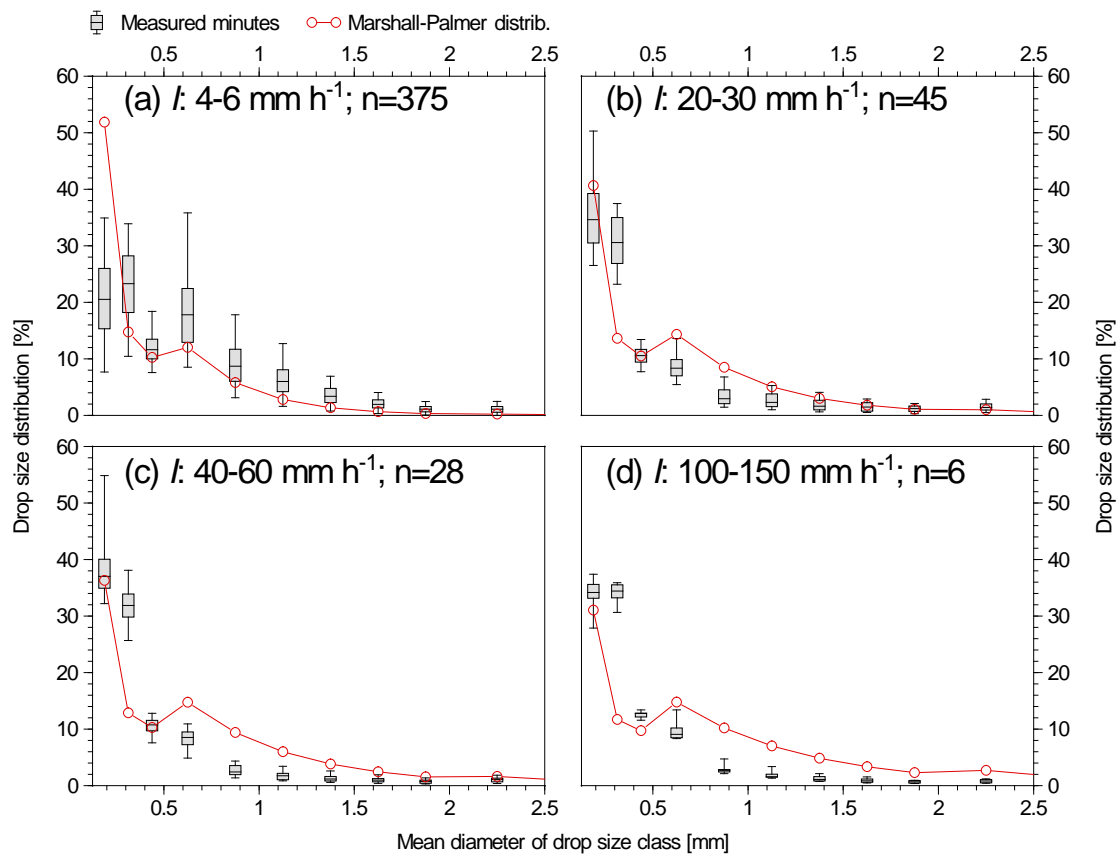


Figure 2.3: Measured drop size distributions for minutes of a specific rainfall intensity range (I ; boxes) compared to the drop size distribution model of Marshall and Palmer (1948). The variation of the Marshall-Palmer distribution for the analysed intensity ranges is small and covered by the diameter of the red marker circles. Exemplarily shown for station Uck1.

Comparing measured drop fall velocities against the theoretical fall velocity model of Gunn and Kinzer (1949; GK) also indicates pronounced deviations (Fig. 2.4). Particularly for the highly erosive rainfall event (Fig. 2.4a), small drops were measured at almost all fall velocities, where for the low erosive rainfall event (Fig. 2.4b) the range of measured

fall velocity is somewhat smaller. A large proportion of small measured drops show higher fall velocities than predicted by the terminal velocity model by GK. For larger drops, the GK distribution describes more or less the measured fall velocities, but a substantial number of large drops show smaller fall velocities. As these large drops are highly relevant for the KE, assuming the GK model leads to an overestimation of KE. The comparison of measured and theoretical drop size and fall velocity distributions indicates that both lead to KE overestimations for large drops.

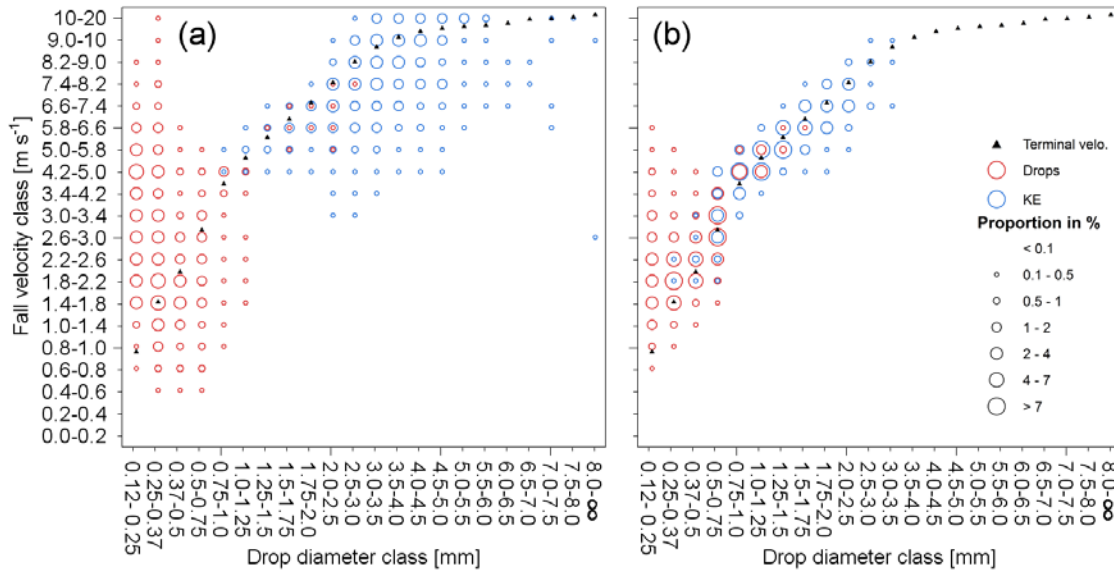


Figure 2.4: Measured proportions of individual drops and rainfall kinetic energies of specific drop size and fall velocity classes. Exemplarily shown for (a) a heavy erosive rain event (sum: 38 mm; I_1 : 253 mm h⁻¹, I_{10} : 162 mm h⁻¹, I_{30} : 74 mm h⁻¹) and (b) a moderate erosive rain event (sum: 11 mm; I_1 : 3 mm h⁻¹, I_{10} : 1.8 mm h⁻¹, I_{30} : 1.5 mm h⁻¹) at the study site Uck1 (see Fig. 2.2). Terminal velocity according to Gunn and Kinzer (1949) is represented in black triangles.

2.3.2 Comparison of measured vs. derived kinetic energy

We analysed the deviation between measured and derived KE by 32 KE-I relations. The majority of KE-I relations show an overestimation of cumulative KE with a large variety of results (Fig. 2.5). The deviation was not uniformly distributed throughout the course of increasing measured KE. In general, there are mainly three kinds of behaviour of the KE-I relations: (i) an exponentially increasing overestimation, (ii) a pronounced underestimation of the strongest 10% of rainfall minutes. (iii) A number of relations do show a conservative behaviour and lead to a constant overestimation (without exponential deviation at high energies) throughout the course of different energy levels (Fig. 2.5). The minutes of highest KE are proportionally more relevant for the total KE of the data series at the Uckermark stations compared to the Rur stations (Fig. 2.5). Hence, 90% of the total

KE was achieved by 13.5% and 14.7% of rainfall minutes for Uck1 and Uck2, respectively (Rur1: 23.3%, Rur2: 20.8%). In contrast, the largest contribution of heavy precipitation minutes was found for station Rur3 (12.6%).

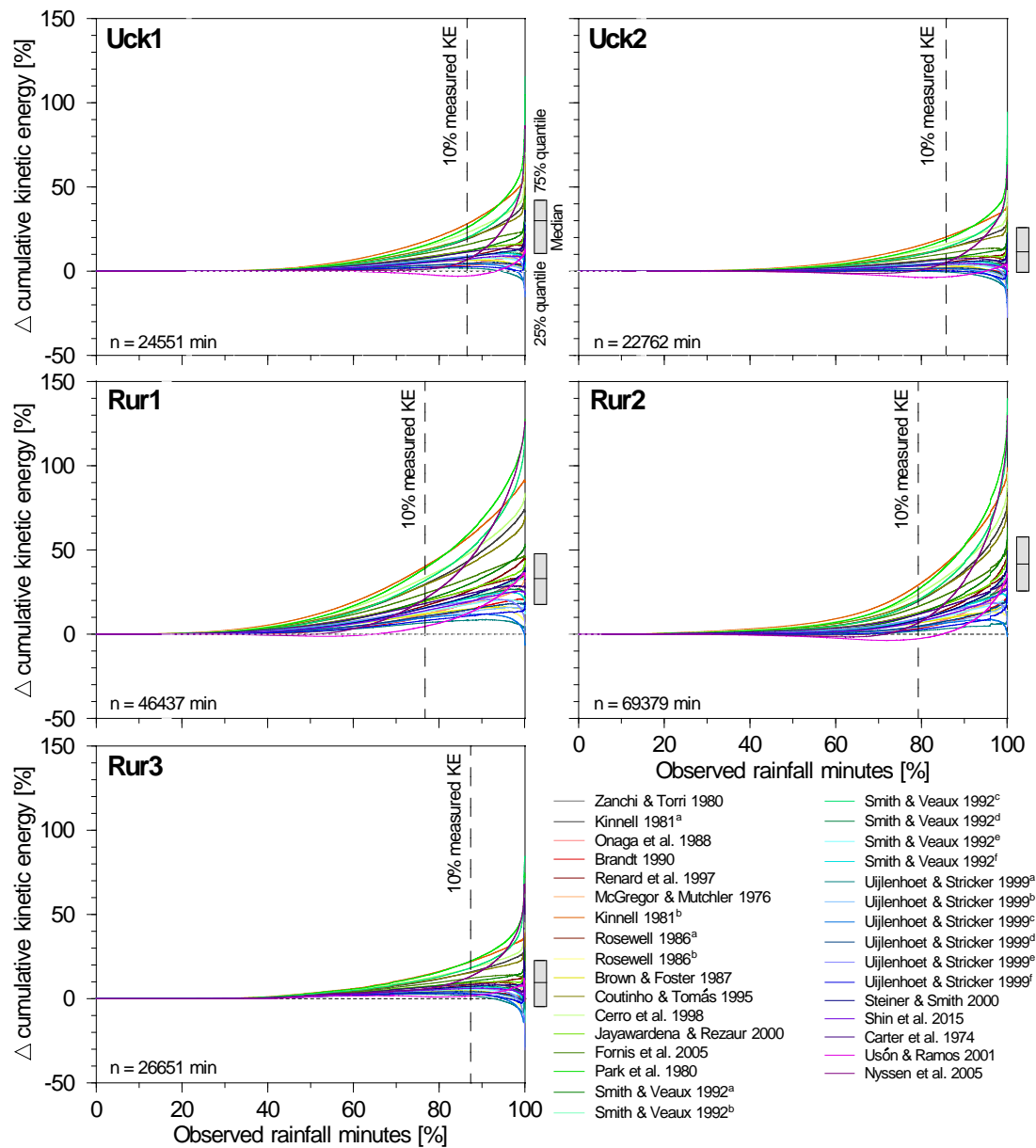


Figure 2.5: Cumulative deviation, increasingly sorted according to measured kinetic energy (KE), between measured and derived KE by 32 different rainfall kinetic energy-intensity relations (see Table 2.1). Vertical dashed line shows 10% of cumulative measured KE sum.

On an annual aggregation level, all years at all stations show a mean overestimation of the 32 KE-I relations compared to the measured KE (Table 2.3). The highest annual deviations are found for the stations Rur1 and Rur2, which are located in the hilly Eifel region. The highest mean deviation of 71% for a measured total annual KE sum of 4.4 kJ m^{-2} was found at station Rur2 in 2015. The lowest annual deviation was shown for station Rur3 with a relative mean deviation of 1% for a total KE sum of 2106 J m^{-2} .

Table 2.3: Annual deviation of 32 kinetic energy-intensity relations to measured kinetic energy over 5 stations and a total of 13 years (see Table 2.2). Relative deviation (%) is given in brackets behind absolute deviation (J m^{-2}). Positive values indicate an overestimation and negative values an underestimation of the measured kinetic energy.

Station	Year	Measured KE [J m^{-2}]	Δ measured KE	
			Mean	Median
Uck1	2015	2152	788 (36.6)	635 (29.5)
	2016	3203	870 (27.2)	700 (21.9)
Uck2	2015	3173	462 (10.9)	273 (8.7)
	2016	4247	742 (8.2)	568 (6.5)
Rur1	2015	6278	3036 (48.4)	2531 (40.3)
	2016	5519	1845 (33.4)	1416 (25.7)
Rur2	2013	4236	1810 (42.7)	1370 (32.3)
	2015	4444	3134 (70.5)	2738 (61.6)
	2016	3133	963 (30.7)	883 (28.2)
Rur3	2013	5846	283 (4.8)	-11 (-0.2)
	2014	1604	906 (56.5)	790 (49.2)
	2015	2106	22 (1)	-66 (-3.1)

2.3.3 Measured vs. derived kinetic energy affecting event erosivity

Analysing event differences for measured and derived KE in relation to erosivity, shows distinct differences between the Uckermark and Rur stations. Uck1 and Uck2 are dominated by events with low rainfall erosivities $< 5 \text{ N h}^{-1}$, while the Rur stations show regularly occurring events of higher rainfall erosivities between 5 and 20 N h^{-1} (Fig. 2.6). Events of long duration (> 2.5 days) can accumulate large quantities of KE but do not have high rainfall intensities and therefore low erosivities. A long duration event at Rur1 shows the largest 95% confidence interval for the 32 KE-I relations, ranging from 1.3 to 3 kJ m^{-2} . Surprisingly, this large range does not cover the measured KE (1.2 kJ m^{-2} ; Fig. 2.6). As already shown by the analysis of minute-wise data, the derived KE distinctively overestimates the measurements, which is indicated by the median PBIAS (average over or underestimation between derived and measured KE values in percent) of all KE-I relations, ranging from 10 to 54% (Table 2.4). KE-I relations originally developed for Spain (Usón and Ramos, 2001) and North Carolina (USA: Smith and De Veaux, 1992e) matched the events of the Uckermark stations best, where KE-I relations theoretically developed from DSDs (Uijlenhoet and Stricker, 1999b) performed best for Rur1 and Rur2. The heavy event at the stations Uck1 and Uck2 in 2016 (Fig. 2.6a) contributes only with 11% and 17% to the total KE but with 46% and 60% of the total rainfall erosivity,

respectively. Although single events have limited impact on the total KE sum of a time series, the relevance of single events for the total rainfall erosivity is high. The Uckermark stations are located 300 m apart, but show substantial differences (Table 2.4). The goodness of fit parameters for the Uckermark stations indicate better estimates compared to the Rur station (Table 2.4). Removing heavy events with a median derived KE greater than 1 kJ m^{-2} does not show high sensitivity for the goodness of fit parameters. Nevertheless, poor estimate quality for the stations Rur1 and Rur2 are indicated by low and partially negative (worse than mean of observations) model efficiency coefficients (Nash and Sutcliffe, 1970).

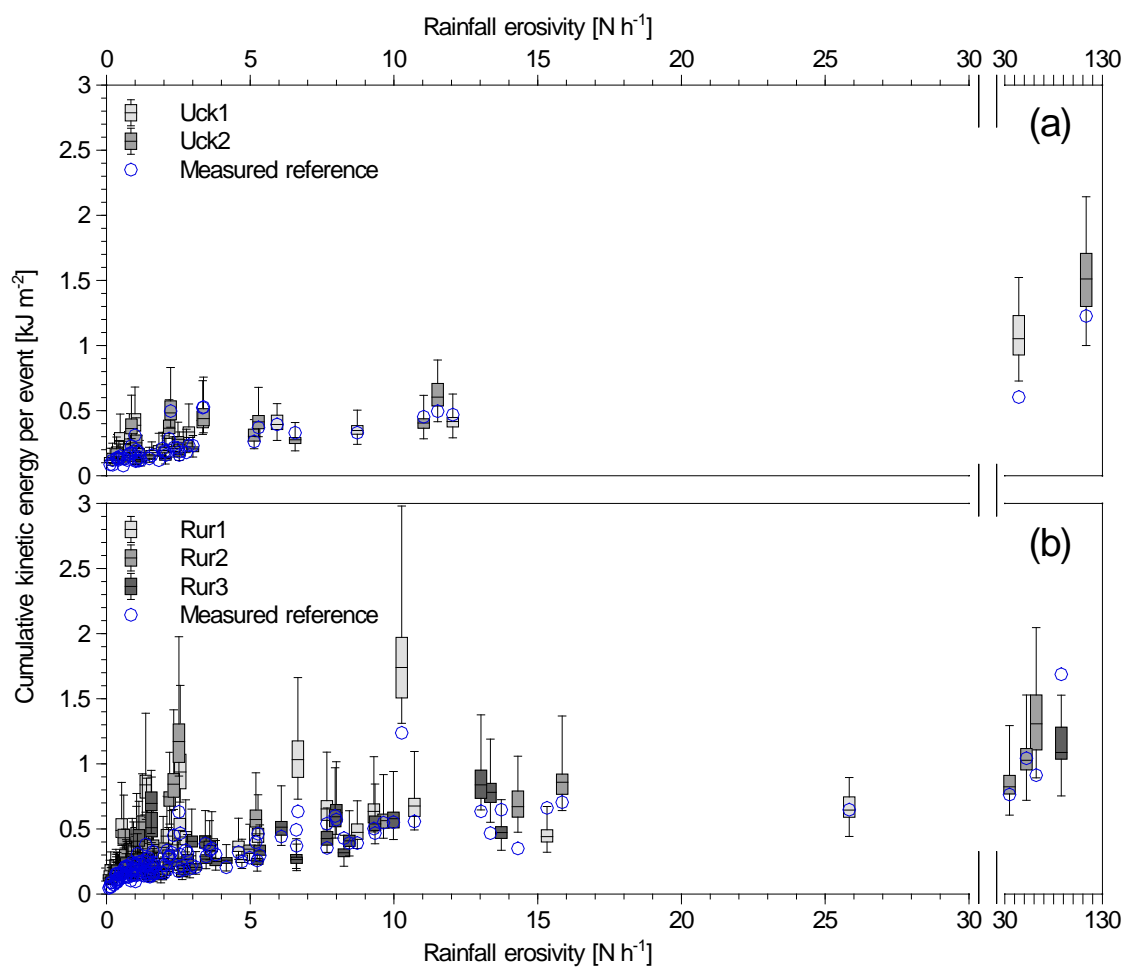


Figure 2.6: Event based kinetic energy derived by 32 different kinetic energy-intensity relations (box-whiskers). Error bars indicate the 95% interval of confidence. The blue circles show the measured kinetic energy.

Table 2.4: Goodness of fit parameters for the median value of 32 kinetic energy-intensity relations against measured kinetic energy. The sensitivity of extreme events is shown in brackets, as events of a derived kinetic energy $> 1 \text{ kJ m}^{-2}$ are excluded from calculation. Root mean square error (RMSE), model efficiency coefficient (MEC), percent bias (PBIAS) and number of observed erosion events (n).

Station	RMSE [J m^{-2}]	MEC	PBIAS [%]	n
Uck1	105 (57)	0.45 (0.77)	24 (17)	26 (25)
Uck2	78 (55)	0.88 (0.81)	11 (9)	26 (25)
Rur1	431 (197)	-2.19 (0.01)	54 (42)	36 (33)
Rur2	178 (178)	0.15 (0.15)	42 (42)	45 (43)
Rur3	190 (194)	0.36 (0.35)	14 (15)	57 (55)

2.3.4 Modelled differences in sediment delivery

Applying the WaTEM/SEDEM model with altered R and C factors in relation to different rainfall KE-I relations shows high variations in sediment delivery (Fig. 2.7). Where the reference runs (based on measured rainfall KE), show for the larger catchments (C1 to C3; Fig. 2.2) moderate sediment delivery ($< 4 \text{ Mg ha}^{-1} \text{ yr}^{-1}$), the highly connected catchment 4 shows annual sediment delivery up to $18 \text{ Mg ha}^{-1} \text{ yr}^{-1}$. Catchment 2, which is the largest catchment that consists of erosional and depositional structures (Fig. 2.8), shows the lowest reaction on different KE-I relations. Contrary to that, the smallest and mainly erosion dominated catchment 4 shows the highest 95% confidence interval in response to alterations in the derived KE from 13 up to $27 \text{ Mg ha}^{-1} \text{ yr}^{-1}$. Interestingly, the model runs of highest sediment delivery show conflicting results in relation to the corresponding reference runs. The year of highest sediment delivery (Rur3, 2013) shows a median underestimation of $5 \text{ Mg ha}^{-1} \text{ yr}^{-1}$, where the second highest year (Rur2, 2015) has a median overestimation of $5.9 \text{ Mg ha}^{-1} \text{ yr}^{-1}$ in catchment 4. Substantial sediment delivery was solely simulated for rainfall data of the Rur stations (Fig. 2.7). The extreme event at the Uckermark stations in 2016 occurred in times of high soil cover and does not cause substantial simulated sediment delivery. Highest sediment delivery of the crop rotation is caused by rape cultivation followed by the first year of winter barley.

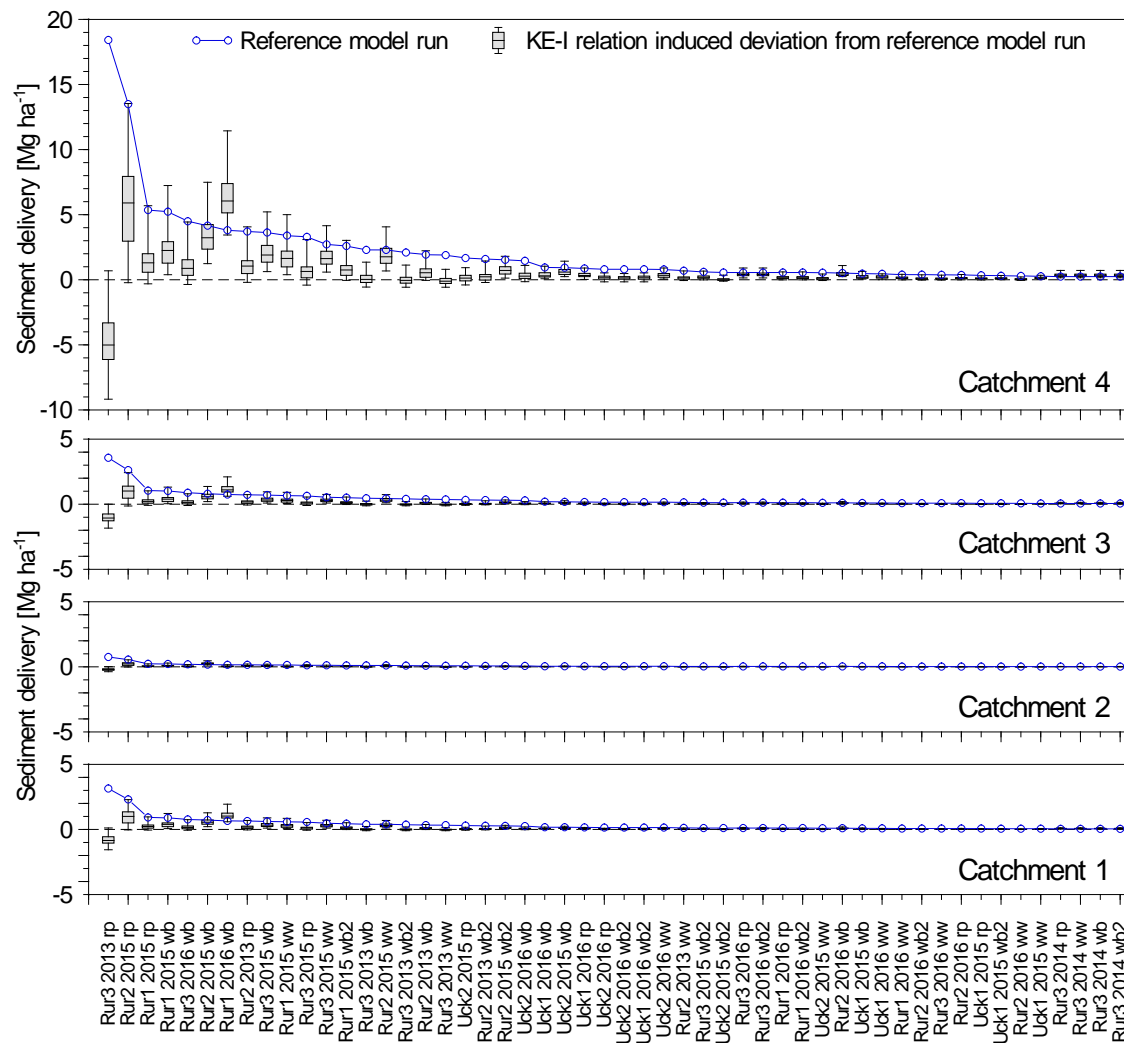


Figure 2.7: Modelled (WaTEM/SEDEM) uncertainty in annual sediment delivery related to 32 different theoretical rainfall kinetic energy-intensity (KE-I) relations (see Table 2.1), altering the R (rainfall erosivity) and C (management) factor of the RUSLE. The blue circles indicate the modelled absolute sediment delivery, whereas the boxes (25 and 75%) and whiskers (5 and 95%) show the deviation between the reference model run and the KE-I relation model runs. The model applies 13 yrs of rainfall data of 5 station to a complete crop rotation in four catchments (see Fig. 2.2; rp: rape, wb: winter barley, ww: winter wheat, ww2: winter wheat second year).

2.4 Discussion

Optical disdrometers have potential error sources e.g. splash from device arm into the sensor, two drops detected as a single drop, horizontal moving drops by wind (Angulo-Martinez et al., 2016). Nonetheless, optical disdrometers enable the continuous observation of rainfall KE dynamics on high temporal resolution. Due to dynamics in DSD according to the type of rainfall, the KE-I relationship is not static for different events and furthermore throughout different event phases (Angulo-Martinez et al., 2016). However, almost all KE-I relations are explicitly developed for one typical DSD of a single distinct meteorological region, rainfall type and utilize static drop size specific fall velocities. Therefore, combined measurements of DSD and corresponding fall velocities by optical

disdrometers are assumed to be the most accurate and available source to measure and analyse rainfall KE dynamics.

2.4.1 High resolution analysis

The minute based analysis shows pronounced deviations in reaction to different rainfall KE-I relations (Fig. 2.5). A few KE-I relations match the total sum of measured KE after the complete time series well, but nonetheless do have a large absolute error, caused by high deviations over the course of different KE levels. The majority of KE-I relations show a distinct overestimation (Fig. 2.5), which is likely to be caused by a large number of drops falling at velocities conflicting common models of terminal velocity (Gunn and Kinzer, 1949; Hinkle et al., 1987; Laws, 1941). We observed a large quantity of small drops (< 0.75 mm) falling at extraordinarily high velocities (Fig. 2.4).

These super-terminal drops are reported in literature and are likely to be caused by

wind effects (Montero-Martinez and Garcia-Garcia, 2016) and fragmentation of fast and large drops (Larsen et al., 2014). Since super-terminal drops have higher energies than estimated from theoretical terminal velocity models, they cause an underestimation of KE-I relations. However, Figure 2.4 shows that the amount of KE caused by drops smaller than 0.75 mm is rather limited for the overall KE estimation. Furthermore, we observed drops falling at substantially lower velocities than expected from terminal velocity models (Fig. 2.4), which were also observed in other studies (Angulo-Martinez et al., 2016; Cerro et al., 1998; Montero-Martinez and Garcia-Garcia, 2016; Petan et al., 2010). Sub-terminal drops cause an overestimation for KE-I relationships and mainly occur in the drop diameter class contributing to the highest amount of rainfall KE (Fig. 2.4). Therefore, sub-terminal drops and the overestimation of large drops in case of high rainfall intensities (Fig. 2.3) are likely to be the reason for the disagreement between measured

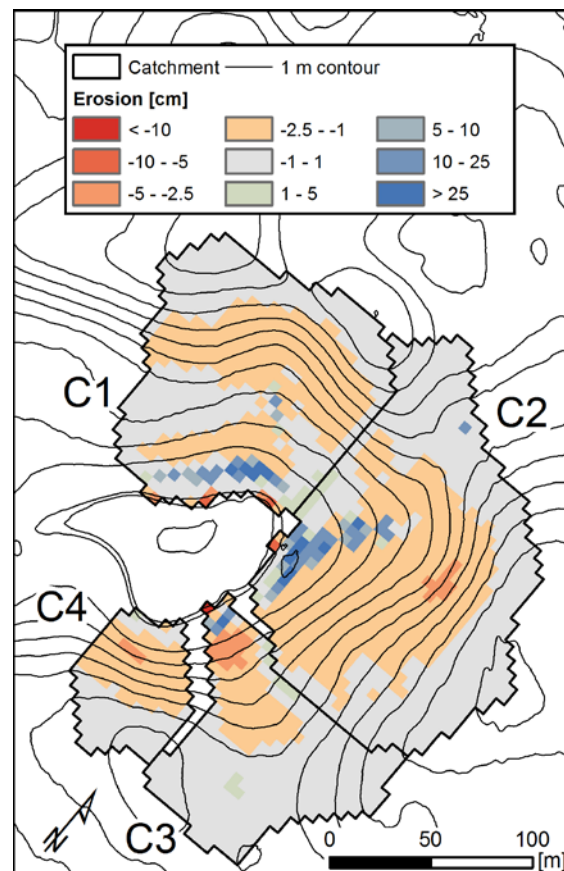


Figure 2.8: Cumulative soil erosion (negative values) and deposition (positive values) by water of all 56 reference model runs based on measured rainfall kinetic energy.

and theoretically derived KE. This general overestimation of KE-I relations is in line with recently published results of Angulo-Martinez et al. (2016). With similar methodology, they reported a minute based positive bias for the KE-I relations compared to optical disdrometer based measured KE.

2.4.2 Regional conditions for event based model input

The most common use of KE-I relations in soil erosion modelling, is to provide event based kinetic energies. Considering the median of all 32 KE-I relations, a distinct positive bias for all stations can also be found on event resolution (Table 2.4). Interestingly, the best matching KE-I relations are not necessarily developed for similar regions or environmental conditions. One could argue that the good performance for Uck1 and Uck2 of the KE-I relation developed for Spain (Usón and Ramos, 2001) is attributed to meteorological similarities, such as convective rainfall of high intensities. However, Usón and Ramos (2001) developed this relation based on data with a maximum rainfall intensity of 20 mm h^{-1} . Since our rainfall records consist of measurements of much higher rainfall intensities (up to 300 mm h^{-1}), the good agreement cannot be attributed to meteorological reasons due to heavy uncertainties by extrapolation.

We found regional differences in estimate quality. The predictions for the Uckermark stations were better compared to the Rur stations (Table 2.4), which is potentially caused by less variation in rainfall types. In contrast to the predominantly cyclonic rainfall in the maritime climate of the Rur stations, the short and heavy convective rainfall in the sub-continental climate of the Uckermark might have less variation in DSD, which leads to a better predictability of static KE-I relations. Furthermore, the stations Rur1 and Rur2 are located in the hilly Eifel region that may cause larger dynamics in rainfall types and corresponding DSD, which may to some extent explain the poor estimate quality at these two particular stations (Table 2.3 and 2.4). Therefore, it is suggested to select the utilized KE-I relation on event level in relation to the rainfall type and not only for a distinct meteorological region.

2.4.3 Soil erosion modelling

The parsimonious WaTEM/SEDEM model showed its reliability in predicting soil erosion estimates in numerous studies for different environments (e.g. Bakker et al., 2008; De Vente et al., 2008; Dlugoß et al., 2012; Nadeu et al., 2015; Van Rompaey et al., 2005; Verstraeten et al., 2002). Due to the artificial input data, a rigorous validation was not possible. However, with respect to the study aim of quantifying the range of possible

uncertainties induced by a variety of KE-I relations and focusing on relative differences, the model performance is assumed to be sufficiently good.

Sediment delivery is substantially affected by the seasonal distribution of rainfall KE occurrence. For the year of the highest KE and R factor, low sediment delivery was simulated because the largest energy proportion occurred during a period of full vegetation cover. Thus, pronounced sediment delivery was solely simulated for the rainfall data of the cyclonic Rur stations due to a higher event frequency. An altered seasonal rainfall distribution would cause much higher sediment delivery and thus our estimates are rather conservative. Soil erosion by water is a highly episodic process, driven by single events (Fiener et al., 2015; Wilken et al., 2017a) and requires a combination of environmental conditions. Unfortunately, extreme events show the highest variation and uncertainty of the KE-I relationship. Figure 2.7 illustrates that the positive bias is not constant throughout all years of highest sediment delivery and can either over or underestimate the reference run considerably. This implies for water erosion modelling, that KE derived from rainfall intensity underlies large uncertainties for rare and highly important extreme events. This is particularly true for physically-oriented models that apply KE-I relations on high temporal resolution. In contrast, on long time scales, the error might to some extent average out when utilizing conceptual models that were originally developed for the prediction of long-term average soil loss such as the USLE (Wischmeier and Smith, 1960).

The majority of environmental studies utilize tipping bucket rain gauges, which have a known underestimation problem of high intensity rainfall (Humphrey et al., 1997; Marsalek, 1981; Shedekar et al., 2016). Since most KE-I relations were developed to be applied on tipping bucket rain gauges, the positive bias might intentionally compensate the mechanically caused underestimation. Petan et al. (2010) showed that the derived KE from tipping bucket rain gauges is distinctively lower compared to the measured KE based on two optical laser disdrometers (Thies-Clima and OTT). However, this would suggest that traditional KE-I relations need to be calibrated for an application on intensity measurements of modern ombrometers. Further research is needed to show the effect of an overestimation by KE-I relations and underestimation by tipping bucket rain gauges.

2.5 Conclusions

We applied various rainfall kinetic energy-intensity (KE-I) relations on five optical disdrometers to assess (i) deviations between measured and theoretically derived kinetic energy (KE), (ii) variations throughout different energy and temporal aggregation levels and

(iii) implications for soil erosion modelling. For all analysed aspects (minute KE, erosive event KE and modelled sediment delivery), a distinct overestimation by the KE-I relations compared to measured KE was found. However, the overestimation is not a systematic offset and shows large variations for high rainfall intensities. Therefore, the prediction of KE causes substantial uncertainties for the simulation of rare and highly important extreme events of soil erosion modelling.

A geographical region is not necessarily the best predictor to determine the most adapted KE-I relation for a study area with heterogeneous rainfall characteristics. Therefore, an event specific selection according to rainfall types is suggested. Our findings demonstrate a need for rainfall type explicit KE-I relations and calibration coefficients of KE-I relations for application on modern optical disdrometers.

Article II

Modelling a century of soil redistribution processes and carbon delivery from small watersheds using a multi-class sediment transport model

Florian Wilken^{1,2,3}, Peter Fiener¹ and Kristof Van Oost⁴: Modelling a century of soil redistribution processes and carbon delivery from small watersheds using a multi-class sediment transport model, *Earth Surface Dynamics*, 5, 113-124, <https://doi.org/10.5194/esurf-5-113-2017>, 2017.

¹Institute for Geography, Universität Augsburg, Germany

²Chair of Soil Protection and Recultivation, Brandenburg University of Technology Cottbus-Senftenberg, Germany

³Institute of Soil Landscape Research, Leibniz-Centre for Agricultural Landscape Research (ZALF) e.V., Germany

⁴Earth & Life Institute/TECLIM, Université catholique de Louvain, Belgium

Published in the journal Earth Surface Dynamics.

Article abstract

Over the last few decades, soil erosion and carbon redistribution modelling has received a lot of attention due to large uncertainties and conflicting results. For a physically based representation of event dynamics, coupled soil and carbon erosion models have been developed. However, there is a lack of research utilizing models which physically represent preferential erosion and transport of different carbon fractions (i.e. mineral bound carbon, carbon encapsulated by aggregates and particulate organic carbon). Furthermore, most of the models that have a high temporal resolution are applied to relatively short time series ($< 10 \text{ yr}^{-1}$), which might not cover the episodic nature of soil erosion. We applied the event-based multi-class sediment transport (MCST) model to a 100-year time series of rainfall observation. The study area was a small agricultural catchment (3 ha) located in the Belgium loess belt about 15 km southwest of Leuven, with a rolling topography of slopes up to 14%. Our modelling analysis indicates (i) that interrill erosion is a selective process which entrains primary particles, while (ii) rill erosion is non-selective and entrains aggregates, (iii) that particulate organic matter is predominantly encapsulated in aggregates, and (iv) that the export enrichment in carbon is highest during events dominated by interrill erosion and decreases with event size.

3.1 Introduction

Numerical models of soil detachment, transport and deposition are important tools for improving our understanding of soil systems and the linkages between the terrestrial and aquatic ecosystems. At present, a wide range of erosion models are available. Conceptual models, such as the RUSLE (Römkens et al., 1997), focus largely on the prediction of long-term sediment production under various environmental and management conditions. In parallel, physically-oriented models have been developed to simulate the routing of soil over complex topographies, taking hydrological and sediment-sorting processes into consideration (e.g. LISEM: De Roo et al., 1996; WEPP: Nearing et al., 1989; EROSION-3D: Schmidt, 1991). These models operate over relatively short timescales, typically one to several events, and are concerned with modelling the detachment and movement of mineral particles. Over the last few decades, they have been instrumental in improving our understanding of erosion processes and currently serve as tools for landscape management.

Erosion-induced changes in biogeochemical cycles, in particular carbon (C) fluxes between soils, the aquatic environment and the atmosphere, have received considerable attention over the past two decades (Quinton et al., 2010; Renwick et al., 2004; Stallard, 1998). However, large uncertainties and conflicting results remain (Kuhn et al., 2009; Lal, 2003; Van Oost et al., 2007), and this has spurred renewed interest in the application of soil erosion models. To date, few soil and SOC erosion models integrate detailed transport processes. There have been attempts to address this issue using single-point models with varying degrees of complexity (Billings et al., 2010; Harden et al., 1999; Liu et al., 2003a; Manies et al., 2001). These models apply prescribed SOC erosion and/or deposition rates and simulate the resulting effects on the soil organic carbon (SOC) profile using CENTURY (Parton et al., 1988) parameterizations. Recently, spatially explicit models that combine erosion models with models of SOC dynamics have been developed (e.g., Changing Relief and Evolving Ecosystems Project (CREEP): Rosenbloom et al., 2001; Yoo et al., 2005; SPEROS-C: Van Oost et al., 2005c; Fiener et al., 2015). Both CREEP and the model presented by Yoo et al. (2005) focus on long-term landscape development (i.e. millennial scale) and diffusive geomorphic processes that occur on undisturbed grasslands. The CREEP model also simulates textural differentiation and preferential transport of the finer fractions by surface wash. Compared to CREEP,

SPEROS-C focuses on shorter timescales (i.e. years to decennia) and agricultural landscapes. It includes spatially distributed water and tillage erosion and dynamically couples SOC turnover (Dlugoß et al., 2012; Van Oost et al., 2005c).

Although these model concepts have facilitated an improved qualitative understanding of SOC erosion and erosion-induced changes in SOC storage, they are largely based on unverified assumptions and simplified process descriptions: First, SOC erosion is mostly approximated as being proportional to the bulk carbon:sediment ratio of topsoils. However, both experimental and modelling studies have clearly shown that erosion preferentially removes and exports SOC (Kuhn et al., 2010; Polyakov and Lal, 2004b; Schiettecatte et al., 2008a, b). This preferential transport results from the fact that SOC is not distributed uniformly throughout the soil, but instead consists of several fractions, characterized by different densities and particle sizes. For example, some SOC is bound to the fine mineral fraction, some is encapsulated in soil aggregates, while another SOC fraction exists as mineral-free particulate organic matter (POM) and has a much lower density (John et al., 2005; Von Lützow et al., 2007). This differentiation is particularly relevant for the C cycle, since for example the C fraction with the highest potential mobilization and transport capacity (i.e. POM due to its low density) is also a very labile fraction (Haynes, 2005). Thus, SOC erosion models should always consider the differential behaviour of sediment particles and SOC fractions when simulating erosion and transport processes. Second, SOC erosion simulation models need to consider relatively long timescales, i.e. several years to decades, as SOC erosion fluxes are relatively small when compared to rates of SOC turnover (Fiener et al., 2015). Current models addressing erosion (e.g. EDCM: Liu et al., 2003a; CENTURY: Parton et al., 1988; WaTEM: Van Oost et al., 2000a; EPIC: Williams, 1995) use a constant average annual soil erosion rate by assuming uniformity. However, empirical observations indicate that soil erosion and sediment delivery are to a large extent controlled by extreme events (Fiener and Auerswald, 2007b). This calls into question whether the effects of erosion on biogeochemical cycles can reasonably be derived from continuous average long-term erosion rates. Event size also influences the extent to which selective transport takes place in erosion processes. For example, interrill erosion, which is a selective process (Kuhn et al., 2010), is more pronounced during smaller erosion events. As a result, there is more enrichment of fine soil fractions, including SOC associated with clay particles, during small events compared to large ones. It is therefore important that SOC erosion models correctly represent the different processes that control selectivity. Furthermore, analysis

on the relative contribution of low intensity (but high frequency) and more extreme (but low frequency) erosion events is required to understand the long-term effect on SOC dynamics. An important limitation of current approaches is therefore the frequent use of the USLE (Wischmeier and Smith, 1978) as a basis for erosion prediction. The USLE was not designed to estimate frequency distributions of soil erosion but is in fact designed to average out variability but is widely used on an annual (Erol et al., 2015; Ligonja and Shrestha, 2015) or monthly (Galdino et al., 2016) resolution.

The main objective of this paper is to use a physically-oriented erosion model the multi-class sediment transport (MCST) model (Fiener et al., 2008; Van Oost et al., 2004) in a numerical experiment to improve our mechanistic understanding of sediment and SOC delivery. To this end, the MCST model is modified to incorporate the natural long-term variability of soil and SOC erosion. Existing empirical observations will be used to assess the model behaviour and to identify potential deficiencies in model process descriptions. Finally, the long-term role of event size on soil and SOC erosion will be evaluated and discussed.

3.2 Methodology

The MCST model (Fiener et al., 2008; Van Oost et al., 2004) combines a soil infiltration component with a kinematic wave routine to produce continuous series of runoff events. The event-based soil erosion component describes detachment as a function of rainfall characteristics, slope and discharge, while transport and deposition are simulated using the Hairsine and Rose (1992b, b) equations. The two-dimensional implementation in a regular grid (1m x 1 m to 5m x 5 m) uses a digital elevation model to route overland flow and sediment redistribution. A detailed model description can be found in Van Oost et al. (2004) and Fiener et al. (2008); here we focus on its main features and modifications made in order to continuously simulate long-term (up to centuries) soil and SOC erosion.

3.2.1 Modelling surface runoff

The model calculates rainfall excess at a fine temporal resolution (minutes to hours) using a modified curve number approach. The original version of the MCST model simulates single rainfall events but is converted into a continuous simulation model as follows. The input of the model is a continuous rainfall series with a time resolution of 10 min. A rainfall-runoff event is identified as a period (i) in which rainfall depth exceeds 2 mm in 24 h (<1% of total runoff excluded) and (ii) which is separated by at least 72 h without

rainfall. Accordingly, a rainfall-runoff event is not necessarily defined by a single hydrograph, but might contain multiple runoff peaks. A moving window of 24 h is used to estimate cumulative rainfall ($P_{i,cum}$) and cumulative abstractions for each time step i (i.e. initial abstraction ($I_{a,cum}$) and continuing abstraction ($F_{a,cum}$) of the curve number method). The excess rainfall hyetograph (R_i) at time step i is calculated as

$$R_i = R_{i,cum} - R_{i-1,cum} \quad (3.1)$$

and

$$R_{i,cum} = (P_{i,cum} - I_{a,cum} - F_{a,cum})I_f, \quad (3.2)$$

where $P_{i,cum}$ (mm) is the cumulative excess rainfall during the last 24 h.

I_f is a scaling factor for rainfall intensity which is calculated as:

$$I_f = \left(\frac{IN_{max10}}{10} \right)^{0.9} \quad (3.3)$$

where IN_{max10} is the maximum 10-minute rainfall intensity (mm h^{-1}).

Flow discharges for each grid cell and time step are calculated by numerically solving the kinematic wave equations (Van Oost et al., 2004). For sheet flow, cross-sectional flow area is calculated assuming a homogeneous flow depth for each raster cell, while for concentrated flow, a relationship between discharge and cross-sectional flow area is used (Govers, 1992). To distinguish between sheet and concentrated flow, a critical shear velocity of 3.5 cm s^{-1} for rill initiation, based on flume experiments conducted by Govers (1985), is used. The model keeps track of changes in the pattern of concentrated flow and rill network development. Finally, sediment movement is described by utilizing an event-based steady-state sediment continuity equation proposed by Yu et al. (1997).

3.2.2 Modelling erosion and deposition

Experimental research has shown that the Hairsine-Rose model provides a physically based description of sediment transport and deposition for multiple sediment classes that differ in terms of settling velocities (Beuselinck et al., 2002a, b). Transport of soil by overland flow is characterized by simultaneous re-entrainment and deposition (i.e. temporary settlement) of sediments:

$$d_i - r_{ri} = \alpha_i C_i v_{si} - \frac{\alpha_i H F}{g} \frac{\delta_i}{(\delta_i - \rho)} \frac{(\Omega - \Omega_{cr})}{D} \frac{M_{di}}{M_{dt}} \quad (3.4)$$

where d_i is the mass rate of deposition per unit area of size class i ($\text{kg s}^{-1} \text{m}^{-2}$), r_{ri} is the rate of sediment re-entrainment for settling velocity class i ($\text{kg s}^{-1} \text{m}^{-2}$), C_i is the mean sediment concentration (settling velocity class i ; kg m^{-3}), α_i is the ratio of the sediment class concentration of flow related to the local sediment class concentration of the parent material, v_{si} is the settling velocity of sediment size class i (m s^{-1}), H is the fractional shielding of the soil by the deposited layer, F is the fraction of stream power used for re-entrainment, g is gravity (m s^{-2}), δ_i is the sediment density of settling velocity class i (kg m^{-3}), ρ is the water density (kg m^{-3}), Ω is the stream power (W m^{-2}), Ω_{cr} is the critical stream power (W m^{-2}), D is the depth of the water flow (m), M_{di} is the mass of sediment class i in the deposited layer (kg m^{-2}), M_{dt} is the total mass of the deposited layer per unit area (kg m^{-2}).

If the local stream power (Ω) is less than a critical threshold (Ω_{cr}), re-entrainment does not occur and deposition of size class i is a function of its specific settling velocity (Beuselinck et al., 1999; Hairsine et al., 2002). If the local stream power exceeds this threshold value, a shielding factor H is calculated to decide whether net erosion or deposition occurs (Hairsine and Rose, 1992a):

$$H = \frac{(\delta - \rho)g \sum v_i C_i}{\delta F(\Omega - \Omega_{cr})} \quad (3.5)$$

If $H \geq 1$, then net deposition, characterized by steady state flow and re-entrainment of previously deposited sediment, occurs. If $H < 1$, net erosion occurs, and soil detachment is modelled as:

$$D_r = aS^{ser} Q^{de} + bS^{sei} \quad (3.6)$$

$$D_{ir} = bI^2 Sf \quad (3.7)$$

where D_r and D_{ir} are the rill detachment rate and the interrill sediment transport to the rill ($\text{kg m}^{-2} \text{s}^{-1}$), respectively, a is the rill erodibility factor, b is the interrill erodibility factor, Q is the rill discharge ($\text{m}^3 \text{s}^{-1}$), S is the local slope gradient, I is the maximum 10 min rainfall intensity, Sf is a slope factor and ser , de and sei are calibration exponents.

Rill erosion is considered to be unselective, i.e. the sediment particle size distribution of the eroded material equals the distribution of the source material at the source location. In contrast, interrill erosion is simulated as a selective process: assuming steady state flow

conditions, Eq. (3.4) is used to estimate the particle size distribution of the sediment detached by interrill erosion and Eq. (3.7) is used to estimate the transport for sediment delivered to the rill network (or that leaves a grid cell when there is no incised rill). This approach is consistent with empirical observations showing that the enrichment of finer sediment particles and SOC in suspended sediment is mainly controlled by the transport capacity of the flow (Schiettecatte et al., 2008b). To represent the amount of primary particles vs. soil aggregates of suspended sediments, the model interpolates the settling velocity for each particle class and grid cell according to the proportion of particles detached by interrill or rill erosion.

The MCST model keeps track of spatio-temporal changes in particle size distribution of the eroded and deposited topsoil sediment within 10 different size fractions. However, the particle size distribution is spatially homogenous and constant throughout the 100-year modelling period.

3.2.3 Model implementation

For our modelling based analysis, we combined data from different sources into a virtual catchment data-set: (i) All basic data (i.e. digital elevation model, soils) were taken from a small first-order catchment in central Belgium, located about 15 km southwest of Leuven. The site has a size of 3 ha with a mean and maximum slope of 7% and 14%, respectively. The catchment consists of diverging convex hillslopes and a central concavity where ephemeral gullying and sediment deposition are frequently observed (Fig. 3.1; Desmet and Govers, 1997). Soils in the catchment are loess-derived, silty-loamy Luvisols, with a clay, silt and sand content of 14%, 82% and 4%, respectively (Desmet and Govers, 1997). (ii) For the 100-year modelling period, high resolution rainfall data (1898-1997; 10-min intervals), measured in Ukkel (Brussels-Capital Region), were used (Fig. 3.1; Verstraeten et al., 2006).

Modelling parameters were derived from earlier studies: (i) We assumed continuous maize cropping, where monthly Curve Number values range between 83 and 89 (Van Oost et al., 2004) to account for seasonal changes in crop cover and soil crusting. This range resulted in runoff volumes that are consistent with field observation (Gillijns et al., 2005). (ii) Two annual tillage operations are assumed to erase the network of rills and ephemeral gullies which may have evolved during preceding erosion events. Apart from removing rills, tillage erosion is not taken into account. (iii) The rill and interrill erodibility parameter values, as well as the slope and discharge exponents (Eq. 3.6 and 3.7), were assumed to be constant over time and space. Therefore, spatio-temporal variability of soil moisture is not accounted for. The parameter values are taken from flume and plot-scale experiments, conducted using soils from the Belgium loess belt (Table 3.1; Van Oost et al., 2004). With these parameters, MCST has already shown to be able to predict the spatial patterns and rates of sediment detachment and transport in the test catchment (Van Oost et al., 2004).

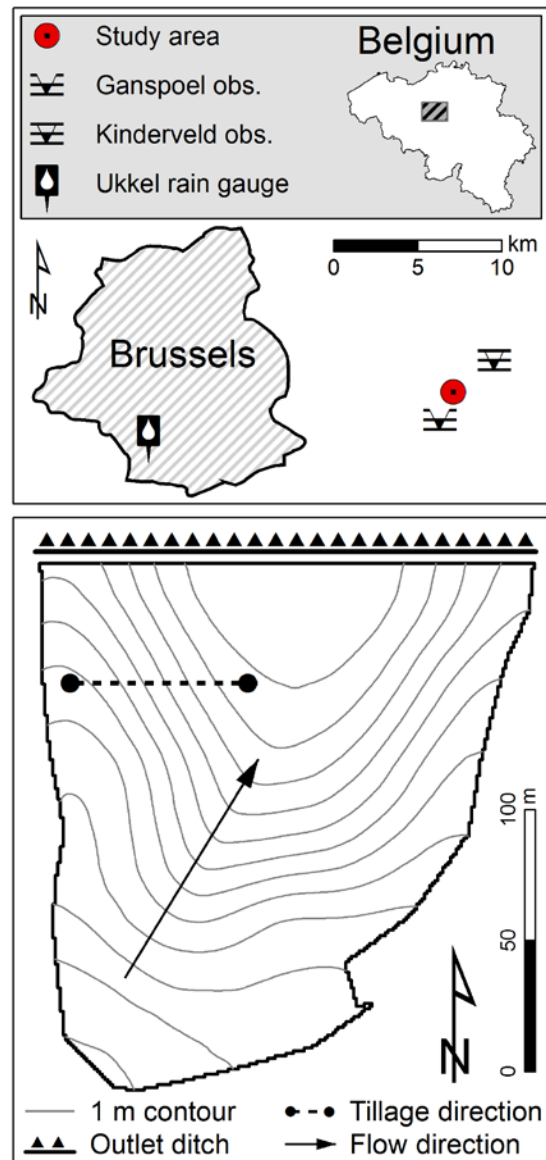


Figure 3.1: Topography and location of the test catchment, location of the Ganspoel and Kinderveld runoff and sediment observation stations and the rain gauge of Ukkel, Brussels-Capital Region.

Table 3.1: Parameter description and model setup.

Symbol	Description	Unit	Range/value
<i>Static parameters</i>			
	sediment density	kg m ⁻³	2600
δ	aggregate density	kg m ⁻³	1300
	particulate organic matter density	kg m ⁻³	1000
ρ	water density	kg m ⁻³	1000
Ω_{cr}	threshold of re-entrainment	W m ⁻²	0.6
g	gravity	m s ⁻²	9.81
v_{si}	settling velocity for class i	m s ⁻¹	2.6 x 10 ⁻⁷ - 5.0 x 10 ⁻³
<i>Dynamic parameters</i>			
R_i	excess rainfall at hyetograph at time step i	mm	
$P_{i,cum}$	cumulative excess rainfall of past 24 h	mm	
$I_{a,cum}$	initial abstraction	mm	
$F_{a,cum}$	continuing abstraction	mm	
d_i	mass rate of deposition for class i	kg s ⁻¹ m ⁻²	
r_{ri}	rate of sediment re-entrainment for class i	kg s ⁻¹ m ⁻²	
C_i	mean sediment concentration for class i	kg m ⁻³	
Ω	stream power	W m ⁻²	
D	depth of water flow	m	
M_{di}	sediment mass of deposited layer for class i	kg m ⁻²	
M_{dt}	total sediment mass of deposited layer	kg m ⁻²	
D_r	rill detachment rate	kg m ⁻² s ⁻¹	
D_{ir}	interrill sediment transport to the rill	kg m ⁻² s ⁻¹	
Q	rill discharge	m ³ s ⁻¹	
I	maximum 10 min rainfall intensity	mm h ⁻¹	
α_i	sediment:parent-material ratio for class i	-	
F	stream power fraction for re-entrainment	-	
H	shielding by deposits	-	
a	rill erodibility factor	-	
b	interrill erodibility factor	-	
S	local slope gradient	-	
Sf	slope factor	-	

In simulation studies, the particle size distribution is typically derived from dispersed sediment samples and therefore reflects the settling velocities of the primary particles of the sediment. However, sediment transport and deposition can also occur in the form of aggregates, particularly for fine textured soils, as is the case in our study area (Beuselinck et al., 2000). Therefore, we considered the particle size distributions of both aggregated soil and primary particles in our simulations. We considered two erosion scenarios. In

erosion scenario 1, both detachment by rill and interrill erosion leads to aggregate breakdown and soil is transported and deposited following the settling velocity classes of primary particles (Fig. 3.2). Furthermore, particulate organic matter (POM) is an individual free floating particle class. In erosion scenario 2, interrill erosion still breaks down aggregates and transports primary particles. In contrast, detachment by rill erosion does not lead to aggregate breakdown and entrains aggregated soil, following the settling velocity classes of aggregated soil (Fig. 3.2). For aggregated soil POM is assumed to be encapsulated in soil aggregates and is not treated as an individual class. Following detachment, the model simulates the transport and deposition of primary particles or aggregated soil based on the erosion type of detachment that they underwent. The particle size distributions of primary particles and aggregated soil were taken from direct measurements ($n=81$) in the Belgian loess belt conducted by (Beuselinck et al., 1999). The grain size distribution for aggregated soil represents the relative difference between fully dispersed and non-dispersed soil in 10 different diameter classes. For these classes, the corresponding settling velocities were calculated according to the model of Dietrich (1982), using a density of 2.6 and 1.3 kg m^{-3} for primary particles and aggregates, respectively. The density of primary particles is assumed to be close to quartz, whereas a pore space of 50% is assumed for aggregates. The settling velocity distributions (Fig. 3.2) show that the aggregated sediments are dominated by fractions with settling velocities between 10^{-4} and 10^{-3} m s^{-1} , i.e. silt-sized particles. In contrast, erosion scenario 1, which solely considers primary particles, shows very low settling velocities relative to aggregated sediments (Fig. 3.2). This results from differences in particle size between the two fractions: aggregated soils contain fewer clay and silt-sized particles, because particles of this size tend to be occluded in aggregates. As a result, aggregates have larger particle sizes and faster settling velocities.

The implementation of SOC characteristics in the model is based on a SOC fractionation study that was carried out with similar soils (Luvisols) from the Belgian loess belt (Doetterl et al., 2012a). In the study of Doetterl et al. (2012a), soil samples were taken at 11 locations along a topographic gradient, from non-eroded to eroding and depositional sites. The results showed that 85% ($\pm 10\%$) of the total SOC was associated with the mineral fraction (clay and silt size), while the remaining 15% ($\pm 3\%$) was POM. To our knowledge, no detailed information is available on the allocation of SOC in particle size fractions from 2 to 63 μm . In terms of simplicity, and given the constraints imposed by the model structure, we considered two types of SOC for both primary particles and aggregated soil: (i) mineral-bound SOC, which represents 90% of the total and is associated with the finest sediment class ($< 2 \mu\text{m}$) and (ii) a POM fraction, which represents 10% of total SOC and is considered a separate class in the model, with a particle size of 250 μm and a density of 1000 kg m^{-3} . Hence, SOC is represented in different particle classes but the model does not account for geochemical processes.

3.2.4 Model evaluation

We evaluated the performance of the model by comparing the predicted characteristics with those that were continuously observed in the Kinderveld and Ganspoel (Table 3.2) agricultural catchments for two observation periods of 3 years each (6 years total observation; Van Oost et al., 2005a). The two catchments are situated approx. 15 km from our study site and are larger but very similar to our site in terms of soil properties and geomorphology. We were unable to directly apply our model to these two agricultural catchments, as our model has high data requirements, which could not be met due to large uncertainties in input data, or in some cases because the data were simply not available. Rather than providing an evaluation on an event-basis, we evaluated the model performance by looking at the characteristics of sediment and SOC delivery, in response to a

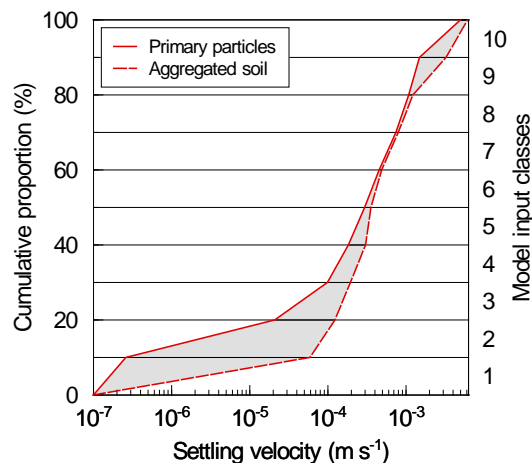


Figure 3.2: Measured cumulative proportion of settling velocity distributions for primary particles and aggregated sediments ($n=81$). The grey area represents the range of possible settling velocities related to different proportions of primary particles or soil aggregates. Right Y-axis shows the settling velocity classes as implemented in the model for primary particles and aggregates (based on particle size distribution measurements conducted by Beuselinck et al., 1999).

range of erosion event-sizes. This provides a first, but stringent, test of model structure and assumptions.

Table 3.2: Area, topographic characteristics, land use and soil of the study area and the two evaluation catchments.

	Study area	Kinderveld	Ganspoel
Area [ha]	3	250	117
Elevation [m]	12	61	39
Mean slope [°]	4.4	3.8	3.4
Arable [%]	100	80.5	76.9
Forest & pasture [%]	0	16.7	9.0
Other [%]	0	2.8	14.1
Clay [%]	14	7-18	
Silt [%]	83	70-80	

3.2.5 Frequency analysis

For an analysis of event-based recurrence intervals, we follow the rainfall event definition given in section 3.2.1 (72 h window). Thereby, some events may contain multiple runoff peaks. The recurrence interval (T) is related to the frequency (P) with which soil erosion (SL) exceeds the value X :

$$T = \frac{1}{P(SL \geq X)}. \quad (3.8)$$

The recurrence interval is expressed in years when T is multiplied by the number of modelled years.

To calculate the frequency of exceedance, monthly soil erosion values were ranked in increasing order, and a rank m is given to each modelled soil erosion event. The exceedance probability for event m is given by:

$$P(SL \geq X)_m = \frac{m}{n+1}, \quad (3.9)$$

where n is the total number of events during the period.

3.3 Results and Discussion

3.3.1 Rainfall/runoff

Application of the rainfall/runoff model over a period of 100 years resulted in 792 individual rainfall/runoff events. The temporal variability of rainfall events is relatively low, as more than 70% of total rainfall is associated with events with a recurrence interval of

less than 1 year. Extreme rainfall events do occur, but their relative contribution to total rainfall is limited (i.e. events with a recurrence interval ≥ 2 years contribute less than 18% of total rainfall). The model simulates that, integrated over the period of simulation, about 10% of the total rainfall does result in surface runoff. This is consistent with field observations in the study area, where an average of 8% was reported by Steegen et al. (2000, 2001). In contrast, the simulated temporal variability in runoff is high, and events with a larger recurrence interval, i.e. ≥ 2 years, make up more than 36% of total runoff. The variability in runoff is higher than that of rainfall because it is controlled by multiple factors, including rainfall amount and intensity, vegetation characteristics, soil surface conditions and the presence and/or absence of a rill/ephemeral gully network at the beginning of an event.

3.3.2 Interrill and rill/ephemeral gully erosion

In the study area, erosion can be found in the mid-slopes, whereas a depositional area is located in the valley bottom (Fig. 3.3). Interrill erosion, modelled here as a function of slope and rainfall intensity, accounts for 14% of total sediment mobilization over a 100-year period. Rainfall intensity is the main factor controlling interrill erosion and explains about 70% ($p < 0.001$) of its variability. In contrast, incised (i.e. rill/ephemeral gully) erosion was modelled as a function of slope and discharge and is therefore mainly controlled by surface runoff ($R^2 = 88\%$; $p < 0.001$). The simulated relative contribution of interrill erosion depends on the suspended sediment concentration (SSC) and the sediment delivery ratio (SDR), which is the fraction of eroded soil that is transported to the catchment outlet. For events with low values for SSC and SDR, the contribution of interrill erosion can account for up to 100% of total sediment mobilization, but this contribution declines rapidly with increasing SSC and SDR (Fig. 3.4). This reflects the role of event size, whereby only larger events produce significant amounts of concentrated erosion once the hydraulic threshold for rill initiation is exceeded. This large contribution of rill

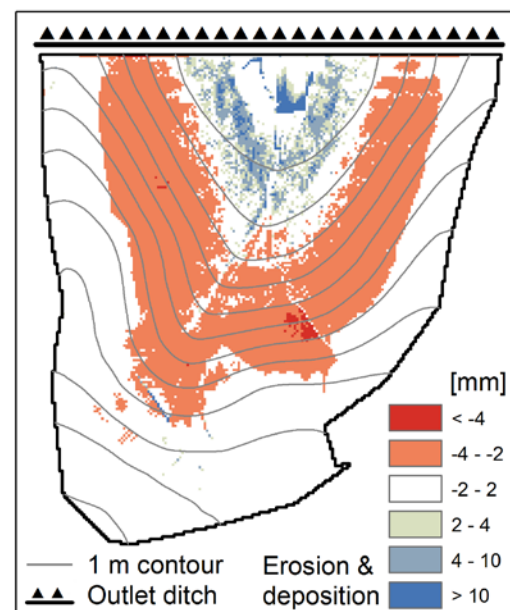


Figure 3.3: Spatial patterns of total soil erosion and deposition after hundred years of simulation. Negative values indicate erosion and positive values deposition.

erosion for sediment delivery was also observed by Wang et al. (2010) in the Kinderveld and Ganspoel catchment. In a modelling study, Wilken et al. (2017b) tested the effect of different rill initiation characteristics on SOC delivery in a catchment of similar loess-derived soils. The results showed that rill erosion widely controls sediment and SOC delivery in catchments with high connectivity.

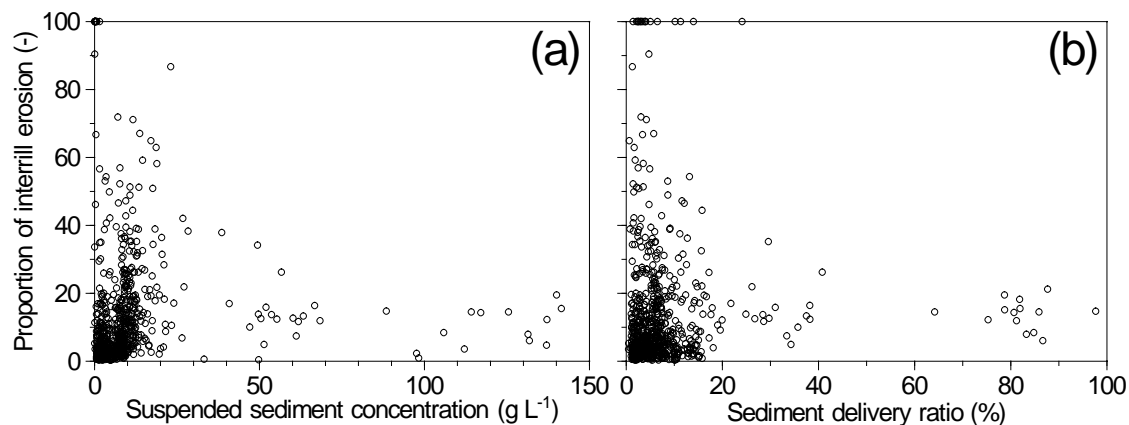


Figure 3.4: Event proportion of interrill erosion contributing to suspended sediment concentration (a) and the sediment delivery ratio (b).

3.3.3 Sediment and carbon mobilization and export under different scenarios

We evaluated two erosion scenarios where different assumptions about particle size distribution are made: erosion scenario 1, where soil is transported and deposited as primary particles and POM is an individual class, and erosion scenario 2 where rill erosion detaches, transports, and deposits aggregated soil and POM is encapsulated in soil aggregates (see section 3.2.3). The simulated long-term enrichment ratio of the deposits for the fine fraction ($< 2 \mu\text{m}$), which results from selective transport and deposition processes, was found to be 0.02 and 0.6 for erosion scenario 1 and 2, respectively. For erosion scenario 1, this implies that the deposition of clay particles and POM is virtually non-existent and also suggests a very efficient export of clay minerals and POM from first-order catchments. However, these results are not consistent with field observations. Data derived from the Belgian Soil Map (Baeyens, 1959) show only small differences between the primary particle size distributions of colluvial and non-eroded agricultural soils in the study area. The reported enrichment ratio for the clay fraction of colluvial soils is 0.8 (Baeyens, 1959). The colluvial sediment is thus only slightly depleted in clay when compared to the source material. Based on this analysis, we consider the results of the simulations for erosion scenario 1 to not be physically valid. In contrast, the results of erosion scenario 2 are qualitatively similar to the observations (Baeyens, 1959), which suggests

that erosion scenario 2 more accurately depicts erosion processes in our study area. This implies that the assumptions made for erosion scenario 2 are appropriate, i.e. interrill erosion detaches and transports primary particles, whereas rill erosion is unselective and detaches and transports soil aggregates. The concept of particle size-selective interrill and non-selective rill erosion which detaches and entrains the entire soil matrix has been documented in numerous studies (Kuhn et al., 2010; Polyakov and Lal, 2004b; Quinton et al., 2001; Schiettecatte et al., 2008b). Following non-selective splash erosion (Parsons et al., 1990; Poesen, 1985; Poesen and Savat, 1980), selectivity is caused by particle size specific deposition differences, where coarser and heavier particles settle out earlier than finer and lighter particles (Schiettecatte et al., 2008a). The model tends to slightly underestimate the deposition of the finest fractions (enrichment of colluvial sediments: 0.6 model versus 0.8 field observations).

The clay enrichment ratios at the outlet of the catchment (i.e. clay exported sediment / clay source material) for the simulated events range between 1 and 4.8 (Fig. 3.5). These ratios are strongly related to the SSC: high enrichment ratios occur when SSC is low, i.e. during small events with a low recurrence interval. In contrast, low enrichment ratios (i.e. close to 1) are associated with events characterized by a high SSC. These findings are in line with other studies (Schiettecatte et al., 2008a, b; Wang et al., 2010) and emphasize the importance of event size. The contribution of interrill erosion is higher for small events and, since interrill erosion is modelled as the detachment and export of individual sediment particles, this results in a higher clay enrichment ratio. Vice versa, the contribution of interrill erosion is small for large events, resulting in enrichment ratios close to 1, since concentrated erosion is assumed to be unselective. The simulated range of enrichment ratios and the relationship between those ratios and SSC are both very similar to that which was observed at the Kinderveld and Ganspoel catchment (Fig. 3.5; Wang et al., 2010).

However, over a simulation period of 100 years, the flux-weighted predicted clay enrichment ratio in exported sediments was found to be 1.4, which is lower than the field-observed ratio of 1.5 - 2.6 for a 6-year period for the Ganspoel and Kinderveld catchments (Wang et al., 2010). We assume that this discrepancy results from difference in sedimentological connectivity, whereas a cascade of selective erosion and deposition processes in the larger catchments lead to stronger enrichment in the delivered fines. In contrast, an earlier study applying MCST in catchments of similar scale (0.7 and 3.7 ha; Fiener et al., 2008) showed a good representation ($R^2 = 0.93$) of the modelled transport of fines compared to 8 years of observations

The simulated enrichment of SOC is directly related to the preferential export of the clay fraction through by interrill erosion. The simulated SOC enrichment ratios are higher than the clay enrichment ratios previously discussed and range between 1 and 9 (Fig. 3.5b). Exported sediment is more enriched in SOC than it is in clay due to the fact that the clay fraction is itself enriched in SOC relative to the bulk soil. The simulated relationship between SSC and SOC enrichment is similar to what was found for clay enrichment, i.e. enrichment is higher when SSC is low. This is again consistent with the Kinderveld and Ganspoel field observations (Wang et al., 2010).

It should be noted that the enrichment of exported clay and SOC was simulated assuming that interrill erosion resulted in the detachment of primary particles while concentrated erosion resulted in the detachment of aggregates. Alternatively, clay and POM fractions could be considered as individual classes in the model. However, due to very low settling velocities, nearly the entire mobilized clay and POM fractions are exported from the

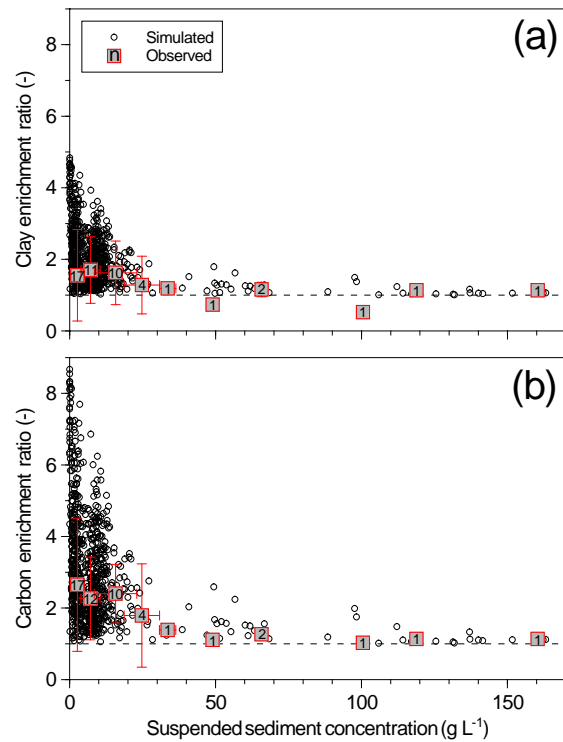


Figure 3.5: Clay (a) and carbon (b) enrichment ratios with respect to simulated and observed (Wang et al., 2010) suspended sediment concentrations (observed n =clay 50/carbon 49). Error bars of measurements represent the 95% confidence interval.

catchment when this is simulated. This is not in line with field observations or with experiments that show that the transport of fine-textured sediments mainly occurs in the form of aggregates (Beuselinck et al., 2000; Wang et al., 2013b).

3.3.4 Frequency and magnitude of erosion and delivery of soil constituents

Based on the 100-year modelling period, we analysed the effect of event-based frequency and magnitude of erosion on mobilisation and delivery of bulk sediment, clay and SOC (Fig. 3.6). We found that for within catchment erosion, a large number of relatively small events (recurrence interval < 1.5 yrs.) account for about half of the cumulative erosion, while larger events (> 10 yrs. recurrence) account for only about 15%.

The SDR was 0.18 over the 100-year simulation period, while the mean erosion rate was $12.5 \text{ Mg ha}^{-1} \text{ yr}^{-1}$. Figure 3.6 clearly shows that larger events play a more important role in determining SDR than they do in determining soil erosion. Approximately 57% of the total sediment delivery comes from events with a recurrence interval less than or equal to 10 years (Fig. 3.6). This is explained by the fact that sediment delivery is not linearly related to runoff amount: once the hydraulic threshold is exceeded

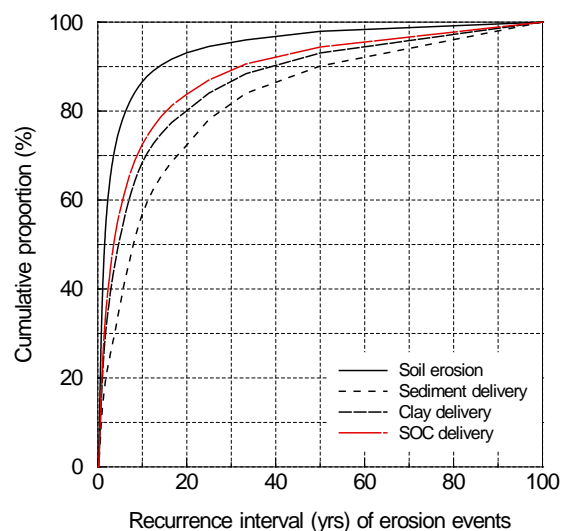


Figure 3.6: Cumulative erosion as well as sediment, clay, and SOC delivery related to event-based recurrence intervals.

(i.e. an extensive network for concentrated flow is established) the sedimentological connectivity is highly enhanced and SDRs can be very large. The simulation of hydrological and sedimentological connectivity requires the introduction of (i) differentiated hydrological behaviours for sheet and concentrated flow, (ii) rill/ephemeral gully network development tracking and (iii) the rill/ephemeral gully network connectivity to the outlet of the catchment. Our simulations show that the highest export rates occurred when the rill/ephemeral gully network was already well established at the beginning of an event. The important role of a rill/ephemeral gully network for the catchment connectivity was also pointed out in other studies (Lopez-Vicente et al., 2013; 2015). However, structures which interrupt the rill/ephemeral gully network potentially reduce the sedimentological connectivity to the outlet and reduce the SDR substantially (Wilken et al., 2017b).

The importance of event size for simulating clay and SOC delivery is also shown in Figure 3.5. Compared to bulk sediment, the delivery of clay and SOC is less driven by rare, large events, since small events with more interrill erosion already deliver relatively large amounts of clay and SOC. In general, the model results underline the importance of a more process-oriented analysis of SOC redistribution, as the effects of small erosion events, e.g. upon aquatic ecosystems, are underestimated when modelling only mean bulk erosion rates.

In order to qualitatively evaluate our predicted temporal patterns for sediment delivery, we compared our results to studies that continuously measured export from small catchments. In one such study, which was carried out in small agricultural catchments in the Belgian loess belt, Steegen et al. (2000) measured sediment delivery over a 3-year period in two first-order streams. The authors found that a single event contributed to more than 40% of the total sediment delivery during the observation period and that the sum of rare and extreme events accounts for 46%. Even more extreme results were reported from a small loess catchment (3.7 ha) in Southern Germany, where a short-term series of single runoff events accounted for up to 67% of total sediment export (> 0.5 mm runoff) over an 8-year period (Fiener et al., 2008). Although a quantitative comparison of the model results with these empirical observations is not possible, as empirical observations in central Europe typically cover far fewer than 100 years, this analysis strongly indicates that the mechanisms incorporated into the MCST model (i) allow for a quantitative representation of the relative importance of both small and large events and (ii) account for event size related sediment and SOC delivery.

3.4 Conclusions

In this study, we incorporated preferential erosion and transport of sediment and soil organic carbon (SOC) fractions into a numerical model of surface runoff and sediment transport. In doing so, we were able to predict the export of these different classes of sediment and SOC from small hilly watersheds, located in a temperate region with fine-textured soils. The model predictions were only consistent with field observations when (i) interrill erosion was simulated as a process that entrains primary particles, (ii) rill erosion is unselective and (iii) low-density POM is encapsulated within soil aggregates and cannot be entrained by interrill erosion. These results suggest that carbon enrichment at the outlet of small watersheds occurs as a result of the selective interrill transport of clay and fine-silt associated carbon. Based on the application of the model over a period of 100 years, we conclude that sediment delivery is a highly episodic process. Our results

show that 63% of the total sediment delivery was caused by 20 single events with a rainfall recurrence > 5 years. This highlights the need to consider sufficiently long timescales when addressing the impact of lateral fluxes of sediment and nutrients on soil processes. However, the dominance of large events is less pronounced in the case of SOC delivery, where only 44% of total delivery is caused by extreme events. This reduced importance is associated with the selective process of interrill erosion and transport. This study highlights the need for an event-based analysis of carbon erosion and delivery in order to assess the overall effect of SOC redistribution on the terrestrial carbon balance.

Article III

Process-oriented modelling to identify main drivers of erosion-induced carbon fluxes

Florian Wilken^{1,2,3}, Michael Sommer^{3,4}, Kristof Van Oost⁵, Oliver Bens⁶, and Peter Fiener¹: Process-oriented modelling to identify main drivers of erosion-induced carbon fluxes, *SOIL*, 3, 83-94, <https://doi.org/10.5194/soil-3-83-2017>, 2017.

¹Institute for Geography, Universität Augsburg, Germany

²Chair of Soil Protection and Recultivation, Brandenburg University of Technology Cottbus-Senftenberg, Germany

³Institute of Soil Landscape Research, Leibniz-Centre for Agricultural Landscape Research ZALF e.V., Germany

⁴Institute of Earth and Environmental Sciences, University of Potsdam, Germany

⁵Earth & Life Institute, TECLIM, Université catholique de Louvain, Belgium

⁶Helmholtz Centre Potsdam GFZ German Research Centre for Geosciences, Germany

Published in the journal SOIL.

Article abstract

Coupled modelling of soil erosion, carbon redistribution, and turnover has received great attention over the last decades due to large uncertainties regarding erosion-induced carbon fluxes. For a process-oriented representation of event dynamics, coupled soil-carbon erosion models have been developed. However, there are currently few models that represent tillage erosion, preferential water erosion and transport of different carbon fractions (e.g. mineral bound carbon, carbon encapsulated by soil aggregates). We couple a process-oriented multi-class sediment transport model with a carbon turnover model (MCST-C) to identify relevant redistribution processes for carbon dynamics. The model is applied for two arable catchments (3.7 and 7.8 ha) located in the Tertiary Hills about 40 km north of Munich, Germany. Our findings indicate the following: (i) redistribution by tillage has a large effect on erosion-induced vertical carbon fluxes and has a large carbon sequestration potential; (ii) water erosion has a minor effect on vertical fluxes, but episodic soil organic carbon (SOC) delivery controls the long-term erosion-induced carbon balance; (iii) delivered sediments are highly enriched in SOC compared to the parent soil, and sediment delivery is driven by event size and catchment connectivity; and (iv) soil aggregation enhances SOC deposition due to the transformation of highly mobile carbon-rich fine primary particles into rather immobile soil aggregates.

4.1 Introduction

Soil organic carbon (SOC) is the largest terrestrial carbon (C) pool and has been identified as a cornerstone for the global C cycle. Globally, approx. 1400 Pg C is stored in the upper meter of soil, with approx. 700 Pg C in the upper 0.3 m (Hiederer and Köchy, 2011). As a result, exchange rates between soil and the atmosphere are a major concern with regards to climate change (Polyakov and Lal, 2004a). Earth system model-based estimates for terrestrial C storage in the year 2100 vary widely, ranging from a sink of approx. 8 Pg C yr⁻¹ to a source of approx. 6 Pg C yr⁻¹ (Friedlingstein et al., 2014). This large uncertainty might even increase if process levels that are at this point not yet implemented in current models are taken into account (Doetterl et al., 2016). One such process is the lateral redistribution of SOC via erosion processes and the effect this has on vertical C fluxes. Global estimates of erosion-induced C fluxes show conflicting results, ranging from a source of 1 Pg C yr⁻¹ to a sink of the same magnitude (for recent reviews see Doetterl et al., 2016; Kirkels et al., 2014). The main reasons for these large differences are a lack of appropriate data (Prechtel et al., 2009), oversimplified modelling approaches that ignore important processes, and differences in measuring approaches, e.g. extrapolating from arable plots (Hooke, 2000; Myers, 1993; Pimentel et al., 1995) vs. measuring continental delivery in river systems (Berhe et al., 2007; Wilkinson and McElroy, 2007). Most challenging in developing and especially testing models that couple process-oriented SOC redistribution with SOC dynamics are the different spatial and temporal scales of the processes at play (Doetterl et al., 2016). Process-oriented erosion models need event-based data to be validated, while SOC dynamics can hardly be observed on time-scales smaller than several decades. Consequently, most existing models that couple soil erosion and SOC turnover processes are based on long-term, USLE-type erosion models that ignore event dynamics. The most widespread of these is SPEROS-C, which was applied on scales ranging from micro- to mesoscale catchments (Fiener et al., 2015; Nadeu et al., 2015; Van Oost et al., 2005c).

The conventional approach to modelling coupled soil erosion and SOC turnover is to treat SOC as a stable part of the bulk parent soil and statistically model (long-term) erosion. However, this approach is likely to lead to biased estimates of both water-erosion-induced SOC redistribution and its effect on vertical C fluxes. Numerous studies have shown that the transport of SOC is selective (Schiettecatte et al., 2008b), controlled by event characteristics (Sharpley, 1985; Van Hemelryck et al., 2010) and soil aggregation (Hu and Kuhn, 2014; 2016). The enrichment of SOC during transport has been explicitly addressed by a

few modelling studies, using different approaches (Fiener et al., 2015; Lacoste et al., 2015). The effects of tillage erosion on vertical C fluxes have not yet been evaluated in detail, although a representation has been accounted for in some modelling studies (Lacoste et al., 2015; Van Oost et al., 2005b).

The aim of this study is to couple a spatially distributed, process-oriented and event-based water erosion model with a tillage erosion model and a SOC turnover model in order to analyse the importance of individual erosion processes in the erosion-induced C balance of agricultural catchments. The study intends to identify relevant processes that should be implemented in less data-demanding, more parsimonious models.

4.2 Materials and Methods

4.2.1 Test site

The test site is located about 40 km north of Munich in the Tertiary Hills, an intensively used agricultural area in southern Germany. The site consists of two small arable catchments ($48^{\circ}29' \text{ N}$, $11^{\circ}26' \text{ E}$; Fig. 4.1), catchments C1 and C2, covering an area of 3.7 and 7.8 ha, respectively. The rolling topography ranges from 454 to 496 m above sea level with a mean slope of 4.2° ($\pm 0.6^{\circ}$) for catchment C1 and 5.3° ($\pm 1.7^{\circ}$) for catchment C2. The soil landscape is characterized by Cambisols and Luvisols (partly redoximorphic), both developed from loess. Furthermore, Colluvic Regosols have developed in depressional areas due to long-term soil translocation processes. In both catchments, the dominant topsoil textures are loam and silty loam with a median grain size diameter between 12.5 and 16.0 μm (Sinowski and Auerswald, 1999). The average SOC content of the Ap horizons is

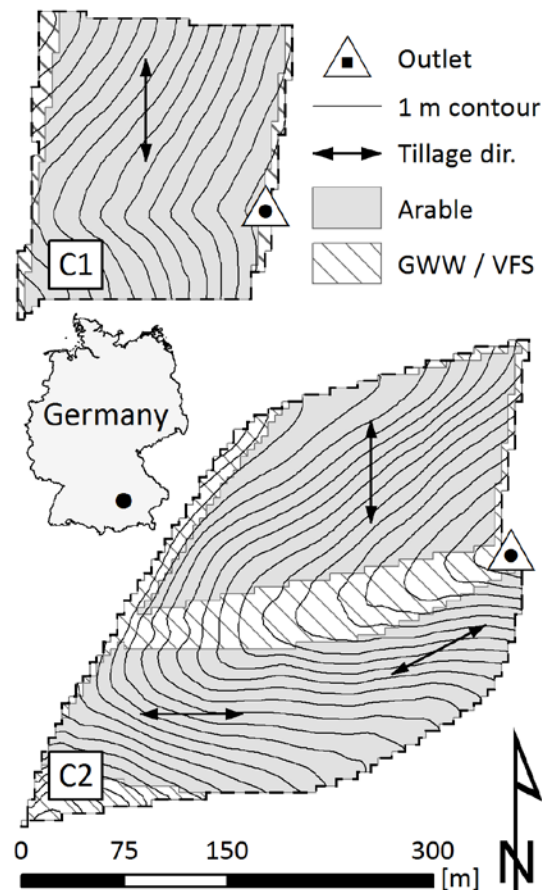


Figure 4.1: Land use, topography and tillage direction for modelled catchments C1 and C2. In catchment C2, a grassed waterway (GWW) is located along the thalweg, while vegetated filter strips (VFS) are located along the upslope and downslope field borders.

3.7 kg m⁻². The mean annual temperature and precipitation is 8.4°C and 834 mm, respectively (measured 1994 to 2001). Agricultural management at the research farm is dedicated to soil conservation: the main cropping principle is to keep soil covered by vegetation or residues as long as possible (Auerswald et al., 2000). The crop rotation during the project was winter wheat (*Triticum aestivum* L.) – maize (*Zea mays* L.) – winter wheat – potato (*Solanum tuberosum* L.). This crop rotation allowed for the cultivation of mustard (*Sinapis alba* L.) cover crops before each row crop (i.e. potato and maize). For implementation, potato ridges were formed before mustard sowing and, later, potato was directly sown into the ridges covered by winterkilled mustard. Maize, on the other hand, was directly sown into the winterkilled mulched mustard (Auerswald et al., 2000). For the established mulch tillage system, the main soil tillage operation was performed with a chisel cultivator (tillage depths approx. 0.2 m). To avoid soil compaction and depressions, which could potentially induce concentrated runoff, wide and low-pressure tires were used on all farming machines (e.g. Fiener and Auerswald, 2007b). Catchment C1 drains one large field with an approx. 2-3 m wide grass filter strip along its downslope border, whereas catchment C2 consists of two fields draining into an approx. 300 m long and 30-40 m wide grassed waterway (Fig. 4.1).

4.2.2 Model description

For our study, we coupled three different models: (i) the process-oriented Multi-Class Sediment Transport Model (Fiener et al., 2008; Van Oost et al., 2004; Wilken et al., 2017a), a spatially distributed and event-based water erosion model with a specific emphasis on grain size selectivity using the Hairsine and Rose equations (Hairsine et al., 1992; Hairsine and Rose, 1991), (ii) a tillage erosion model following a diffusion-type equation adopted from Govers et al. (1994), which derives tillage erosion from topography and tool-specific tillage erosion coefficients, and (iii) the Introductory Carbon Balance Model (ICBM; Andr en and K atterer, 1997; K atterer and Andr en, 2001), which models SOC turnover. The ICBM calculates yearly SOC dynamics using two SOC pools (“young” and “old”) and four C fluxes (C input from plants, mineralisation from the young and the old pool, and humification). Both the tillage erosion and ICBM model were adapted from SPEROS-C, which couples annual water erosion (based on the RUSLE; Renard et al., 1996), tillage erosion and SOC turnover (Fiener et al., 2015; Nadeu et al., 2015; Van Oost et al., 2005c). In the following, we describe only those features of the coupled MCST-C model (Multi-Class Sediment Transport and Carbon dynamics model)

that had to be adapted in order to couple the models or for the introduction of SOC-specific transport mechanisms. An overview of the main model concepts of MCST-C is given in Fig. 4.2. For more details regarding the three coupled models and processes modelled therein, we refer the reader to the original publications (see above).

4.2.3 Representation of grain-size-specific soil and associated SOC

The representation of soil texture and SOC in the model is three-dimensional. The horizontal distribution of grain-size-specific soil and SOC is grid-based, while the vertical distribution is represented by ten 10 cm layers. The two uppermost layers are assumed to be homogeneously mixed due to tillage. The grain size distribution is represented in 14 primary particle classes, described by class median particle diameter, particle density and the class proportion relative to the bulk soil (kg kg^{-1}). The median class diameter is calculated by a logarithmic function that takes grain diameter class boundaries into account (Scheinost et al., 1997). The standard procedure (e.g. sieve-pipette method; Casagrande, 1934; DIN, 2002) to determine grain size distributions destroys soil aggregates in a pre-processing step and therefore only represents the primary particle distribution. However, soil aggregation has a large effect on the fall velocity distribution of soils and reduces the transport distance of SOC-rich material (Hu and Kuhn, 2014; 2016). Therefore, to account for soil aggregation, two water-stable aggregate classes have been introduced following the hierarchy model of Oades (1984), which describes microaggregate formation inside macroaggregates: silt-sized small microaggregates (6.3 – 53 μm , median diameter (D50): 18 μm ; Tisdall and Oades, 1982) and microaggregates (53 – 250 μm , D50: 115 μm ; Six et al., 2002). In model parametrization, the small microaggregates are exclusively formed out of primary particles with diameters less than 6.3 μm , whereas microaggregates are formed from those with diameters less than 53 μm (i.e. the lower diameter boundary of the aggregate class). As a result, aggregation causes a certain number of primary particles to be moved into the aggregate classes. Hence, the absolute amount of soil aggregation is controlled by the availability of fine primary particles, i.e. sandy soils are less aggregated compared to clayey soils. Macroaggregates (250–2000 μm) are neglected since they are rather immobile during selective interrill erosion and are assumed to break into smaller aggregates during extreme events with high-precipitation kinetic energies (Legout et al., 2005; Oades and Waters, 1991; Tisdall and Oades, 1982). Furthermore, particulate organic matter (POM) is not treated as an individual class, as POM is assumed to be predominantly encapsulated within soil aggregates (Beuselinck et al., 2000; Wang et al., 2013a; Wilken et al., 2017a).

SOC transport is associated with various primary particle and aggregate classes. Based on the literature (Doetterl et al., 2012a; Von Lützow et al., 2007), it is assumed that mineral bound SOC is primarily attached to fine particles ($< 6.3 \mu\text{m}$) or included in soil aggregates. To keep the mass balance, SOC in water-stable aggregates is allocated based on the SOC content of the primary particles that form these aggregates. This leads to a conservative estimate of SOC in aggregates, as measurements show that aggregates tend to encapsulate more C than found attached to mineral primary particles (Doetterl et al., 2012a). As small microaggregates in the model consist solely of primary particles with diameters less than $6.3 \mu\text{m}$, their C content equals that of the fine primary particles. Microaggregates show a somewhat smaller C content, since the larger primary particles from which they are also made tend to have less associated SOC.

4.2.4 Continuous tracking of catchment dynamics

In its original version, the MCST model treats events individually without considering changes caused by previous events. For a continuous application, the water erosion module of MCST-C simulates single events and keeps track of the following redistribution related changes in the catchment: spatial and vertical changes in (i) the grain size distribution and (ii) SOC content and (iii) the development of a rill network, which remains until the next tillage operation. A layer-specific mixture module continuously updates for spatial changes in the vertical grain size distribution and its associated SOC content, changes which are caused by selective redistribution of water and non-selective tillage erosion. In the case of net deposition, new material with a different grain size distribution is added to the top of the plow horizon (layer 1 and 2). Subsequently, the grain size distribution of the plow layer is mixed and assumed to be homogeneous. Furthermore, deposition leads to an upward movement of the layer borders such that soil material from the plow layer becomes incorporated into the subsoil layers. Any C content moving below 1 m depth is summarized and assumed to be stable in time. In contrast, erosion lifts new material from the subsoil horizons upwards. Assuming that the deepest horizon represents the original loess, the properties of uplifted subsoil remain constant, delivering infinite material of the same grain size distribution and C content.

4.2.5 Model validation

For a truly rigorous validation of MCST-C, there are numerous long-term data requirements: event-based data for surface runoff, sediment delivery and SOC delivery, long-term data regarding changes in spatially distributed SOC stocks, spatially distributed C

loss and gain due to crop harvesting, and C input via plants and manure application. In addition to these validation data requirements, model input data would also be required over decades for a long-term validation. The research project (Auerswald et al., 2000), which is the basis of this study provided a very comprehensive database. However, continuous monitoring was ‘only’ carried out for 8 years (1994 to 2001), and SOC inventories span roughly a decade (first inventory in 1990/91, second in 2001). Therefore, measured changes in SOC stocks are too small to be used for a long-term model validation (requires approx. 50 years; see implementation).

In consequence, we only use the measured continuous event-based surface runoff and sediment delivery from catchment C1 to validate the modelled erosion. The runoff was collected at the lowest point of the catchment (Fig. 4.1), which was bordered by a small earthen dam. From the dam, the runoff was transmitted via an underground tile outlet (diameter 0.29 m) to a measuring system consisting of a Coshocton-type wheel runoff sampler (for details regarding the procedure and the precision of the measurements see Fiener and Auerswald, 2003). Corresponding precipitation was measured using a tipping bucket rain gauge of 0.2 mm volume resolution. To determine single erosion events, the precipitation data are filtered in two steps: first, all events with cumulative precipitation > 5 mm and without a 6 h gap in recorded precipitation are considered single erosion events. Second, we included all the largest events accounting for 90% of total observed runoff. The model is not able to predict erosion under soil frost; hence, winter events, indicated by air temperatures below zero, are removed.

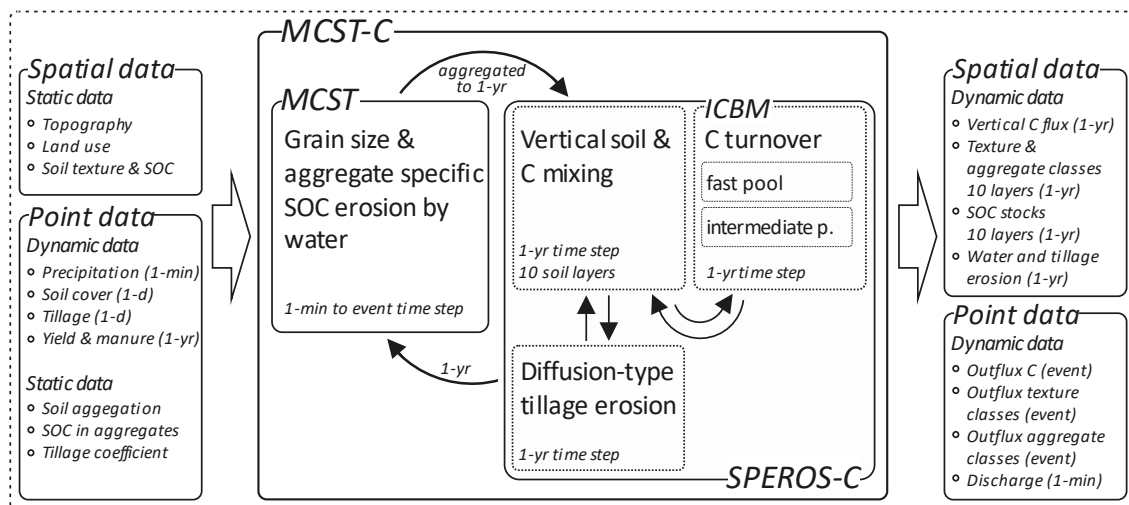
As the original MCST model was previously tested in catchment C1 (Fiener et al., 2008), we did not explicitly calibrate the surface runoff and erosion model. Instead, observed runoff and sediment delivery data was used to test whether our changes to the model still result in a reasonable model performance.

4.2.6 Model implementation

To run and test MCST-C, a variety of measured input data and parameters are required. This input data are partly calculated from measured data at the research farm and partly taken from literature (Table 4.1; Fig. 4.2).

Table 4.1: Main input data and parameters used in the Multi-Class Sediment Transport and Carbon dynamics model (MCST-C).

Description	Unit	Temporal resolution	Range / value
Digital elevation model	m	static	(5 x 5 m) 454 - 496
Land use	-	daily	-
Soil cover	%	biweekly	0 - 100
Curve number per crop to be modified by cover and soil crusting	-	daily	38 - 88
Tillage roughness and direction	m	vegetation period	0 - 0.25
Hydraulic roughness arable land	s m ^{-1/3}	biweekly	0.016 - 0.101
Hydraulic roughness grass strip	s m ^{-1/3}	static	0.20
Yield	kg m ⁻²	at harvest	0.6 - 4.3
Manure	kg C m ⁻²	at fertilisation	0 - 0.13
Tillage operation	-	daily	-
Soil bulk density	kg m ⁻³	static	1350
Initial texture	µm	static	0.04 - 2000
Primary particle density	kg m ⁻³	static	2650
Small microaggregate density	kg m ⁻³	static	1300
Microaggregate density	kg m ⁻³	static	1300
Small microaggregate median diameter	µm	static	18
Microaggregate median diameter	µm	static	115

**Figure 4.2: Modelling scheme of the Multi-Class Sediment Transport and Carbon dynamics model (MCST-C)**

To model surface runoff and erosion, the most important input data requirements are (i) precipitation, measured at two meteorological stations about 100 to 300 m from the catchments using 0.2 mm tipping buckets, (ii) a lidar 5 m x 5 m digital elevation model, (iii) soil data taken from a 50 m x 50 m raster sampled during the soil survey in 1990/91 (Sinowski et al., 1997), and (iv) soil cover data, measured biweekly during the vegetation period, monthly in autumn and spring, and before and after each soil management operation (1993-1997). A tillage transport coefficient (k_{til}) of 169 kg m⁻¹ yr⁻¹ was utilized for

contour tillage by a chisel, following Van Muysen et al. (2000). For SOC redistribution and modelling of vertical C fluxes, the most important model inputs were yields and manure application, a topsoil SOC map (12.5 m x 12.5 m; Sinowski et al., 1997) and assumptions regarding the allocation of C to different texture classes and in different aggregates. As texture and aggregate C allocation was not measured, we took measured data from Doetterl et al. (2012a) and scaled these measurements according to the available bulk SOC (see Section 4.2.3: Representation of grain-size-specific soil and SOC). The parameters for the C turnover model are taken from Dlugoß et al. (2012), who worked under similar environmental conditions with loess-derived soils in a small catchment in western Germany. The C turnover decline with depth was determined by an inverse modelling approach and found a mean turnover rate of 0.268 year⁻¹ for the young pool and 0.002 year⁻¹ for the old pool over the 1 m soil profile. Further details regarding the monitoring data are given in Fiener and Auerswald (2003, 2007b) and Fiener et al. (2008).

As indicated above, it is difficult, if not impossible, to identify erosion-induced changes in SOC and vertical C fluxes if measurements or modelling efforts do not cover decadal time spans. Therefore, a 50-year synthetic input data set and parameter set was created for MCST-C in order to analyse C dynamics. This data set is based on the 8 years of measured data used to validate the erosion component of the model. First, a time series of precipitation was established by randomly choosing the data of one of the eight measured years (see Section 4.2.5: Model validation) and applying it for the first 42 years of the time series. This was followed by the original 8 measured years to reach the total of 50 years. Next, this precipitation time series was combined with synthetic land use and soil management data representing two full crop rotations (1994 to 2001), which were repeatedly used for all 50 years. This combination leads to a wide variety of precipitation events (time step 1 min) occurring for different daily soil covers by vegetation as a major driver of soil erosion. In contrast to the erosion dynamics, C inputs via plants and manure are repeated every 8 years, which ignores any potential change in management and yields within the modelling period. The synthetic input data were applied for both catchments for the purpose of comparability.

4.2.7 Analysis of process-specific, erosion-induced C fluxes

Various model setups were chosen (Table 4.2) to analyse the effects of different erosion processes upon lateral SOC redistribution and the resulting vertical C fluxes. All of these model runs were compared to the 50-year reference run that was validated for the 8-years monitoring phase at the research farm (1994-2001). In general, we tested the effect of a

number of water erosion processes and compared the relevance of water vs. tillage erosion. Firstly, the critical shear stress of rill initiation (τ_{crit}) was varied by $\pm 50\%$ in comparison to its reference run value (0.9 Pa) in order to change the proportion of interrill vs. rill erosion, whereas interrill erosion is a selective SOC transport process and rill erosion is unselective. The reference run value for τ_{crit} was derived from flume experiments in loamy, loess-derived soils (Giménez and Govers, 2002) similar to those found at the test site. Next, the aggregation level was varied in an analogous way to modify the allocation of soil primary particles into the small microaggregate and microaggregate classes (Fig. 4.3). In another model run, grain size selectivity was switched off in order to produce a similar behaviour to more parsimonious models, which only erode bulk soil (Table 4.2).

Table 4.2. Model parameterisation to analyse the effects of different erosion processes upon C fluxes. Model runs are abbreviated as follows: reference run (*Ref*), without tillage erosion (*Til_{off}*), water erosion without grain size selectivity (*GS_{off}*), high threshold for rill initiation (*Ril_{lo}*), low threshold for rill initiation (*Ril_{hi}*), without soil aggregation (*Agg_{off}*), low soil aggregation (*Agg_{lo}*), high soil aggregation (*Agg_{hi}*), without water erosion (*Wa_{off}*), low tillage erosion (*Til_{lo}*), and high tillage erosion (*Til_{hi}*).

Processes	Parameter [unit]	<i>Ref</i>	<i>Til_{off}</i>	<i>GS_{off}</i>	<i>Ril_{lo}</i>	<i>Ril_{hi}</i>	<i>Agg_{off}</i>	<i>Agg_{lo}</i>	<i>Agg_{hi}</i>	<i>Wa_{off}</i>	<i>Til_{lo}</i>	<i>Til_{hi}</i>
Water erosion												
with vs. w/o tillage erosion	[-]	+ [#]	-	+	+	+	+	+	+	+	+	+
with vs. w/o grain size selectivity	[-]	+	+	-	+	+	+	+	+	+	+	+
varying rill/interrill erosion	τ_{crit}^{\dagger} [Pa]	0.9	0.9	0.9	1.35	0.45	0.9	0.9	0.9	0.9	0.9	0.9
varying small micro & microaggregates	[%]	60	60	60	60	60	0	30	90	60	60	60
Tillage erosion												
with vs. w/o water erosion	[-]	+	+	+	+	+	+	+	+	-	+	+
varying tillage intensity	k_{til}^* [kg m ¹ yr ⁻¹]	169	0	169	169	169	169	169	169	169	85	254

[#] + and - indicates if a process is modelled or not; [†] critical shear stress for rill initiation; * tillage erosion coefficient.

To analyse the sensitivity of C fluxes to water and tillage erosion, we first compared model runs with pure water or pure tillage erosion. Secondly, we varied the reference run k_{til} coefficient of 169 kg m⁻¹ yr⁻¹ by $\pm 50\%$. All model runs altered only a single parameter, with all other parameters retaining their reference run values. Parameter variations and the abbreviations for each of the model runs are given in Table 4.2.

4.2.8 Analysis of erosion-induced C fluxes

To compare vertical C fluxes from erosional and depositional sites, the corresponding total and mean C flux was calculated on an annual basis. To isolate the C fluxes that result solely from erosion processes, we first calculate all vertical C fluxes excluding erosion processes and then subtract these from the vertical C fluxes including erosion processes. In the following results section, positive C fluxes indicate an erosion-induced C gain for the catchment (input to the soil), while negative fluxes indicate an erosion-induced loss (from soil to the atmosphere or SOC delivery from the catchment by run-

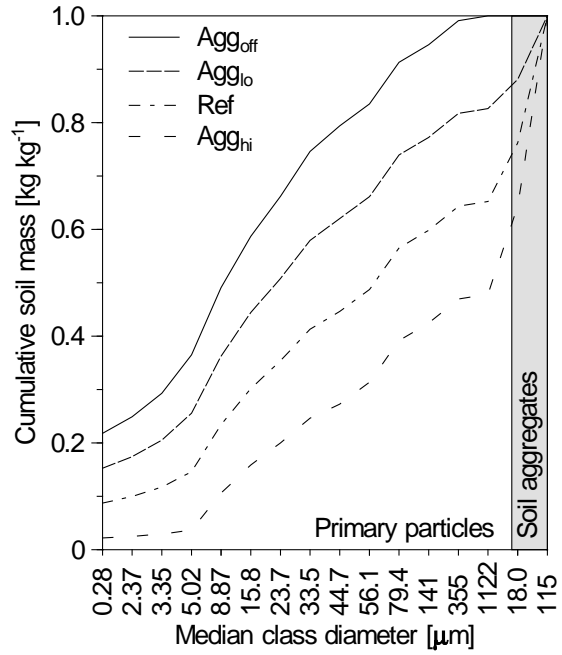


Figure 4.3: Median class diameter distribution (14 primary particle and 2 aggregate classes) in the plow layer assuming different aggregation levels, as described in Table 4.2.

off). Subsequently, erosional and depositional sites were spatially subdivided and an average vertical C flux in kg C m^{-2} was calculated. Finally, the erosion-induced C balance of the catchment was calculated as the sum of the total vertical C flux and laterally delivered SOC.

4.3 Results

4.3.1 Validation

A number of goodness-of-fit parameters (Table 4.3) indicate a sufficient model performance to simulate event runoff and sediment delivery for the 8-year observation period. The Nash-Sutcliffe efficiency and coefficient of determination

Table 4.3: Model performance, as described by the Nash-Sutcliffe efficiency (NSE; Nash and Sutcliffe, 1970), root mean square error (RMSE), coefficient of determination (R^2), and Spearman’s rank correlation coefficient (RHO).

	NSE	RMSE	R^2	RHO
Runoff	0.83	5.6 mm	0.94	0.89
Sediment delivery	0.92	165 kg/ha	0.95	0.71

for runoff (NSE = 0.83; R^2 = 0.94) and sediment delivery (NSE = 0.92; R^2 = 0.95) are particularly satisfactory. However, a root mean square error of 165 kg ha^{-1} for sediment delivery indicates difficulties in predicting some small events.

4.3.2 Long-term erosion-induced C fluxes

The simulated tillage and water erosion shows distinct spatial patterns (Fig. 4.4). The highest rates of tillage erosion are found along the upslope boundaries of the arable field and on hilltops. The main areas for tillage-induced deposition are at the downslope arable field boundaries and in concavities (Fig. 4.4). Due to the well-established soil conservation system, water erosion takes place over a much smaller spatial extent and is limited to the main hydrological flow path, while deposition is dominantly found in the vegetated filter strips and grassed waterway (Fig. 4.4).

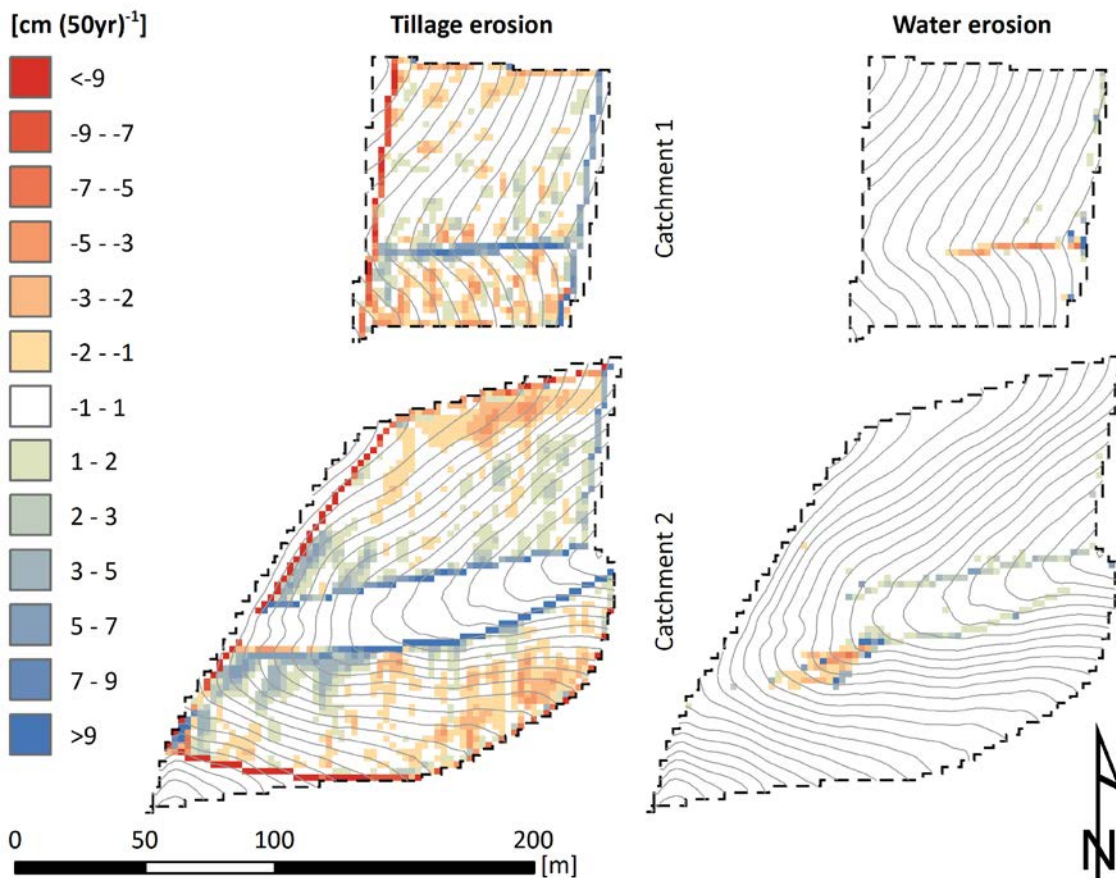


Figure 4.4: Spatial patterns of tillage and water erosion for the 50-year simulation period of the reference run.

The reference run (validated against sediment delivery in catchment C1, 1994-2001) shows positive vertical C fluxes at erosional sites over the 50-year simulation period, with a cumulative flux of $40 \text{ g m}^{-2} (50 \text{ yr})^{-1}$ in C1 and to $59 \text{ g m}^{-2} (50 \text{ yr})^{-1}$ in C2 (Fig. 4.5: Ero1, Ero2). The depositional C fluxes show a cumulative C loss of $-27 \text{ g m}^{-2} (50 \text{ yr})^{-1}$ and $-30 \text{ g m}^{-2} (50 \text{ yr})^{-1}$ for C1 and C2, respectively (Fig. 4.5: Dpo1, Dpo2). Lateral SOC delivery is mainly driven by three heavy erosion events causing 58% and 53% of the total SOC delivery in C1 and C2, respectively. The total SOC delivery in C1 is $-15.6 \text{ g m}^{-2} (50 \text{ yr})^{-1}$ and in C2 is $-6.5 \text{ g m}^{-2} (50 \text{ yr})^{-1}$ (Fig. 4.5: Del1, Del2). In C1, the

source function of lateral SOC delivery exceeds the sink function of vertical SOC sequestration and leads to a net C loss of $-5.7 \text{ g m}^{-2} (50 \text{ yr})^{-1}$ (Fig. 4.5: Bal1, Bal2). In contrast, catchment C2 is a net C sink of $4.6 \text{ g m}^{-2} (50 \text{ yr})^{-1}$.

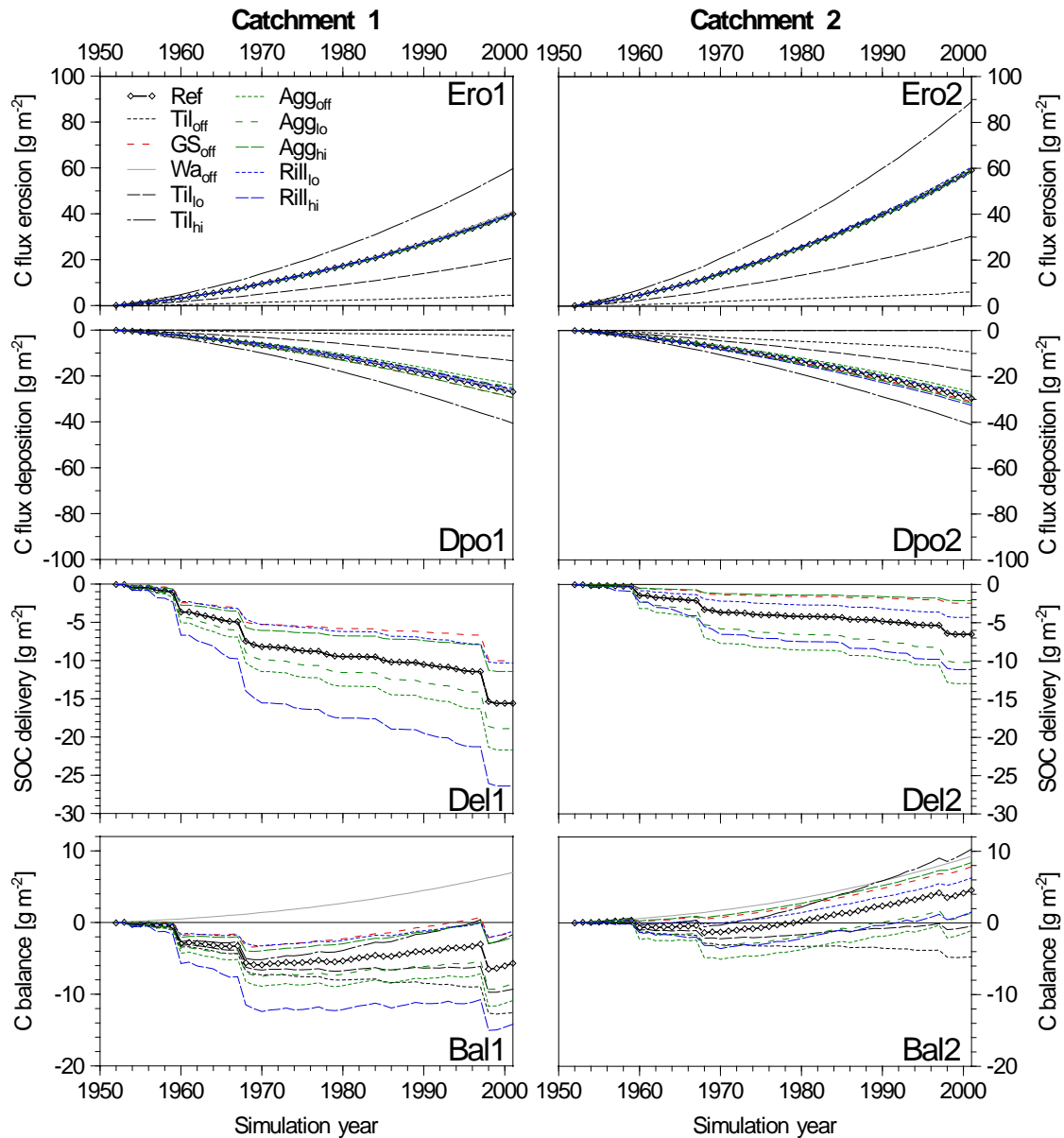


Figure 4.5: Simulated cumulative vertical C fluxes for erosional (Ero1, Ero2) and depositional (Dpo1, Dpo2) sites, lateral C delivery (Del1, Del2) and catchment C balance (Bal1, Bal2) for catchment C1 and C2. For details regarding the model runs and corresponding abbreviations see Table 4.2.

The event-based SOC enrichment in delivered sediments, compared to parent soil, ranges from 1.1 to 2.7 (2.4 mean) for C1 and from 2.5 to 2.7 (2.7 mean) for C2 over the 50-year time span (Fig. 4.6). Subdividing the events into tertiles (33% parts) according to sediment delivery, the mean enrichment in C1 is 2.5 ($n=67$) for the low tertile (i.e. smallest 33% of all event-specific sediment delivery masses), 1.4 ($n=6$) for the middle tertile and 1.2 ($n=2$) for the high tertile (Fig. 4.6). In contrast, more or less no variation in SOC enrichment was modelled for C2 (Fig. 4.6).

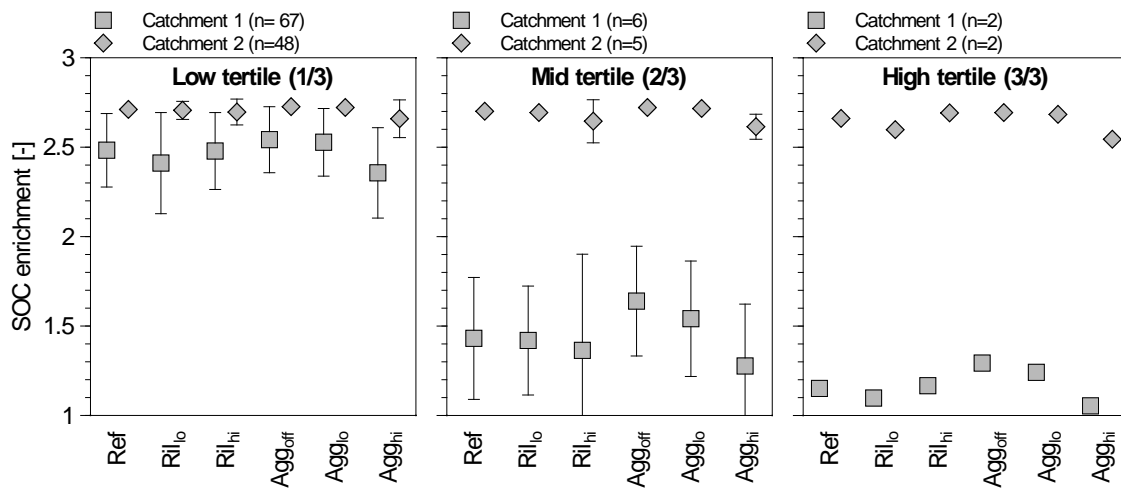


Figure 4.6: Event-size-specific simulated mean SOC enrichment in delivered sediments of catchment C1 and C2. Error bars indicate one standard deviation. Panels A, B, and C represent the smallest, middle, and largest 33.3% of all event-specific sediment delivery masses. For details regarding different model runs and abbreviations see Table 4.2.

4.3.3 Importance of individual erosion processes for long-term erosion-induced C fluxes

Vertical C fluxes show a large response to changes in the k_{til} coefficient but a negligible response to varying levels of water erosion (Fig. 4.5: Ero1, Ero2, Dpo1, Dpo2). Cumulative C flux at erosional and depositional sites is found to be lowest when no tillage (Til_{off}) is simulated and highest for strong tillage (Til_{hi}). When pure tillage erosion is simulated (Wa_{off}) in catchment C1, a C sequestration of $7 \text{ g m}^{-2} (50 \text{ yr})^{-1}$ is simulated (Fig. 4.5: Bal1). The majority of processes in catchment C2 lead to an erosion-induced C gain for the catchment. The highest C sequestration in catchment C2 is found for high tillage erosion (Til_{hi} : $10.3 \text{ g m}^{-2} (50 \text{ yr})^{-1}$). In contrast, catchment C2 acts as a source when there is no tillage (Til_{off} : $-4.8 \text{ g m}^{-2} (50 \text{ yr})^{-1}$), as well as when tillage erosion is low (Til_{lo} : $-0.4 \text{ g m}^{-2} (50 \text{ yr})^{-1}$; Fig. 4.5: Bal2).

Lateral SOC delivery is solely caused by water erosion. The model shows its smallest levels of lateral SOC delivery when grain size selectivity is ignored (GS_{off}), and delivered sediments therefore have the same SOC concentration as the parent soil (C1: $-10 \text{ g m}^{-2} (50 \text{ yr})^{-1}$; C2: $-2.4 \text{ g m}^{-2} (50 \text{ yr})^{-1}$). This effect is less pronounced for catchment C2 (Fig. 4.5: Del1, Del2). Catchment C1 shows the largest SOC delivery when the threshold for rill initiation is low (Ril_{hi} : $-26.3 \text{ g m}^{-2} (50 \text{ yr})^{-1}$). In catchment C2, the highest lateral SOC delivery is achieved when there is assumed to be no soil aggregation (Agg_{off} : $-13.0 \text{ g m}^{-2} (50 \text{ yr})^{-1}$). If water erosion is taken into account, catchment C1 is a net C

source ranging from 1.3 (GS_{off}) to 14.2 (Ril_{hi}) $\text{g m}^{-2} (50 \text{ yr})^{-1}$. In contrast, the tillage-induced sequestration potential of catchment C2 exceeds SOC delivery in most water erosion model runs, leading to a positive erosion-induced C balance (sink) as long as soil aggregation is included (Agg_{off} : $-1 \text{ g m}^2 (50 \text{ yr})^{-1}$; Fig. 4.5: Bal1-Bal2).

Variations in SOC enrichment of delivered sediments is generally rather small for all model runs (Fig. 4.6). The most pronounced effect on SOC enrichment results from different aggregation levels (Agg_{off} , Agg_{lo} , Agg_{hi}). However, differences in SOC enrichment were much more pronounced between the catchments. While C2 show high enrichment ratios (> 2.5) for all events, the enrichment ratios strongly decline with increasing event size in C1 (Fig. 4.6: B-C).

4.4 Discussion

4.4.1 Vertical C fluxes

Tillage erosion dominates the erosion-induced vertical C fluxes in both catchments. Without water erosion (Wa_{off}), total tillage-erosion-induced C sequestration potential was 7 and 9 $\text{g m}^2 (50 \text{ yr})^{-1}$ in catchment C1 and C2, respectively. The higher sequestration potential in catchment C2 results from steeper slopes and more field boundaries, where tillage erosion is most pronounced (Fig. 4.4). This offsets its smaller relative proportion of arable land. However, this field boundary effect (Fig. 4.4) might be overestimated as we did not update the digital elevation model during the 50-year simulation period. The response of vertical C fluxes to changes in tillage erosion strength (Til_{lo} ; Til_{hi}) further underlines the dominance of tillage redistribution in determining these fluxes (Fig. 4.5). This dominance results, in part, from the soil conservation system established at the research farm. Indeed, when compared to conventional soil management practices, water erosion was reduced by roughly a factor of 20 (Fiener and Auerswald, 2007a) in both catchments, while tillage erosion intensity (k_{til}) was only reduced by a factor of about 3 times smaller (Van Oost et al., 2006) as a result of the soil conservation system. However, independent from the soil tillage management, it is obvious that tillage erosion needs to be taken into account for reasonable estimates of vertical erosion-induced C fluxes on arable land (see also Van Oost et al., 2005b). Moreover, it should be noted that modelling tillage erosion is associated with large uncertainties since it is controlled by a large number of parameters (e.g. tool geometry and type, up-down or contour tillage, speed, depth, soil characteristics; Van Muysen et al., 2000; Van Oost and Govers, 2006). This uncertainty is illustrated by the large range of k_{til} coefficients which can be found in the literature (e.g. for chisel k_{til} :

70 to 657 kg m⁻¹ yr⁻¹; Van Oost and Govers, 2006). Interestingly, different water erosion processes hardly affected the vertical erosion-induced C fluxes. This is even true for model parametrisations with very pronounced rill erosion (*Rilhi*) and large sediment fluxes, because rills only affect a small area. Deposition is also restricted to a small number of raster cells (Fig. 4.4), particularly in the grassed waterway of catchment C2. The model does not account for changes in C mineralization at depositional sites that may occur as a result of aggregate breakdown shortly after deposition (Hu et al., 2016; Van Hemelryck et al., 2010; 2011). However, the potential underestimation of C mineralisation at depositional sites is assumed to be small (< 2% at a loess site in Belgium; Van Hemelryck et al., 2011). In addition, various drivers of additional C mineralisation at depositional sites have been discussed in literature (soil moisture, crusting and crust recovery, deposition of large macroaggregates; Van Hemelryck et al., 2010; 2011) but there is still a substantial lack in process understanding. At this moment, this issue makes it difficult to transfer the specific experimental results into a modelling framework addressing other environmental conditions.

Overall, to achieve accurate estimates of vertical erosion-induced C fluxes, it seems to be more important to improve the representation of tillage erosion in the model, rather than focusing on detailed process-oriented water erosion modelling, which is less important for vertical C fluxes.

4.4.2 Lateral C fluxes

In contrast to vertical C fluxes, lateral erosion-induced C fluxes are substantially affected by a number of event-specific processes. To assess these processes, a spatially distributed process-oriented modelling approach is needed.

Our synthetic 50-year data set (based on the 1994-2001 observations) produces three large SOC delivery events, representing nearly 60% of the total SOC delivery in both catchments (Fig. 4.5: Del1-Del2). This underlines the importance of accounting for individual events, particularly for the enrichment of SOC in delivered sediment (Fig. 4.6). However, it should be noted that SOC enrichment is mostly affected by catchment characteristics (Fig. 4.6: B-C). While catchment C1 follows the expected behaviour, i.e. decreasing SOC enrichment with increasing event size (Auerswald and Weigand, 1999; Menzel, 1980; Polyakov and Lal, 2004b; Sharpley, 1985), and is in good agreement with the results of Wang et al. (2010) for similar soils in the Belgian loess belt, event size had hardly any effect on the SOC enrichment in catchment C2, where any larger particles, including ag-

gregates, are deposited in the grassed waterway due to consistently high hydraulic roughness throughout the year. Hence, a parsimonious approach solely relating annual erosion magnitude to SOC enrichment (e.g. Fiener et al., 2015 using the model SPEROS-C) might fail on the landscape scale due to varying inter-field connectivity characteristics of catchments. Underlining the results of recent studies (e.g. Hu and Kuhn, 2016), it seems to be essential to take detailed processes into account during erosion, transport, and deposition in order to accurately capture the SOC enrichment of delivered sediments. In our modelling example, neglecting enrichment would lead to a 36% underestimation of the total SOC delivery in catchment C1 and an even more extreme 63% underestimation in catchment C2. This large difference between catchment C1 and C2 suggests that the relevance of SOC enrichment in delivered sediments is controlled not only by event size but also by the catchment connectivity to the outlet.

SOC enrichment in delivered sediments is mainly controlled by the physical properties (e.g. soil texture) of the parent soil (Foster et al., 1985). Soil aggregation transforms unconsolidated fine primary particles, a highly mobile SOC fraction, into soil aggregates, a fraction in which SOC is far less mobile. Hu and Kuhn (2016) showed that soil aggregation reduces the transport distance and potentially enhances terrestrial SOC deposition up to 64%. We found a similar trend: upon increasing the aggregation level of the model from non-aggregated (*Agg_{off}*) to heavily aggregated (*Agg_{hi}*) soil conditions, we found an increase in SOC deposition for both catchment C1 (47%) and C2 (83%). However, while soil texture clearly plays an important role, inter-field connectivity can be the dominant process driving lateral SOC delivery on the landscape scale. This is demonstrated by catchment C2, which shows its largest SOC delivery when it is assumed that there is no soil aggregation. Unfortunately, representing soil aggregation in models is challenging due to a pronounced seasonality (Angers and Mehuys, 1988; Coote et al., 1988; Six et al., 2004; Wang et al., 2010) and complex spatial patterns related to soil nutrients, moisture, grain size distribution, management practices, erosion, and soil biota (Denef et al., 2002). Especially for landscape-scale applications, this high degree of complexity needs to be substantially reduced in a conceptual way. In general, static soil parameters might underestimate dynamic feedbacks, but they are a necessary simplification for landscape-scale modelling approaches.

4.4.3 Erosion-induced C balance of different catchments

Under the same precipitation and field conditions, the simulated erosion-induced C balance of catchment C1 and C2 show opposing results (Fig. 4.5: Bal1-Bal2). While catchment C1 acts as a C source for the majority of simulated processes (controlled primarily by SOC delivery), the presence of the grassed waterway for catchment C2 substantially reduces lateral SOC delivery and leads the catchment to function as a C sink for most simulated processes. For both catchments, the majority of simulation years show a positive erosion-induced C balance (sink). However, three heavy erosion events in catchment C1 exceeded the positive cumulative vertical flux. Therefore, we underline that any analysis of landscape-scale erosion-induced C balances must consider inter-field connectivity.

4.5 Conclusions

In this study, the effect of individual soil organic carbon (SOC) redistribution processes on SOC dynamics is assessed by utilizing a coupled process-oriented erosion and carbon (C) turnover model. The erosion component of the model was successfully validated against a continuous 8-year data set of surface runoff and sediment delivery. The model was able to estimate the relevance of different processes in terms of their impact on vertical and lateral C fluxes for two catchments with distinct characteristics over an artificial time series of 50 years. We found that tillage erosion dominates on-field soil redistribution and vertical erosion-induced C fluxes on arable land, while water erosion processes have a much more limited effect. However, episodic lateral SOC delivery is critically important for the carbon balance. Ignoring SOC enrichment in delivered sediments leads to a pronounced underestimation of delivered SOC. Soil aggregates substantially reduce SOC delivery by turning highly mobile fine primary particles into less mobile soil aggregates. In general, the erosion-induced C balance is largely affected by inter-field deposition related to catchment connectivity.

Our results underline the importance of having an accurate and spatially distributed representation of tillage erosion. The episodic nature of water erosion calls for a sufficiently long simulation period and the inclusion of grain-size-selective transport in order to address the enrichment of delivered SOC. Furthermore, we stress the need for future investigations on seasonal and spatial variations in soil aggregation for a conceptual model implementation.

Article IV

Uncertainties in assessing tillage erosion – how appropriate are our measuring techniques?

Peter Fiener¹, Florian Wilken^{1,2}, Detlef Deumlich², José A. Gómez³, Gema Guzmán³, Robert Hardy⁴, Emilien Aldana-Jague⁵, John Quinton⁴, Michael Sommer^{2,6}, Kristof Van Oost⁵, and Robert Wexler¹.: Uncertainties in assessing tillage erosion – how appropriate are our measuring techniques?, *Geomorphology* (*submitted).

¹Institute of Geography, University Augsburg, Germany

²Institute of Soil Landscape Research, Leibniz-Centre for Agricultural Landscape Research ZALF e.V., Germany

³Institute for Sustainable Agriculture, Spanish National Research Council, Department of Agronomy, Spain

⁴Lancaster Environment Centre, Lancaster University, UK

⁵ Earth & Life Institute, TECLIM, Université catholique de Louvain, Belgium

⁶Institute of Earth and Environmental Sciences, University of Potsdam, Germany

Submitted to the journal Geomorphology as is, except for minor formatting changes.

Article abstract

Tillage erosion on arable land is a very important process leading to a net downslope movement of soil and soil constituents. Tillage erosion rates are commonly in the same order of magnitude as water erosion rates and can be even higher, especially under highly mechanized agricultural soil management. Despite its prevalence and magnitude, tillage erosion is still understudied compared to water erosion. The goal of this study was to bring together experts using different techniques to determine tillage erosion and use the different results to discuss and quantify uncertainties associated with tillage erosion measurements. The study was performed in North-Eastern Germany on a 10 m by 50 m plot with a mean slope of 8%. Tillage erosion was determined after two sequences of seven tillage operations (simulating about 10-14 yrs. of cultivation). Two different micro-tracers (magnetic iron oxide mixed with soil and fluorescent sand) and one macro-tracer (passive radio-frequency identification transponders (RFIDs), size: 3 x 20 mm) were used to directly determine soil fluxes. Moreover, tillage induced changes in topography were measured for the entire plot with two different terrestrial laser scanners and an unmanned aerial system for structure from motion topography analysis. Based on these elevation differences, corresponding soil fluxes were calculated. The mean translocation distance of all techniques was 0.57 m per tillage pass, with a relatively wide range of mean soil translocation distances ranging from 0.39 to 0.72 m per pass. A benchmark technique

could not be identified as all used techniques have individual error sources, which could not be quantified. However, the translocation distances of the used macro-tracers were consistently smaller than the translocation distances of the micro-tracers (mean difference $-26\pm 12\%$), which questions the general assumption of non-selective soil transport via tillage operations. This study points out that tillage erosion measurements, carried out under almost optimal conditions, are subject to major uncertainties that are far from negligible.

5.1 Introduction

Soil erosion, especially on arable land, is a major environmental threat (Montanarella et al., 2016; Pimentel, 2006) negatively affecting on-site soil properties and leading to substantial off-site damage (Pimentel and Burgess, 2013). Moreover, lateral soil fluxes due to soil erosion are important modulators of biogeochemical cycles within soils (Doetterl et al., 2016; Quinton et al., 2010), and also substantially affect carbon and nutrient cycling in inland waters (Battin et al., 2009; Tranvik et al., 2009). Soil erosion is most commonly understood as a process driven by water and wind that redistributes soil within the terrestrial environment and transfers it to water courses. However, since the early 1990s there has been a growing awareness of tillage as another important agent of soil erosion and redistribution (Govers et al., 1993; Lindstrom et al., 1990; Lobb et al., 1995). Tillage on sloping land leads to a net downslope displacement of soil, even if up- and downslope tillage directions are alternated (Govers et al., 1999). The major difference between tillage and water or wind erosion is: (i) that tillage erosion occurs on a regular basis and is not driven by rare extreme events; and (ii) that soil is solely redistributed within fields and hence the process does not lead to off-site damage. Tillage erosion typically occurs on convex slopes while soil accumulation takes place in concavities (Govers et al., 1999). Hence, tillage and water erosion tends to take place at different landscape positions: tillage mobilizes soil from hilltops which are minimally affected by water erosion to the thalwegs where the highest rates of water erosion occur (Govers et al., 1994).

Various authors have shown that tillage erosion rates on arable land are at least in the same order of magnitude as water erosion rates (Li et al., 1999; Van Oost et al., 2006) and might be even higher than water erosion rates in drier or less convective storm dominated areas (Sommer et al., 2008). Despite, its prevalence and magnitude, tillage erosion is still understudied compared to water erosion: a Web-of-Knowledge search for articles including the topic 'water erosion' or 'tillage erosion' resulting in roughly 10-times more results for 'water erosion' (260 vs. 2222; May 2017).

There are a variety of techniques presented in the literature for determining tillage erosion rates. These can be categorized as either tracer-based, those that determine topographic change or directly determine the movement of soil. For tracing methods, tracers are either added before performing individual or series of tillage operations or are *in-situ* tracers, e.g. ^{137}Cs (Van Oost et al., 2006), used to estimate long-term erosion rates. Tracers added before tillage experiments have the advantage that tillage erosion can be isolated from long-term erosion, which is always a combination of different erosion processes. The added tracers can be subdivided into macro-tracers (diameter > 2 mm) and micro-tracers (diameter as soil particles or solutes absorbed by soil colloids). Micro-tracers are applied as solutes sprayed onto soil, e.g. sodium chloride solution (Barneveld et al., 2009), or mixed with natural soil and applied in trenches within the experimental plots, e.g. magnetic particles (Zhang and Li, 2011) or Chloride (often as KCL) (Lobb et al., 1999). The recovery of the tracer after the experiment is either performed via soil sampling and/or if possible, e.g. in case of magnetic tracers, with instruments measuring *in-situ* concentrations as used by Guzmán et al. (2013) at plot scale, but for water erosion. Typical macro-tracers are coloured stones (Kietzer, 2007; Logsdon, 2013; Thapa et al., 1999; Tiessen et al., 2007; Turkelboom et al., 1997; Zhang and Li, 2011) and different types of metal, mostly aluminium cubes (Barneveld et al., 2009; De Alba et al., 2006; Lindstrom et al., 1990; Van Muysen et al., 2002; Van Oost et al., 2000b), which are often individually numbered. In addition, approaches that attempt to mimic soil with the intention to more realistically simulate soil movement, coloured aggregates (Dupin et al., 2009) have been used. The main advantage of these macro-tracers is that in most cases the movement of individual, numbered particles can be tracked. The main disadvantage is the very time-consuming application and especially recovery of the particles from the tilled soil layer. The most widely used *in-situ* tracer to determine tillage (or total) erosion is ^{137}Cs resulting from atom bomb testing in the 1950s and 60s (Govers et al., 1996; Heckrath et al., 2005; Kietzer, 2007; Quine et al., 1994; Quine et al., 1996; Van Oost et al., 2003). Tillage erosion rates are estimated by comparing the ^{137}Cs activities at different slope positions and soil depths with those of reference sites, which should not be affected by any soil erosion or deposition. A similar approach is based on other naturally occurring tracers, e.g. Jordanova et al. (2011) used the natural magnetism in different soil horizons to determine tillage erosion and deposition due to different depths of these horizons. The advantage of using such kind of natural tracers is that these represent long-term tillage erosion. Apart from technical issues with these techniques, their major disadvantage is that they do not

only measure tillage erosion, as the pattern of tracer redistribution results from the combination of various erosion types (Van Oost et al., 2006).

Techniques to estimate tillage erosion from changes in topography vary widely regarding their spatial and temporal resolution. In several studies, the slight step in topography, introduced by tillage at the upslope boundary, allowed the translocation of soil material to be determined due to tillage at the upslope end of experimental plots (Kimaro et al., 2005; Turkelboom et al., 1997). This, so-called step method, has been combined with the installation of soil collecting trenches at the downslope end of the experimental plots (Kimaro et al., 2005; Turkelboom et al., 1997). Another method for the determination of elevation differences is the determination of the soil depth above a known reference point buried below the tillage depth, e.g. a concrete block as in Sadowski and Sorge (2005).

Photogrammetry was used by Vandaele et al. (1996) to carry out a longer-term and larger-scale estimate of tillage erosion. They determined temporal patterns of elevation differences using sequential stereoscopic aerial photographs from the Belgium loess belt (1947-1996). Their findings underlined the importance of tillage erosion in the region, with the most severe surface lowering occurring on hilltops and on hillslope convexities (Vandaele et al., 1996). More recently, high-resolution digital elevation models (DEMs) in combination with digital aerial photographs have improved long-term analysis of landscape changes (Deumlich et al., 2014) and recent advances in image acquisition and software have, over the past decades, made novel measurement techniques for geomorphological change detection affordable. Terrestrial laser scanner (TLS) and unmanned aerial system (UAS) together with structure from motion (SfM) techniques have been utilized in several morphological change detection studies. On arable land the majority of these studies have focused on rill and gully erosion features (d'Oleire-Oltmanns et al., 2012; TLS: Eltner and Baumgart, 2015; UAS: Eltner et al., 2015; Peter et al., 2014; Vinci et al., 2015). A recent study by Pineux et al. (2017) investigated spatial elevation changes at the catchment scale, utilizing multi-temporal DEMs of difference (DoD) using UAS based SfM (UAS/SfM). However, as with natural tracers, the changes in topography result from a combination of erosion processes, which need to be unravelled for tillage erosion to be studied.

The results of tillage erosion studies (e.g. summarized in Van Oost et al., 2006) have been used to develop and parameterize a number of tillage erosion models of different complexity. The most widely used is a diffusion-type approach developed by Govers et al. (1994) that simulates tillage erosion as a function of local slope and a tillage transport

coefficient k_{till} . The tillage transport coefficient generalizes several parameters (e.g. tillage speed, implement shape, soil physical properties) and needs to be determined experimentally (e.g. Heckrath et al., 2006; Kosmas et al., 2001; Van Muysen et al., 2000) or calculated from empirical relationships based on experiments (Van Muysen and Govers, 2002; Van Muysen et al., 2002). An overview of different k_{till} values for different soils, tillage depths, tillage directions, implements and speeds as well as plough layer bulk density is given in Van Oost et al. (2006). However, our knowledge of the changes in k_{till} for different tillage techniques is very limited (De Alba et al., 2006; De Alba et al., 2004), and data regarding reduced tillage are especially rare (Van Oost et al., 2006). Apart from models using the diffusion-type approach (e.g. WaTEM-SEDEM or SPEROS-C: Fiener et al., 2015; Van Oost et al., 2000a; Van Oost et al., 2005c; Van Rompaey et al., 2001) there are other, more complex models taking a larger number of parameters into account, e.g. tillage direction, on-field objects, or complex field boundary effects (TILDA: Quine and Zhang, 2004; CATT: Vanwallegem et al., 2010; TELEM: Vieira and Dabney, 2011).

All commonly used tillage erosion models are developed and tested against tillage erosion measurements. To represent individual tillage management practices, these models need to be parameterized by experimentally determined tillage erosion rates. As indicated above, there is still a lack in knowledge regarding model parameters, especially for the large number of different tillage implements (size, depths, shape etc.). However, to establish a substantial data-base of model parameters to simulate tillage erosion, we first need more information regarding the comparability of different methods to determine tillage erosion. Experimentation is critical for determining the parameters used to drive tillage erosion models. Therefore, it is vital to understand how the experimental technique deployed influences the derivation of the model parameters and how these differences translate in to uncertainty surrounding predictions of tillage erosion. Here for the first time we directly compare a range of methodologies for determining tillage erosion simultaneously in the field. In addition, the work contributes new knowledge on the redistribution of soil in reduced tillage systems and the potential of new tracer methods and topographic change techniques to quantify tillage erosion rates.

The main aims of the study are (i) to quantify and compare tillage-induced soil redistribution using different tracers and high-resolution topography measurements, and (ii) to quantify and discuss potential model uncertainties resulting from different model parameters derived from different measuring techniques.

5.2 Materials and Methods

5.2.1 Test site and experimental design

The experimental site was located near the village of Polßen (53.157° North; 13.962° East) about 80 km North-East of Berlin, Germany. It represents the typical topography of previously glaciated, hummocky ground moraines. The soils in this region are strongly affected by landscape position. Extremely eroded Calcaric Regosols (IUSS, 2015) are often located at the hilltops, whereas moderately to strongly eroded Luvisols can be found along the slope, and colluvial, partly groundwater-influenced soils are located in closed depressions (Gerke et al., 2010; Sommer et al., 2008). The subcontinental climate in the area is characterized by a mean annual precipitation of approximately 500 mm a⁻¹ and a mean annual air temperature of 8.9°C (CLINO-1981-2010 for the meteorological stations Gruenow and Angermuende). The region is intensively used for agricultural production with large fields (>20 ha) and cultivated using heavy farming equipment since the early 1970s (Sommer et al., 2008).

The experiment was performed between 03/04/16 and 08/04/16 on a convex upslope, located within a large (ca. 50 ha) field where winter wheat had been planted in autumn. Overall, an area of 15 m x 85 m was prepared with an inner plot of 10 m x 50 m where the tracers were placed (Fig. 5.1). To homogenize the soil and bury the germinated wheat on the test field, the plot was firstly tilled (03/04/16) with a mouldboard plough to a depth of 0.25 m and then smoothed with a roller.

Subsequently, the time after initial plot preparation is referred to as t_0 . For the (reduced) tillage erosion

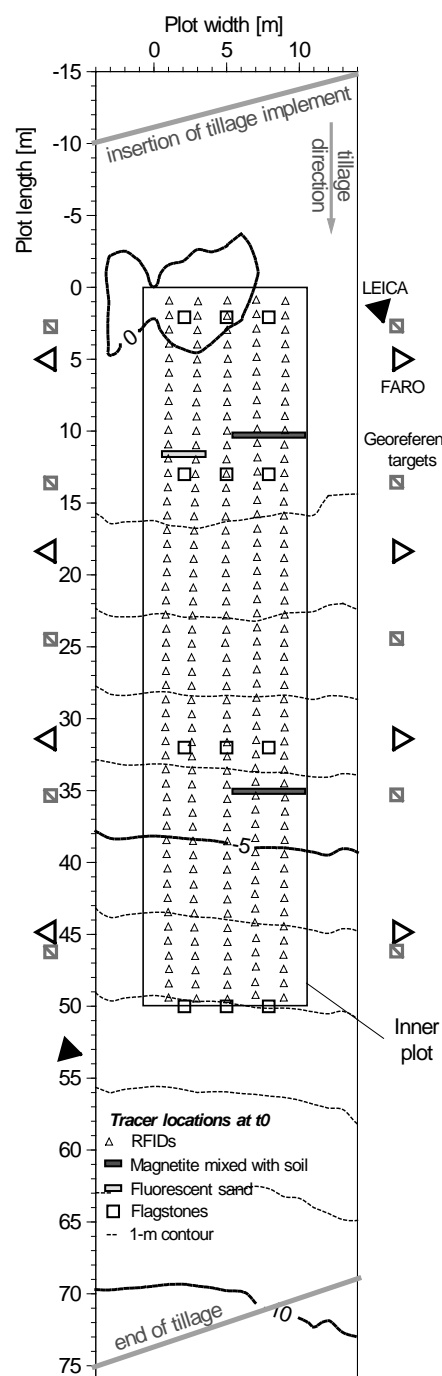


Figure 5.1: Topography of the test site, location of tracers at the beginning of the experiment (t_0), TLS scan positions, and location of georeferenced targets for TLS and UAV/SfM measurements.

experiment, two sequences of seven downslope tillage operations consisting of a combination of a cultivator and a roller (Fig. 5.2) were applied on 04/04/16 and 06/04/16. Subsequently, the time after the first and second tillage sequence is referred to as t1 and t2, respectively. The cultivator, a Tiger 4 AS (HORSCH Maschinen GmbH; Germany), consisted of a series of disks, tines and a roller, and tilled the soil to a depth of 0.15 m without inverting but disrupting and mixing the soil. The tillage width of the cultivator was 5 m, requiring three parallel down-slope operations for one cultivation of the plot. The tractor speed during tillage was approximately 6 km h⁻¹. The roller had a width of 7.5 m, hence only two passes were necessary for rolling the plot.



Figure 5.2: Cultivator (left) and roller (right) used during the experiment.

To monitor potential bulk density changes between t0 and t2, it was measured at 20 locations within the inner plot (centre of 5 x 5 m rasters) at two depths (0.06 to 0.12 m and 0.18 to 0.24 m, resp.) using Kopecky cylinders with a diameter of 0.08 m (volume $3.0 \times 10^{-4} \text{ m}^3$; Table 5.1).

Table 5.1: Bulk density and stone content measured after preparation of the plot with one-time ploughing to a depths of 0.25 m (t0) and at end of the experiment after 14-times tillage with the field cultivator to a depths of 0.15 cm (t2).

Parameter	Soil depth (m)	Time	Mean	Standard Dev.	Min	Max	n
Bulk density incl. stones (t m ⁻³)	0.06-0.12	t0	1.53	0.08	1.36	1.70	20
		t2	1.60	0.08	1.48	1.79	19
	0.18-0.24	t0	1.56	0.11	1.40	1.78	20
		t2	1.67	0.13	1.47	1.88	20
Stone content (mass-%)	0.06-0.12	t0	14	4.3	9	25	20
		t2	13	3.9	7	22	20

5.2.2 Tracer techniques

Micro-tracers

Magnetic iron oxide mixed with soil

A total of 312 kg of soil were mixed by serial dilutions with magnetic iron oxide (subsequently referred as magnetic tracer) in order to increase the average background concentration of soil by two orders of magnitude following the protocol of Guzmán et al. (2010). Magnetic iron oxide mainly binds to the fine particle fraction (clay and silt) of the soil. The mixture was applied at t_0 in two trenches of 5.0 m x 0.35 m x 0.15 m (width, length, depths, resp.) the upper and middle right side of the plot (Fig. 5.1). Volumetric magnetic susceptibility at the beginning of the trial and after every tillage sequence (t_1 and t_2) was measured using a MS2 sensor and a MS2D field probe (Bartington Instruments, UK). The device penetrates the soil and integrates the signal with depth (10% of the signal is associated to a depth of response of 0.06 m). A 0.90 m x 2.50 m grid (X, Y) was set out, with a more dense measuring grid (Y distance: 1.25 m) at areas close to the initial tagged trenches. In order to calibrate the signal of the field probe and allow conversion of the volumetric magnetic susceptibility into mass of tracer, total of 18 random locations (including originally untagged areas and trenches) were sampled before and after the first seven tillage passes at different depths (0-0.05, 0.05-0.10 and 0.10-0.15 m). Their magnetic susceptibility was determined using a MS2B laboratory meter (Bartington®) as described by Guzmán et al. (2015; 2013). Additionally, samples below the tillage layer (interval 0.15-0.20 m) were taken and analysed in the laboratory to evaluate and calibrate the field probe.

Fluorescent sand

The fluorescent tracer is commercially-available (Partrac Ltd; UK) and consists of natural quartz particles (D50: 70 μm) coated with a green fluorescent pigment. A Panasonic Lumix GH4 camera was used with an orange 490 nm long pass filter (Knight Optical; UK) to enhance the contrast between the soil and the tracer. Images were taken during the night or under darkened conditions using an external LED light source (wavelength 450 nm) with diffusing plates to produce the fluorescent response. An intensity-based method, similar to that of Hardy et al. (2016) was utilized to analyse the amount of tracer in the images. The intensity-based method used the numeric pixel values from the green colour channel in the camera and differentiates between the background intensity of the soil and the fluorescent tracer. Therefore, a reduction of the tracer concentration and corresponding soil flux can be derived. At t_1 a trench (3.0 x 0.4 x 0.15 m; Fig. 5.1) was filled

with the fluorescent tracer particles and the intensity-based method used to determine the tracer redistribution was used at t₂. Therefore, the visible surface intensity was determined and the depths distribution of the tracer was measured in five 1.0 x 0.2 x 0.15 m trenches down-slope the tracer application trench (distance: 2.5, 5.0, 7.5, 10.0, 12.5 m).

Macro-tracer

Passive radio-frequency identification transponder

Commercially-available passive radio frequency identification (RFID; HID Global, Germany) transponders were used together with a newly designed prototype detection antenna (diameter 0.2 m; TECTUS Transponder Technology, Germany) to tag soil movement along the inner plot. RFID transponders (n=250), grouted in glass cylinders (3 mm x 20 mm), were inserted to a soil depth of 0.075 m (mid tillage depth) along five rows (spacing of rows and along slope 2 and 1 m, resp.; Fig. 5.1). At t₁ and t₂ the RFID transponders were re-located with the detection antenna, and the new location of the transponders was determined with a total station (TS 06 plus R1000; Leica, Germany). Individual horizontal displacement distances of the RFID transponders were calculated, both along and perpendicular to the slope and tillage direction.

5.2.3 Topographical techniques

Flagstones

Concrete flagstones (n=12; 0.25 m x 0.25 m x 0.03 m) were buried at t₀ at different slope positions in a mean depth of 0.42 m (Fig. 5.1). To relocate the flagstones after the tillage sequences, 3M™ Full-Range Markers (3M™, US; 0.38 m diameter) were buried underneath the flagstones. The markers allow for a precise relocation of the flagstones after the tillage sequences by using a 3M™ Dynatel™ Locator (detection range of about 2.5 m). The change in soil depths above the flagstones at the tillage sequences t₁ and t₂ were measured with a 0.8 m long soil probe (steel needle). Measurements at t₁ and t₂ were corrected for changes in bulk density and hence surface elevation (see below).

Terrestrial laser scanning

Two different impulse wave terrestrial laser scanners (TLSs), a Leica (Scanstation C10; Leica, Germany) and a Faro (Focus 3D; FARO, US), were used during the experiment. The Leica TLS has a lower spatial resolution with a scanning range of approx. 300 m, while the Faro TLS has a higher spatial resolution with a maximum scanning range of approx. 50 m. The Leica scans were performed from two locations at the upper and lower end of the plot, while the Faro scans were taken from eight locations (four on each side

of the plot; Fig. 5.1). An average resolution depending of distance between scanner and soil surface of 4.4×10^3 and 175×10^3 points per m^2 was achieved for the Leica and Faro scanner, respectively. Each scan took about 60 min with the Leica and about 12 min per scan with the Faro.

To georeference the scans, 10 static black and white targets were equally distributed along the down slope plot borders (Fig. 5.1) and independently located for each time step ($t_0 - t_2$) with a total station (TS 06 plus R1000; Leica, Germany). The reference coordinates were used to register the TLS data into a single merged point cloud for t_0 , t_1 , and t_2 using the Leica software Cyclone 9 (Leica, Germany). Digital elevation models of different grid size resolutions of the merged point clouds were processed in CloudCompare 2.6.2 (cloudcompare.org). Subsequently, DoDs were calculated using R for statistical computing 3.2.2 (R Development Core Team, Austria) and ArcGIS 10.4.1 (ESRI, US).

UAS/SfM

DEMs for the time steps t_0 and t_2 were calculated using UAS/SfM technique. Therefore, a hybrid Sony $\alpha 5000$ camera with a 20.1 MP (5456×3064 pixel) resolution was mounted on a gyro-stabilised gimbal to a multicopter UAS platform. The UAS was a custom build hexacopter with a double rotor setup on three arms (RcTakeOff, Belgium). The images (t_0 : $n=99$ images; t_2 : $n=88$ images) were recorded from nadir angle with a 16 mm focal length, f 3.5-5.6 OSS (equivalent 24 mm) and an average flight elevation of 15 m. The TLS black and white targets were also used for referencing the SfM approach. SfM calculations were carried out using PhotoScan Professional version 1.0.4 (Agisoft; Russia) and for further point cloud processing, the software CloudCompare 2.6.2 (cloudcompare.org) was used. The average point cloud density of the inner plot is 75×10^3 points per m^2 .

5.2.4 Determine change in topography

To calculate spatially distributed erosion and deposition from the different TLSs and UAS/SfM based DEMs at t_0 , t_1 and t_2 , it was necessary to correct these DEMs for bulk density changes during the experiment. Therefore, the measured changes in bulk density (t_0 and t_2 ; Table 5.1) were used to correct for the settling of the soil surface during the experiment. It was assumed that the increase in bulk density solely happened in the tillage layer between t_0 and t_1 as complete disruption was reached after seven tillage operations and soil loosed during the pre-experimental mouldboard ploughing should be settled. Calculating a change in soil surface elevation, using the mean bulk density (Table 5.1), leads to an overall elevation correction of the soil surface for the initial DEM (t_0) by -13.2 mm.

5.2.5 Calculating downslope soil flux from tracer movement and topography changes

To derive soil translocation distances and translocation rates from the different measuring techniques two approaches are applied: (i) The soil translocation distance was directly derived from the measured translocation distance of the respective tracer. The underlying assumptions here are that the translocation distance of the used tracer represents the translocation distance of the tilled soil layer, the transport distances of the tracer are normally distributed and hence the mean transport distance adequately represents its movement, and the tracers are more or less homogeneously moved throughout the depth profile of the tillage layer. The distribution of the tracer movement was tested with all tracers and any depths dependence was tested according to depth profiles of the fluorescent tracer along the slope and point measurements of the magnetic tracer. For the RFIDs a mean or median translocation distance in the inner plot was calculated from the movement of all recovered individual RFIDs; non-recovered RFIDs were assumed to travel the mean distance determined from those that were recovered. Due to the large number of RFIDs distributed over the inner plot (Fig. 5.1), it was also possible to calculate movement parallel and perpendicular to the slope. Moreover, movement at different slope positions could be determined between t_0 and t_1 as well as t_1 and t_2 , respectively. In case of the micro-tracers the mean or median translocation distance was derived from the distribution of the measured tracer intensity (magnetic susceptibility and fluorescence) downslope the application trenches. It is important to note that in case of the magnetic susceptibility the bulk magnetic susceptibility of the plough layer is measured, while in case of the fluorescence only the distribution of particles on the soil surface was determined. Compared to the RFIDs it was only possible to determine tracer movements from one (fluorescent tracer) and two locations (magnetic tracer) and one time step. Based on the translocation distance a mean soil translocation rate was calculated following Eq. 1, while using the measured mean bulk density (Table 5.1) and a mean tillage depths of 0.15 m (Van Oost et al., 2006).

$$Q_s = \rho_b \cdot \bar{d} \cdot D \quad (5.1)$$

where Q_s the rate of soil translocation (kg m^{-1}); ρ_b is the soil bulk density (kg m^{-3}); \bar{d} is the tillage translocation distance (m), and D is the tillage depths (m).

Based on 0.5 m x 0.5 m rasters DEMs determined from the three different topographical techniques, the average translocation distance and soil translocation rate is calculated. The soil flux calculation starts at the insertion of the tillage implement (plot length location about -12.5 m; Fig. 5.1) in downslope direction corresponding to the tillage direction.

Hence, the volume of soil loss in downslope direction can be determined based on the accumulated loss in elevation per grid cell (product of elevation difference and grid size). Therefore, the soil flux from the source area (area above inner plot; Fig. 5.1) translocated into the inner plot can be determined by the total soil volume lost in the source area. To route soil loss throughout all slope positions of the inner plot, the soil loss volume was determined by iteratively adding 1 m segments to the source area until the end of the plot was reached. The tillage translocation distance (\bar{d}_i ; m) at each 1 m segment i is calculated as

$$\bar{d}_i = \frac{V_i}{W \cdot D} \tag{5.2}$$

where V is the volume of soil loss (m^3), D is the tillage depths (m) and W is the plot segment width (m).

5.3 Results

5.3.1 Translocation of tracers

All the tracers showed a substantial downslope movement after 7 and 14 tillage passes (Fig. 5.3), with a maximum movement of up to 18 m recorded for an individual RFID during one of the tillage sequences. Across all the tracers mean translocation distances per tillage pass had a substantial range of 0.23 to 0.71 m that depended on the tracer and slope position. Deriving a probability density function of the mean tracer movement per tillage pass of all RFIDs between t_0 and t_1 (recovery rate 79%) as well as t_1 and t_2 (recovery rate 75%) indicates, that a forward movement of RFIDs only occurred parallel to the slope, while perpendicular to the slope the mean movement was close to zero (Fig.

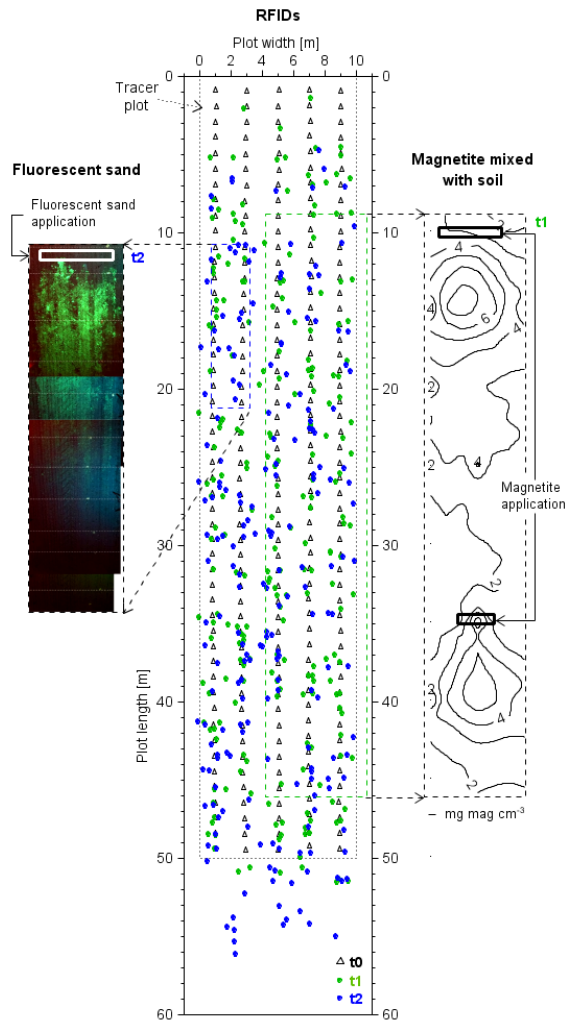


Figure 5.3: Translocation of individual RFIDs (t_0 to t_1 and t_1 to t_2); translocation of magnetic tracer mixed with soil from trenches 1 and 2 (t_0 to t_1) given as lines of equal magnetisation ($mg\ mag\ m^{-3}$); translocation of fluorescent sand from trench 3 (t_1 to t_2) given as mosaic of colour images taken under an external light-source.

5.4). Hence, we subsequently only analysed the movement of tracers in downslope direction.

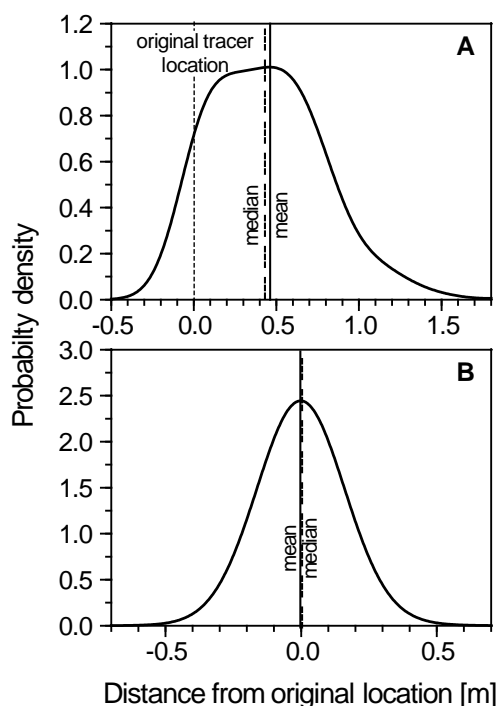


Figure 5.4: Mean and median translocation of all RIFDs per tillage pass (t0-t1 and t1-t2); in slope direction (A) and perpendicular to slope direction (B).

Comparing the movement of the RFIDs located around the micro-tracer trenches (max. distance up- and downslope of application trench ≤ 5 m) with the movement of magnetic tracer (two trenches [Fig. 5.1]; t0 to t1) and fluorescence tracer (one trench [Fig. 5.1]; t1 to t2) indicates a substantial difference in movement between the micro-tracer to the macro-tracer (Fig. 5.5; Table 5.2). In all cases the micro-tracers exhibit a larger translocation distance, while their behaviour at different slope positions is consistent, e.g. at upper and lower trench of magnetic tracer (Fig. 5.5A vs. Fig. 5.5B). Larger transport distances were measured for all tracers at steeper slopes. The mean translocation distance per tillage pass was $26 \pm 12\%$ smaller for the RFIDs compared to the micro-tracers (Table 5.2).

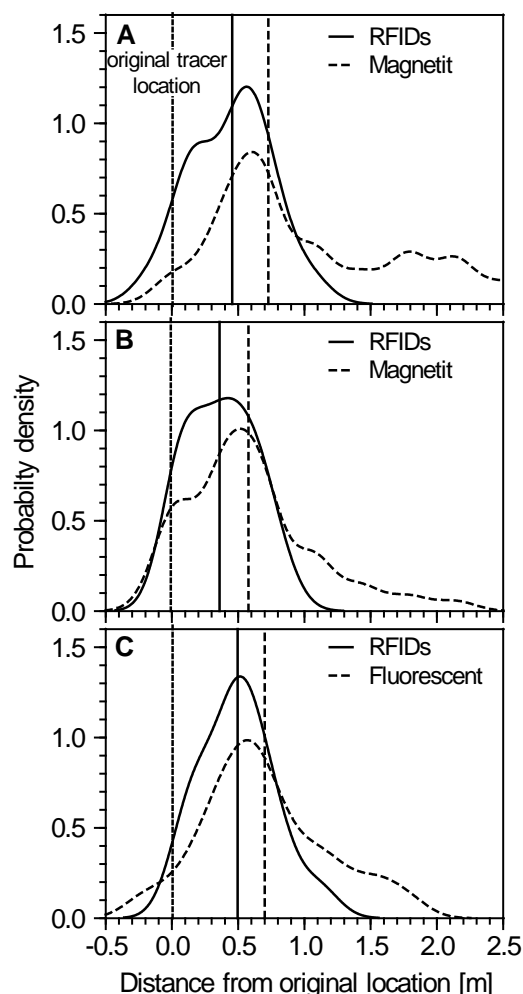


Figure 5.5: Comparison of mean translocation distance per tillage pass of different tracers. RFIDs vs. magnetic tracer translocation from upper (A) and lower trench (B) between t0 and t1. RIFDs vs. fluorescent tracer translocation from upper trench between t1 and t2; It is important to note that in case of the RFIDs slope segments (max. distance up- and downslope of micro-tracer application trenches ≤ 5 m) are compared against tracers distributed along small trenches (see Fig. 5.1). The solid and dashed vertical line shows the average transport distance of the RFIDs and the corresponding micro-tracer, respectively.

behaviour at different slope positions is consistent, e.g. at upper and lower trench of magnetic tracer (Fig. 5.5A vs. Fig. 5.5B). Larger transport distances were measured for all tracers at steeper slopes. The mean translocation distance per tillage pass was $26 \pm 12\%$ smaller for the RFIDs compared to the micro-tracers (Table 5.2).

Measurements of the fluorescent tracer in five soil pits (0-0.15 m) downslope of the tracer application trench at distances of 2.5, 5.0, 7.5, 10.0 and 12.5 m indicate some soil disturbance along the soil profile (Fig. 5.6) without an obvious systematic depths dependency. The surface measurements of the fluorescent tracer indicate that after 7 tillage passes only 17% of the tracer is still located in the area above the first soil pit (2.5 m below application trench). Hence, it was assumed that the depths measurements represent 83% of all fluorescent mate-

Table 5.2: Mean tracer translocation at magnetic tracer trenches and at fluorescent trench according to probability density functions.

Tracer	Tracer origin	Time of measurement	Mean translocation per tillage [m]
Magnetic tracer	Upper trench	t1	0.71
RFIDs	Upper trench	t1	0.44
Magnetic tracer	Lower trench	t1	0.59
RFIDs	Lower trench	t1	0.37
Fluorescent tracer	Upper trench	t2	0.70
RFIDs	Upper trench	t2	0.50

rial to be detected, while ignoring potentially small tracer amounts moved more than 15 m below the application trench. Under this assumption the relative amount of the fluorescent tracer and its mean translocation distance in each of the 0.01 m soil layers could be calculated (Table 5.3). According to this calculation, no systematic depths dependency in amount and translocation distance ranging from 0.68 to 0.83 m per tillage pass (mean ± sd: 0.76 ± 0.05 m) can be detected. This finding is corroborated through six magnetic tracer measurements in three depths (0-0.05 m, 0.05-0.10 m, 0.10-0.15 m) downslope of the tracer application trenches (1.25 m, 2.5 m, 3.75 m, 5.0 m) which only showed slightly higher, but insignificant ($p < 0.05$) values for the soil movement in the upper topsoil layer (0-0.05 m). Both the fluorescent and the magnetic tracer indicate that the different transport distances of the tracers cannot be explained from the different application depths of 0-0.15 m in case of the micro-tracers and 0.075 m in case of the RFIDs, respectively.

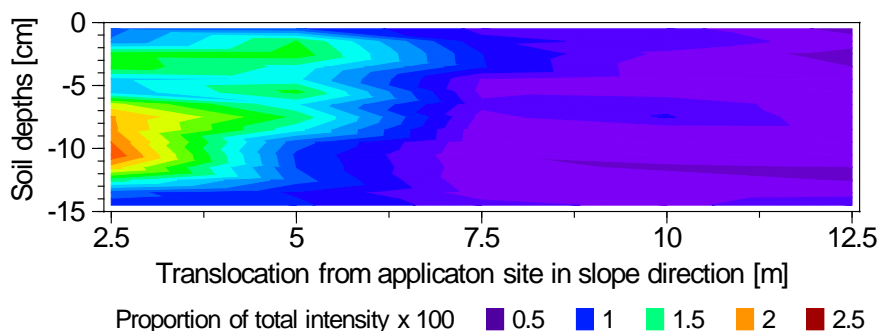


Figure 5.6: Soil depths-dependent translocation distance of fluorescent sand during seven tillage passes; translocation from upper trench between t1 and t2.

Table 5.3: Mean soil translocation distance per tillage pass in different 1-cm soil layers and relative translocation amount in each of the 1-cm soil layer.

Soil depths [cm]	Translocation distance [m]	Relative amount translocated per layer [%]
Surface	0.69	
0...1	0.71	5.90
1...2	0.81	6.81
2...3	0.81	7.29
3...4	0.79	7.06
4...5	0.76	6.48
5...6	0.77	6.64
6...7	0.80	7.19
7...8	0.83	7.61
8...9	0.78	7.20
9...10	0.74	6.90
10...11	0.74	6.91
11...12	0.71	6.55
12...13	0.70	6.13
13...14	0.68	5.52
14...15	0.74	5.82
0...15	0.76	100

5.3.2 Change in topography

The DoDs between the start and end of the experiment ($t_0 - t_2$) show good agreement in spatially distributed erosion and deposition patterns for all measuring techniques (Fig. 5.7). The absolute elevation differences between the TLS systems at the time t_0 to t_1 accurately match for both the flagstone positions and the gridded DEM data (Table 5.4). The TLS systems indicate a substantially lower loss for the tillage sequence t_1 to t_2 compared to t_0 to t_1 . However, for tillage sequence t_1 to t_2 the Leica shows a lower soil loss than the Faro. In contrast to the TLS systems the UAV/SfM show a net soil gain within the inner plot between t_0 and t_2 (Table 5.4). The flagstone point measurements for t_0 to t_2 are in the same range as the TLS measurements, but show major deviations compared to the TLS systems for the individual tillage sequences (Table 5.4).

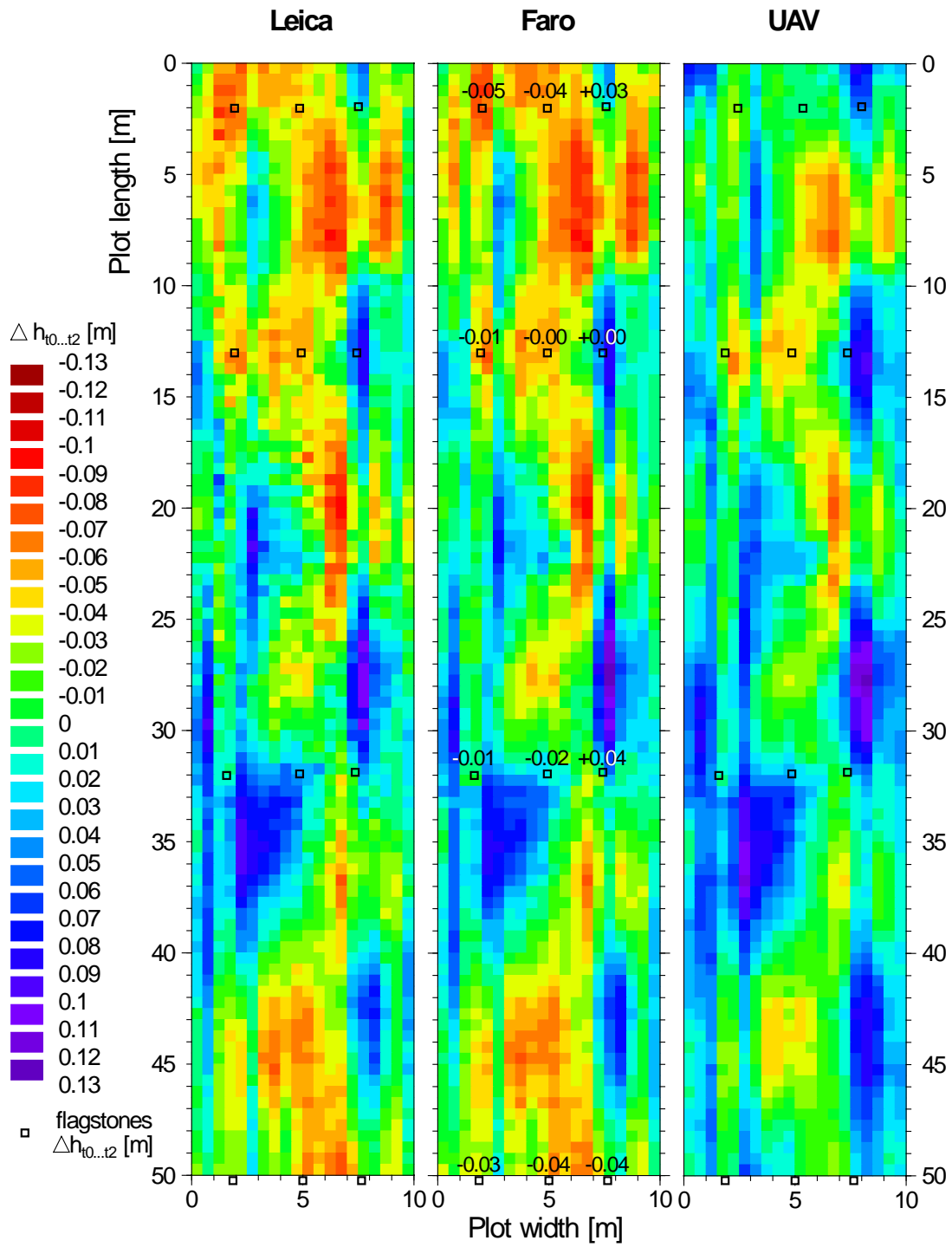


Figure 5.7: Difference in topography between t2 and t0 for all measuring systems. High-resolution data degraded to 0.5 x 0.5 m. Elevation differences derived from the flagstone technique are given in the mid (Faro) DoD map.

5.3.3 Soil translocation distances and translocation rates

Based on Eq. 1, the depths-in-dependence of tracer movement (Table 5.3) and the close to normal distribution of tracer movement (Fig. 5.4 and Fig. 5.5) we calculated the mean soil translocation distance and rate per tillage pass for each original tracer location. For the florescent and the magnetic tracers soil

Table 5.4: Comparison of changes in topography at the flagstone positions and for the TLS system and the UAS for the entire inner plot.

	Δh t1-t0 [cm]		Δh t2-t1 [cm]		Δh t2-t0 [cm]		n
	Mean	SD	Mean	SD	Mean	SD	
<i>At flagstone positions</i>							
Flagstones	-2.4	3.3	1.1	2.7	-1.3	3.0	12
Leica	-0.8	2.4	-0.4	3.1	-1.1	4.7	
Faro	-0.9	2.6	-1.0	3.4	-1.9	5.0	
UAV					0.4	3.9	
<i>0.5 x 0.5 raster inner plot</i>							
Leica	-0.8	3.0	-0.1	2.8	-0.8	3.7	2000
Faro	-0.6	2.9	-0.3	2.8	-0.9	3.8	
UAV					1.1	3.4	

translation was determined for the upper and lower trench locations at the tillage sequence t0-t1 and t1-t2, respectively (Fig. 5.8). For the RFIDs, soil translocation was calculated for ten 5 m segments of the inner plot (Fig. 5.1) for both tillage sequences. Compared to the single trenches or segments along the slope soil translocation was derived in 1 m segments from the DoDs of the TSL systems using Eq. 5.1 and Eq. 5.2. Soil translocation was not calculated for the UAS/SfM system, as the point of implement insertion was unfortunately not recorded.

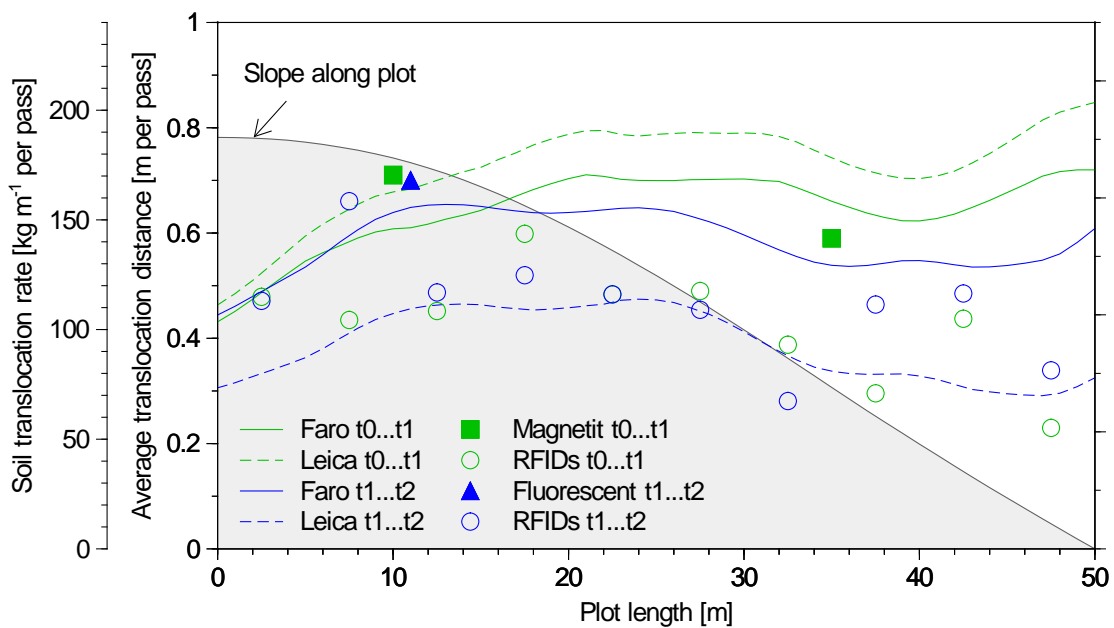


Figure 5.8: Average soil translocation distance and rate derived from the different methods used between t0 and t1 and t1 and t2; movement of tracers it is indicated at the location where the tracers were originally applied; it is important to note that the movement of RFIDs is calculated in 5 m segments averages the mean movement of 4 to 31 RFIDs (mean n per segment = 20.8).

The soil translocation distances and rates from the different techniques show some consistencies but also some substantial differences (Fig. 5.8). The Faro and the micro-tracer distances and rates are very similar and additionally the Faro translocation do not substantially change between t0-t1 and t1-t2. In contrast, the Leica translocation shows some substantial difference between t0-t1 and t1-t2, with a difference in mean translocation rates of 80.6 kg m⁻¹ per pass (difference of t1-t2 relative to t0-t1 is 47%). As expected from the tracer flux calculations, the RFID-based soil translocation distances and rates are substantially smaller than those of the micro-tracers, and are closest to the Leica derived data for the tillage sequence between t1-t2. Comparing all data (both tillage sequences) for the areas around the tracer trenches (between 7.5 m and 17.5 m and 32.5 m and 42.5 m) indicates, that the different techniques result in a substantial variability of derived soil translocation rates ranging from 105.6 to 170.4 kg m⁻¹ per pass at the upper trench area and from 80.9 to 175.6 kg m⁻¹ per pass for the lower trench area. Even more extreme differences can be recognized for the down slope end of the inner plot where four-fold differences between RFID-based and Leica-based translocation rates are found (t0-t1; Fig. 5.8).

5.4 Discussion

5.4.1 Implications of measurement uncertainties

A number of studies were performed over the last two decades reporting different soil translocation rates for different soils (properties, conditions) and tillage techniques (tillage speed, direction, depths, type of implement etc.) determined from a variety of measurement techniques (e.g. Barneveld et al., 2009; Kietzer, 2007; Logsdon, 2013; Van Muysen et al., 2002; Van Oost and Govers, 2006). Van Oost et al. (2006) provide a comprehensive overview of results acquired until 2006. From these data it is obvious that there are substantial differences for similar tillage categories (e.g. mouldboard tillage), which were mostly interpreted as differences resulting from differences in soil properties (bulk density) and in tillage technique (especially tillage depths, tillage speed, and tillage direction; Van Oost et al., 2006). However, uncertainties associated to different measuring techniques used in different studies were not systematically analysed.

Assuming that the results of the individual techniques presented in this study are of comparably quality to those referred to by Van Oost et al. (2006), our work indicates that substantial uncertainties in estimated tillage erosion rates not only results from different experimental set-ups but also from the different techniques used. For those areas of the

tested slope where the different techniques can be directly compared we could identify substantial differences in soil translocation rates per tillage pass (upper trench: 106 to 170 kg m⁻¹ per pass, difference 60%; lower trench: 81 to 176 kg m⁻¹ per pass, difference 118%; Fig. 5.8). Comparing the mean translocations rate from six measuring techniques and two tillage sequences against the corresponding individual measurements ranges from an underestimation of -32.8 kg m⁻¹ (-21.6%) to an overestimation of 41.3 kg m⁻¹ (33.6%). When using experimental results to parametrize tillage erosion models (Dlugoß et al., 2012; Van Oost et al., 2005b), these measurement uncertainties need to be added to uncertainties based on the transfer of measured tillage erosion rates from one test site to another modelling region. The relevance of this uncertainty was recently illustrated by Wilken et al. (2017b), who coupled a water and tillage erosion and soil organic carbon model to analyse erosion-induced carbon (C) fluxes in a small catchment. Varying tillage erosion by $\pm 50\%$ substantially changed the modelled erosion-induced C balance of the catchment, which was overall more important for the C balance than water erosion (Wilken et al., 2017b). In general, it can be concluded that tillage erosion measurement uncertainties of the magnitude found in this study can substantially affect results of studies dealing with erosion-induced changes in soil properties of arable land.

5.4.2 Specific uncertainties of different tillage erosion measuring techniques

Micro-tracer methods disturb the natural soil structure as a trench is filled with artificial or artificially manipulated soil material. This causes uncertainties regarding the transport and mixing properties of the tracer particles into the natural soil structure. If applied in a trench, the fluorescent tracer concentration can reach the detectable saturation level. In consequence, the peak concentration might not be accurately determined and causes uncertainties in the translocation calculation, which is based on fluorescence intensity proportions. RFID macro-tracers enable the tracking of individual particles at distinct slope positions. However, the experiment showed $26\pm 12\%$ lower translocation distances determined by the stone-sized RFID macro-tracers compared to soil-sized micro-tracers (Table 5.2). This calls the general assumption that tillage erosion is a non-selective process of homogenous movement throughout the tillage layer into question. Few studies already speculated about different transport distances between soil and stone sized tracers (Barneveld et al., 2009; Dupin et al., 2009; Logsdon, 2013), but did not investigate this in detail. Nevertheless, it is likely that a potential grain size selectivity of tillage erosion is affected by soil conditions and tillage implement type. Soil cohesiveness may control whether the soil is disrupted and selectively mixed or homogeneously transported in large

clods that encapsulate stone-sized particles. Due to a series of tillage operations under rather dry conditions, the soil was highly disrupted during the experiment, which might have supported selectivity compared to a single tillage operation. Furthermore, a potential grain size selectivity of tillage translocation is likely to be tillage implement specific as some implements are designed to invert topsoil and not to disrupt and entirely mix it. High-resolution topography change measurements can provide spatial movement of the tillage layer and are not affected by potential grain size selective transport. However, the technique needs to be corrected for elevation changes related to bulk density differences that are subject to spatial variations (Gifford and Roderick, 2003). As TLS and UAS/SfM devices are based on optical techniques, information gaps occur behind objects leading to shaded areas. Due to soil surface roughness, the shaded areas become larger with increasing distance to the scan device as the incidence angle of the laser beam becomes smaller (Fig. 5.9). Due to the linear interpolation of shaded areas, the TLS scanners systematically overestimate the elevation of remote scan positions. As illustrated in Figure 5.9 this effect increases with increasing surface roughness. Due to the smooth rolled soil surface (about 2.5 cm roughness), the wheel tracks were the most problematic element in this study. This is especially true as the depths of the wheel tracks were deeper at t_0 because of a very loose soil following the pre-experimental mouldboard ploughing and rolling. The consequence was that the long range scans with the Leica, from two positions only (Fig. 5.1), could only partly see into the wheel tracks, and therefore potentially underestimates deposition in these wheel tracks between t_0 and t_1 , and hence overestimate erosion rates. In general, an image acquisition from nadir that prevents flat incidence angles is a major advantage of the UAS/SfM technique (Fig. 5.9).

To unify different TLS scenes or photogrammetric images, georeferenced ground control points (GCPs) are required. On arable land, plane surfaces or clear structures are not present and scene overlay depends on GCPs. As TLS devices operate from a static position on ground, less GCP are required compared

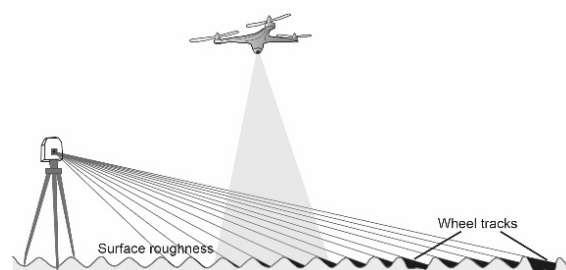


Figure 5.9: Schematic figure of scan angle and shadowing effect of the laser scanners compared to UAV/SfM.

to the moving UAV/SfM. Hence, a dense network of GCPs is of key importance for an UAV/SfM approach on arable land to measure tillage erosion. In this experiment the UAS/SfM approach lead to similar patterns but showed an elevation offset compared to

the TLS measurements. This somewhat unsatisfactory result might be improved using more GCPs or add stable linear features along the measuring plot, which improved SfM processing. However, it was challenging to detect small (< 1 cm) changes in topography if these changes had not resulted from changes in linear features (e.g. erosion rills), which makes a change detection easier. Similar problems in detecting changes on non-linear soil erosion features were shown in a UAS/SfM study of Pineux et al. (2017).

Based on our experiment it was not possible to determine one measuring technique as benchmark as all applied techniques are subject to different technique-specific error sources. However, it is clear that using only one technique to determine tillage erosion, as done in the majority of studies, will lead to large uncertainties in calculated tillage erosion rates.

5.5 Conclusions

Under controlled conditions, different tillage translocation measuring techniques (three tracers and three topographical methods) were applied in a macro-plot experiment with two tillage sequences each consisting of seven tillage operations. The different techniques produce a relatively wide range of soil translocation rates for the same slope positions, with deviations to the mean of all measurements between -32.8 kg m^{-1} (-21.6%) and 41.3 kg m^{-1} (33.6%). This large measurement-induced variation indicates substantial uncertainties in determining tillage erosion, which points to the need to utilise more than one method in tillage erosion studies. The associated uncertainty should be especially taken into account if using results of tillage erosion experiments to parameterize models. All used techniques have potential error sources, which could not be individually quantified. Hence, no benchmark result could be obtained, which probably makes the mean translocation rate out of all six methods the most appropriate estimate. However, the consistently smaller translocation distances of the used macro-tracers, which were on average $26 \pm 12\%$ smaller than the translocation distance of the two micro-tracers, questions the general assumption of non-selective transport and homogenous movement of the tillage layer by management operations into question. At least under dry and disrupted soil conditions, as tested in this experiment, macro-tracers may not accurately represent the flux of soil-sized particles.

As compared to water erosion, there is still a lack in standardized measurements and the overall number of measurements for different management practices is relatively small, which makes a reasonable model parametrisation challenging. Overall, this study points

out that tillage erosion measurements, carried out under almost optimal conditions, are subject to major uncertainties that need to be carefully considered in soil erosion studies.

6 Summary and general discussion

Conflicting results have spurred an ongoing debate about the global role of soil erosion on soil organic carbon (SOC) dynamics. These uncertainties especially originate from insufficient input data and missing processes in soil erosion and SOC dynamics modelling. Within four articles, this PhD-thesis addresses uncertainties related to input data and missing processes in soil erosion and SOC dynamics modelling.

Article I deals with uncertainties in theoretical rainfall kinetic energy-intensity (KE-I) relations that are implemented in widely used soil erosion models (e.g. USLE; Wischmeier and Smith, 1978). Continuous direct measurements of rainfall kinetic energy (KE) are hardly available and need to be derived from rainfall intensity measurements. Due to large variations in drop size and fall velocity distributions, numerous KE-I relations were developed and calibrated for different meteorological regions. Within this study, a comparison of directly measured against derived rainfall KE based on 32 KE-I relations was carried out and applied on a USLE based model. The simulated sediment delivery showed a pronounced response to the different KE-I relations up to a 95% confidence interval from 13 to 27 Mg ha⁻¹ yr⁻¹. It was pointed out that no specific KE-I relation was able to perform equally good for each station and all types of rainfall events, which means that drop size and fall velocity distributions are highly dynamic and are not static for a meteorological region. Therefore, these large inter and intra rainfall event variations, which were also observed in an optical disdrometer study by Angulo-Martinez et al. (2016), and supports the findings of Salles et al. (2002) that KE-I relations are more suitable for specific rainfall types than for meteorological regions. Furthermore, a pronounced overestimation for all stations of the KE-I relations compared to the measured KE was found that is in line with the findings of Angulo-Martinez et al. (2016). These conflicting results are potentially caused by sub-terminal drops (also identified in other studies: Angulo-Martinez et al., 2016; Cerro et al., 1998; Montero-Martinez and Garcia-Garcia, 2016; Petan et al., 2010) that fall at slower speeds than predicted by traditional models of drop size (Marshall and Palmer, 1948) and fall velocity (Gunn and Kinzer, 1949) distributions. Modern ombrometers, which are less sensitive to measurement errors compared to the standard Hellmann tipping bucket rain gauges (e.g. wind drift, high intensities; Humphrey et al., 1997; Marsalek, 1981; Shedekar et al., 2016), potentially need a calibration for KE-I relationships developed from traditional measurements.

Article II assesses the role of an event-based preferential SOC transport and corresponding SOC enrichment in delivered sediments. Therefore, a unique 100-yrs high-resolution (10 min intervals) rainfall data set was simulated with the process-oriented MCST-C model in an arable catchment of the Belgian loess belt. The results are in line with the concept of selective interrill and non-selective rill erosion shown in numerous other studies (Kuhn et al., 2010; Polyakov and Lal, 2004b; Quinton et al., 2001; Schiettecatte et al., 2008b). Modelled SOC enrichment of small interrill dominated events are highest, where enrichment decreases with event size due to a higher contribution of rill erosion. Over the 100-yrs simulation period, small events accounted for substantially more (82%) SOC in delivered sediments compared to the parent soil concentration. Nevertheless, single extreme events are of high importance for sediment and SOC delivery, as 20 single events contributed to 63% and 44% of total sediment and SOC delivery, respectively. Monitoring studies by Steegen et al. (2000) and Fiener et al. (2008) support the important role of single events and emphasize the need for long-term observations of event-level processes on the long-term catchment carbon (C) balance. Ignoring SOC enrichment processes in soil erosion modelling leads to a substantial underestimation of delivered SOC that biases the results of large-scale modelling studies.

For the follow up publication of **Article III**, the MCST-C model was improved in order to represent various detailed soil erosion and SOC redistribution processes. To account for erosion-induced changes of vertical soil-atmosphere fluxes, the model was coupled to a tillage erosion (SPEROS-C: Van Oost et al. 2000, based on diffusion-type equation: Govers et al., 1997) and C turnover model (ICBM; Andr en and K atterer, 1997). For an isolated analysis on the effect of specific processes, simulation runs with altered or removed processes were compared against the reference run. These model based comparisons were applied on two catchments with different hydrological and sedimentological connectivity characteristics over an synthetic 50-yrs rainfall series. The first catchment is a single field with a relatively high connectivity to the outlet, where the connectivity of the second catchment is limited due to a grassed waterway established along the thalweg. The results are in line with Article II and show that lateral fluxes by water erosion are highly event driven as almost 60% of sediment delivery is based on three single events but small events show an enhanced contribution to SOC delivery (36% and 63%) in both catchments due to enrichment processes. C enrichment in delivered sediments is not only controlled by event size and type of erosion, but also by catchment connectivity properties. Due to the constantly high roughness and prevention of rill erosion in the grassed

waterway, coarse primary particles are deposited even at extreme events. This leads to a substantial reduction of delivered sediments, but also to constantly high SOC enrichment ratios as solely fine primary particles are transported to the outlet. Hence, the relevance of specific processes is also subject to catchment connectivity properties. In consequence, the contribution of rill erosion is much more important for the highly connected catchment as the rill network can emerge in close proximity to the outlet and therefore limits deposition. In contrast, alterations in grain size distribution based on soil aggregation show a larger response to the catchment of limited connectivity. This is caused by transport capacity limitations within the grassed waterway, which are not sufficient to transport soil aggregates or coarse particles to the outlet. Within the study site, soil conservation practices reduced water erosion (factor of about 20; Fiener and Auerswald, 2007a) much more efficient than tillage erosion (factor of about 3; Van Oost et al., 2006). Hence, the SOC sequestration potential of water erosion on vertical C fluxes was mainly lower compared to tillage erosion as tillage translocation caused the majority of on-site redistribution, occurred on a regular basis without sediment and SOC delivery. While the highly connected catchment is for most scenarios a C source for the atmosphere, the catchment of limited connectivity is a C sink due to substantial tillage-induced SOC sequestration that offsets the reduced sediment delivery by the grassed waterway. It was shown that distinct erosion processes have a pronounced effect on SOC delivery and turnover that needs to be addressed in large-scale modelling approaches for an appropriate simulation of the catchment C balance.

Article IV: Numerous experimentally determined tillage transport coefficients for different tillage implements and practices are reported in literature with an average of 236 kg m^{-1} per pass and large variations $\pm 172 \text{ kg m}^{-1}$ per pass ($n=33$; Van Oost and Govers, 2006). As tillage erosion has shown to be a highly sensitive driver of erosion-induced C dynamics, an experiment was carried out to assess potential uncertainties in measuring techniques for the determination of tillage translocation. Within the experiment, two sequences of seven downslope tillage operations were applied on a $15 \times 85 \text{ m}$ plot. Tillage translocation was measured using two soil-sized micro-tracers and a stone-sized macro-tracer. Topographical changes were determined using two terrestrial laser scanners (TLS) and unmanned aerial system based structure from motion (UAS/SfM) techniques. The general assumption of a non-selective transport of the tillage layer is called into question due to consistently shorter translocation distances by the stone-sized

macro tracers compared to the soil-sized micro tracers. This study provides first evidence for different transport distances related to the tracer size that was already hypothesized in a few studies (Barneveld et al., 2009; Dupin et al., 2009; Logsdon, 2013). Under controlled conditions, the relative deviation to the mean result of all measurement techniques range from -21.6% to 33.6%. These substantial measuring-induced differences point at large parametrization uncertainties, which need to be carefully taken into account for soil erosion and SOC dynamics modelling.

This PhD-thesis contributes to the debate about the role of soil erosion on SOC dynamics and addresses uncertainties that enhance conflicting results. Global approaches for soil erosion and SOC dynamics modelling lacks appropriate data with sufficient spatio-temporal resolution. However, even under controlled conditions of field and plot scale studies large uncertainties are found. These uncertainties are based on assumptions (e.g. selection of most suitable KE-I relation), input data (e.g. tillage erosion parametrization) and missing processes that lead to fundamental differences in simulated results. Nearing et al. (1999) showed in a replicated field plot experiment a range in the coefficient of variation between the replicates from 14% to 150% for heavy and small events, respectively. This problem illustrates the large unknown variability of soil erosion with complex micro-scale processes at play that cannot be taken into account. This plot scale variability can be assumed to be averaged out under spatio-temporal aggregation (Wendt et al., 1986). Hence, process-oriented soil erosion and C dynamics modelling needs to strengthen the process understanding to develop robust generalizations to bridge the gap between spatio-temporal scales of short-term processes and their effects on long-term SOC dynamics that can be applied in large scale studies.

7 Conclusion and outlook

Uncertainties in input data and oversimplifications in soil erosion and carbon (C) dynamics modelling were identified and quantified. Therefore, deviations between directly measured and derived kinetic energies (KE) on sediment delivery were assessed. Subsequently, the process-oriented water erosion model MCST was coupled to a tillage (SPEROS-C) and C turnover (ICBM) model. The model was successfully validated and used to quantify potential uncertainties regarding specific sediment and soil organic carbon (SOC) redistribution processes. An insight on uncertainties in tillage erosion measurements was achieved by a plot experiment utilizing various tracers and topographical measuring techniques.

The main findings of this PhD thesis are (i) a distinct overestimation of the KE-I relations in comparison between the directly measured and derived KE. This suggests that traditional KE-I relations need to be calibrated for modern ombrometer measurements. (ii) It was indicated that drop size and fall velocity distributions are highly dynamic and do not necessarily correspond to the meteorological region but rather to the type of rainfall. Hence, the selection of the most appropriate KE-I relation should be individually selected for the type of rainfall event. (iii) Both modelling studies distinctively pointed out the important role of event-based water erosion modelling as grain size selective transport and deposition causes substantially more SOC delivery compared to widely used static average erosion rates with assumed parent soil SOC concentrations. (iv) Soil physical properties like the characteristic proportion of interrill vs. rill erosion and soil aggregation substantially alter sediment and SOC delivery. (v) The relevance of process-oriented modelling on global scale was shown, but cannot be achieved as data and computational requirements cannot be matched. Hence, event-based processes need to be highly generalized and implemented to conceptual models that are suitable for large-scale simulations. (vi) It was shown that the effect of water erosion on vertical C fluxes can be minor (e.g. under soil conservation practices), where tillage erosion has major impact on vertical C fluxes with a pronounced SOC sequestration potential. The results of this thesis suggest that tillage erosion has to be taken into account for accurate projections on erosion-induced SOC dynamics. (vii) However, measurements of tillage translocation are subject to uncertainties that can have substantial impact on the results of soil erosion and C dynamics modeling.

Uncertainties originating from input data and ignored process-level control mechanisms in soil erosion and C dynamics modelling are far from negligible. Global soil erosion and C dynamics modelling faces the task of generalizing and implementing complex processes to conceptual models.

References

- Aldana-Jague, E., Sommer, M., Saby, N. P. A., Cornelis, J. T., Van Wesemael, B., and Van Oost, K.: High resolution characterization of the soil organic carbon depth profile in a soil landscape affected by erosion, *Soil & Tillage Research*, 156, 185-193, 2016.
- Amundson, R., Berhe, A. A., Hopmans, J. W., Olson, C., Sztein, A. E., and Sparks, D. L.: Soil and human security in the 21st century, *Science*, 348, 2015.
- Andr n, O. and K tterer, T.: ICBM: The introductory carbon balance model for exploration of soil carbon balances, *Ecological Applications*, 7, 1226-1236, 1997.
- Angers, D. A. and Mehuys, G. R.: Effects of cropping on macro-aggregation of a marine clay soil, *Canadian Journal of Soil Science*, 68, 723-732, 1988.
- Angulo-Martinez, M., Begueria, S., and Kysely, J.: Use of disdrometer data to evaluate the relationship of rainfall kinetic energy and intensity (KE-I), *Science of the Total Environment*, 568, 83-94, 2016.
- Auerswald, K., Albrecht, H., Kainz, M., and Pfadenhauer, J.: Principles of sustainable land-use systems developed and evaluated by the Munich Research Alliance on agro-ecosystems (FAM), *Petermanns Geographische Mitteilungen*, 144, 16-25, 2000.
- Auerswald, K., Fiener, P., and Dikau, R.: Rates of sheet and rill erosion in Germany - A meta-analysis, *Geomorphology*, 111, 182-193, 2009.
- Auerswald, K. and Weigand, S.: Eintrag und Freisetzung von P durch Erosionsmaterial in Oberfl chengew ssern, *VDLUFA-Schriftenreihe*, 50, 37-54, 1999.
- Aufdenkampe, A. K., Mayorga, E., Raymond, P. A., Melack, J. M., Doney, S. C., Alin, S. R., Aalto, R. E., and Yoo, K.: Riverine coupling of biogeochemical cycles between land, oceans, and atmosphere, *Frontiers in Ecology and the Environment*, 9, 53-60, 2011.
- Baeyens, L.: Verklarende tekst bij het kaartblad Tervuren 102E. Bodemkaart van Belgie, Geologisch-Instituut, Gent, Belgium, 1959.
- Bakker, M. M., Govers, G., Van Doorn, A., Quetier, F., Chouvardas, D., and Rounsevell, M.: The response of soil erosion and sediment export to land-use change in four areas of Europe: The importance of landscape pattern, *Geomorphology*, 98, 213-226, 2008.
- Barneveld, R., Bruggeman, A., Sterk, G., and Turkelboom, F.: Comparison of two methods for quantification of tillage erosion rates in olive orchards of north-west Syria, *Soil & Tillage Research*, 103, 105-112, 2009.
- Battin, T. J., Luysaert, S., Kaplan, L. A., Aufdenkampe, A. K., Richter, A., and Tranvik, L. J.: The boundless carbon cycle, *Nature Geoscience*, 2, 598-601, 2009.
- Bentley, W.: Studies of raindrops and raindrop phenomena, *Monthly Weather Review*, 10, 450-456, 1904.
- Berhe, A. A., Harden, J. W., Torn, M. S., and Harte, J.: Linking soil organic matter dynamics and erosion-induced terrestrial carbon sequestration at different landform positions, *Journal of Geophysical Research*, 113, G04039, 2008.
- Berhe, A. A., Harte, J., Harden, J. W., and Torn, M. S.: The significance of the erosion-induced terrestrial carbon sink, *Bioscience*, 57, 337-346, 2007.
- Beuselinck, L., Govers, G., Hairsine, P. B., Sander, G. C., and Breynaert, M.: The influence of rainfall on sediment transport by overland flow over areas of net deposition, *Journal of Hydrology*, 257, 145-163, 2002a.
- Beuselinck, L., Govers, G., Steegen, A., and Quine, T. A.: Sediment transport by overland flow over an area of net deposition, *Hydrological Processes*, 13, 2769-2782, 1999.
- Beuselinck, L., Hairsine, P. B., Sander, G. C., and Govers, G.: Evaluating a multiclass net deposition equation in overland flow conditions, *Water Resources Research*, 38, 1-11, 2002b.
- Beuselinck, L., Steegen, A., Govers, G., Nachtergaele, J., Takken, I., and Poesen, J.: Characteristics of sediment deposits formed by intense rainfall events in small catchments in the Belgian Loam Belt, *Geomorphology*, 32, 69-82, 2000.
- BGR: Erodierbarkeit der Ackerb den durch Wasser in Deutschland, Bundesanstalt f r Geowissenschaften und Rohstoffe, 2014.

- Billings, S. A., Buddemeier, R. W., Richter, D., Van Oost, K., and Bohling, G.: A simple method for estimating the influence of eroding soil profiles on atmospheric CO₂, *Global Biogeochemical Cycles*, 24, 1-14, 2010.
- Brandt, J.: Simulation of the size distribution and erosivity of raindrops and throughfall drops, *Earth Surface Processes and Landforms*, 15, 687-698, 1990.
- Brown, L. C. and Foster, G. R.: Storm erosivity using idealized intensity distributions, *Transactions of the American Society of Agricultural Engineers*, 30, 379-386, 1987.
- Carter, C. E., Greer, J. D., Braud, H. J., and Floyd, J. M.: Raindrop characteristics in South Central United States, *Transactions of the American Society of Agricultural Engineers*, 17, 1033-1037, 1974.
- Casagrande, A.: Die Aräometermethode zur Bestimmung der Korngrößenverteilung von Böden, Arthur Casagrande, Berlin, 1934.
- Cerro, C., Bech, J., Cordina, B., and Lorente, J.: Modeling rain erosivity using disdrometric techniques, *Soil Science Society of America Journal*, 62, 731-735, 1998.
- Chabbi, A., Lehmann, J., Ciais, P., Loescher, H. W., Cotrufo, M. F., Don, A., SanClements, M., Schipper, L., Six, J., Smith, P., and Rumpel, C.: Aligning agriculture and climate policy, *Nature Clim. Change*, 7, 307-309, 2017.
- Chappell, A., Baldock, J., and Sanderman, J.: The global significance of omitting soil erosion from soil organic carbon cycling schemes, *Nature Clim. Change*, 6, 187-191, 2016.
- Coote, D. R., Malcolm-McGovern, C. A., Wall, G. J., Dickinson, W. T., and Rudra, R. P.: Seasonal variation of erodibility indices based on shear strength and aggregate stability in some Ontario soils, *Canadian Journal of Soil Science*, 68, 405-416, 1988.
- Coutinho, M. A. and Tomas, P. P.: Characterization of raindrop size distributions at the Vale Formoso Experimental Erosion Center, *Catena*, 25, 187-197, 1995.
- d'Oleire-Oltmanns, S., Marzloff, I., Peter, K. D., and Ries, J. B.: Unmanned aerial vehicle (UAV) for monitoring soil erosion in Morocco, *Remote Sensing*, 4, 3390-3416, 2012.
- De Alba, S., Borselli, L., Torri, D., Pellegrini, S., and Bazzoffi, P.: Assessment of tillage erosion by mouldboard plough in Tuscany (Italy), *Soil & Tillage Research*, 85, 123-142, 2006.
- De Alba, S., Lindstrom, M., and Schumacher, T. E.: Soil landscape evolution due to soil redistribution by tillage: a new conceptual model of soil catena evolution in agricultural landscapes, *Catena*, 58, 77-100, 2004.
- De Roo, A. P., Wesseling, C. G., and Ritsema, C. J.: LISEM: A single-event physically based hydrological and soil erosion model for drainage basins. I: Theory, input and output, *Hydrological Processes*, 10, 1107-1117, 1996.
- De Vente, J., Poesen, J., Arabkhedri, M., and Verstraeten, G.: The sediment delivery problem revisited, *Progress in Physical Geography*, 31, 155-178, 2007.
- De Vente, J., Poesen, J., Verstraeten, G., Van Rompaey, A., and Govers, G.: Spatially distributed modelling of soil erosion and sediment yield at regional scale in Spain, *Global and Planetary Change*, 60, 393-415, 2008.
- Denef, K., Six, J., Merckx, R., and Paustian, K.: Short-term effects of biological and physical forces on aggregate formation in soils with different clay mineralogy, *Plant and Soil*, 246, 185-200, 2002.
- Desmet, P. J. J. and Govers, G.: Two-dimensional modelling of the within-field variation in rill and gully geometry and location related to topography, *Catena*, 29, 283-306, 1997.
- Deumlich, D.: Erosive Niederschläge und ihre Eintrittswahrscheinlichkeit im Norden Deutschlands, *Meteorologische Zeitschrift*, 8, 155-161, 1999.
- Deumlich, D., Dannowski, R., and Völker, L.: Historische und aktuelle Geoinformation - Grundlage in der Agrarlandschaftsforschung *Zeitschrift für Geodäsie, Geoinformation und Landmanagement*, 139, 329-341, 2014.
- Dietrich, W.: Settling velocity of natural particles, *Water Resources Research*, 18, 1615-1626, 1982.
- DIN: DIN ISO 11277: 2002-08 Bodenbeschaffenheit - Bestimmung der Partikelgrößenverteilung in Mineralböden - Verfahren mittels Siebung und Sedimentation, Beuth Verlag, Berlin, 2002.
- Dlugoß, V., Fiener, P., and Schneider, K.: Layer-specific analysis and spatial prediction of soil organic carbon using terrain attributes and erosion modeling, *Soil Science Society of America Journal*, 74, 922-935, 2010.

- Dlugoß, V., Fiener, P., Van Oost, K., and Schneider, K.: Model based analysis of lateral and vertical soil C fluxes induced by soil redistribution processes in a small agricultural watershed, *Earth Surface Processes and Landforms*, 37, 193-208, 2012.
- Doetterl, S., Berhe, A. A., Nadeu, E., Wang, Z., Sommer, M., and Fiener, P.: Erosion, deposition and soil carbon: A review on process-level controls, experimental tools and models to address C cycling in dynamic landscapes, *Earth-Science Reviews*, 154, 102-122, 2016.
- Doetterl, S., Cornelis, J. T., Six, J., Bodé, S., Opfergelt, S., Boeckx, P., and Van Oost, K.: Soil redistribution and weathering controlling the fate of geochemical and physical carbon stabilization mechanisms in soils of an eroding landscape, *Biogeosciences*, 12, 1357-1371, 2015.
- Doetterl, S., Six, J., Van Wesemael, B., and Van Oost, K.: Carbon cycling in eroding landscapes: geomorphic controls on soil organic C pool composition and C stabilization, *Global Change Biology*, 18, 2218-2232, 2012a.
- Doetterl, S., Van Oost, K., and Six, J.: Towards constraining the magnitude of global agricultural sediment and soil organic carbon fluxes, *Earth Surface Processes and Landforms*, 37, 642-655, 2012b.
- Dupin, B., de Rouw, A., Phantahvong, K. B., and Valentin, C.: Assessment of tillage erosion rates on steep slopes in northern Laos, *Soil & Tillage Research*, 103, 119-126, 2009.
- Eltner, A. and Baumgart, P.: Accuracy constraints of terrestrial Lidar data for soil erosion measurement: Application to a Mediterranean field plot, *Geomorphology*, 245, 243-254, 2015.
- Eltner, A., Baumgart, P., Maas, H. G., and Faust, D.: Multi-temporal UAV data for automatic measurement of rill and interrill erosion on loess soil, *Earth Surface Processes and Landforms*, 40, 741-755, 2015.
- Erol, A., Koskan, O., and Basaran, M. A.: Socioeconomic modifications of the universal soil loss equation, *Solid Earth*, 6, 1025-1035, 2015.
- Fiener, P. and Auerswald, K.: Effectiveness of grassed waterways in reducing runoff and sediment delivery from agricultural watersheds, *Journal of Environmental Quality*, 32, 927-936, 2003.
- Fiener, P. and Auerswald, K.: Möglichkeiten der Abfluss- und Stofftransportkontrolle durch landwirtschaftliche Maßnahmen und ihre Kombination im Landschaftsmaßstab, *Rostock 2007*, 2007a, 23-36.
- Fiener, P. and Auerswald, K.: Rotation effects of potato, maize and winter wheat on soil erosion by water, *Soil Science Society of America Journal*, 71, 1919-1925, 2007b.
- Fiener, P., Dlugoß, V., and Van Oost, K.: Erosion-induced carbon redistribution, burial and mineralisation - Is the episodic nature of erosion processes important?, *Catena*, 133, 282-292, 2015.
- Fiener, P., Govers, G., and Van Oost, K.: Evaluation of a dynamic multi-class sediment transport model in a catchment under soil-conservation agriculture, *Earth Surface Processes and Landforms*, 33, 1639-1660, 2008.
- Fornis, R. L., Vermeulen, H. R., and Nieuwenhuis, J. D.: Kinetic energy-rainfall intensity relationship for Central Cebu, Philippines for soil erosion studies, *Journal of Hydrology*, 300, 20-32, 2005.
- Foster, G. R., Young, R. A., and Neibling, W. H.: Sediment composition for nonpoint source pollution analyses, *Transactions of the American Society of Agricultural Engineers*, 28, 133-139, 1985.
- Franzluebbers, A. J.: Achieving soil organic carbon sequestration with conservation agricultural systems in the southeastern United States, *Soil Science Society of America Journal*, 74, 347-357, 2010.
- Friedlingstein, P., Andrew, R. M., Rogelj, J., Peters, G. P., Canadell, J. G., Knutti, R., Luderer, G., Raupach, M. R., Schaeffer, M., van Vuuren, D. P., and Le Quere, C.: Persistent growth of CO₂ emissions and implications for reaching climate targets, *Nature Geoscience*, 7, 709-715, 2014.
- Galdino, S., Sano, E. E., Andrade, R. G., Grego, C. R., Nogueira, S. F., Bragantini, C., and Flosi, A. H. G.: Large-scale modeling of soil erosion with RUSLE for conservationist planning of degraded cultivated brazilian pastures, *Land Degradation & Development*, 27, 773-784, 2016.

- Gerke, H. H. and Hierold, W.: Vertical bulk density distribution in C-horizons from marley till as indicator for erosion history in a hummocky post-glacial soil landscape, *Soil & Tillage Research*, 125, 116-122, 2012.
- Gerke, H. H., Koszinski, S., Kalettka, T., and Sommer, M.: Structures and hydrologic function of soil landscapes with kettle holes using an integrated hydropedological approach, *Journal of Hydrology*, 393, 123-132, 2010.
- Gifford, R. M. and Roderick, M. L.: Soil carbon stocks and bulk density: spatial or cumulative mass coordinates as a basis of expression?, *Global Change Biology*, 9, 1507-1514, 2003.
- Gillijns, K., Poesen, J., and Deckers, J.: On the characteristics and origin of closed depressions in loess-derived soils in Europe - A case study from central Belgium, *Catena*, 60, 43-58, 2005.
- Giménez, R. and Govers, G.: Flow detachment by concentrated flow on smooth and irregular beds, *Soil Science Society of America Journal*, 66, 1475-1483, 2002.
- Govers, G.: Relationship between discharge, velocity and flow area for rills eroding loose, non-layered materials, *Earth Surface Processes and Landforms*, 17, 515-528, 1992.
- Govers, G.: Selectivity and transport capacity of thin flows in relation to rill erosion, *Catena*, 12, 35-49, 1985.
- Govers, G., Lobb, D. A., and Quine, T. A.: Preface - Tillage erosion and translocation: emergence of a new paradigm in soil erosion research, *Soil & Tillage Research*, 51, 167-174, 1999.
- Govers, G., Quine, T. A., Desmet, P. J. J., and Walling, D. E.: The relative contribution of soil tillage and overland flow erosion to soil redistribution on agricultural land, *Earth Surface Processes and Landforms*, 21, 929-946, 1996.
- Govers, G., Quine, T. A., and Walling, D. E.: The effect of water erosion and tillage movement on hillslope profile development: a comparison of field observation and model results. In: *Farm land erosion in temperate plains environments and hills*, Wicherek, S. (Ed.), Elsevier, Amsterdam, 1993.
- Govers, G., Vandaele, K., Desmet, P., Poesen, J., and Bunte, K.: The role of tillage in soil redistribution on hillslopes, *European Journal of Soil Science*, 45, 469-478, 1994.
- Gregorich, E. G., Greer, K. J., Anderson, D. W., and Liang, B. C.: Carbon distribution and losses: erosion and deposition effects, *Soil & Tillage Research*, 47, 291-302, 1998.
- Gunn, R. and Kinzer, D.: The terminal velocity of fall for water droplets in stagnant air, *J. Meteorology*, 6, 243-248, 1949.
- Guzmán, G., Barron, V., and Gomez, J. A.: Evaluation of magnetic iron oxides as sediment tracers in water erosion experiments, *Catena*, 82, 126-133, 2010.
- Guzman, G., Laguna, A., Canasveras, J. C., Boulal, H., Barron, V., Gomez-Macpherson, H., Giraldez, J. V., and Gomez, J. A.: Study of sediment movement in an irrigated maize-cotton system combining rainfall simulations, sediment tracers and soil erosion models, *Journal of Hydrology*, 524, 227-242, 2015.
- Guzman, G., Vanderlinden, K., Giraldez, J. V., and Gomez, J. A.: Assessment of spatial variability in water erosion rates in an olive orchard at plot scale using a magnetic iron oxide tracer, *Soil Science Society of America Journal*, 77, 350-361, 2013.
- Hairsine, P. B., Beuselinck, L., and Sander, G. C.: Sediment transport through an area of net deposition, *Water Resources Research*, 38, Art. No. 1086 JUN, 2002.
- Hairsine, P. B., Moran, C. J., and Rose, C. W.: Recent developments regarding the influence of soil surface characteristics on overland flow and erosion, *Australian Journal of Soil Research*, 30, 249-264, 1992.
- Hairsine, P. B. and Rose, C. W.: Modeling water erosion due to overland flow using physical principles. 1. Sheet flow, *Water Resources Research*, 28, 237-243, 1992a.
- Hairsine, P. B. and Rose, C. W.: Modeling water erosion due to overland flow using physical principles. 2. Rill flow, *Water Resources Research*, 28, 245-250, 1992b.
- Hairsine, P. B. and Rose, C. W.: Rainfall detachment and deposition: Sediment transport in the absence of flow-driven processes, *Soil Science Society of America Journal*, 55, 320-324, 1991.
- Harden, J. W., Sharpe, J. M., Parton, W. J., Ojima, D. S., Fries, T. L., Huntington, T. G., and Dabney, S. M.: Dynamic replacement and loss of soil carbon by eroding cropland, *Global Biogeochemical Cycles*, 13, 885-901, 1999.
- Hardy, R. A., Pates, J. M., Quinton, J. N., and Coogan, M. P.: A novel fluorescent tracer for real-time tracing of clay transport over soil surfaces, *Catena*, 141, 39-45, 2016.

- Haynes, R. J.: Labile organic matter fractions as central components of the quality of agricultural soils: An overview. In: *Advances in Agronomy*, Vol 85, Sparks, D. L. (Ed.), *Advances in Agronomy*, 2005.
- Heckrath, G., Djurhuus, J., Quine, T. A., Van Oost, K., Govers, G., and Zhang, Y.: Tillage erosion and its effect on soil properties and crop yield in Denmark, *Journal of Environmental Quality*, 34, 312-324, 2005.
- Heckrath, G., Halekoh, U., Djurhuus, J., and Govers, G.: The effect of tillage direction on soil redistribution by mouldboard ploughing on complex slopes, *Soil & Tillage Research*, 88, 225-241, 2006.
- Herbrich, M., Gerke, H. H., Bens, O., and Sommer, M.: Water balance and leaching of dissolved organic and inorganic carbon of eroded Luvisols using high precision weighing lysimeters, *Soil & Tillage Research*, 165, 144-160, 2017.
- Hiederer, R. and Köchy, M.: *Global soil organic carbon estimates and the harmonized world soil database*, Publications Office of the EU, Luxembourg, 2011.
- Hinkle, S. E., Heermann, D. F., and Blue, M. C.: Falling water drop velocities at 1570 m (5150 ft) elevation, *Transactions of the ASAE*, 30, 15, 1987.
- Hooke, R. L.: On the history of humans as geomorphic agents, *Geology*, 28, 843-846, 2000.
- Houghton, R. A.: Balancing the global carbon budget, *Annual Review of Earth and Planetary Sciences*, 35, 313-347, 2007.
- Hu, Y. and Kuhn, N. J.: Aggregates reduce transport distance of soil organic carbon: Are our balances correct?, *Biogeosciences*, 11, 6209-6219, 2014.
- Hu, Y. X., Berhe, A. A., Fogel, M. L., Heckrath, G. J., and Kuhn, N. J.: Transport-distance specific SOC distribution: Does it skew erosion induced C fluxes?, *Biogeochemistry*, 128, 339-351, 2016.
- Hu, Y. X. and Kuhn, N. J.: Erosion-induced exposure of SOC to mineralization in aggregated sediment, *Catena*, 137, 517-525, 2016.
- Humphrey, M. D., Istok, J. D., Lee, J. Y., Hevesi, J. A., and Flint, A. L.: A new method for automated dynamic calibration of tipping-bucket rain gauges, *Journal of Atmospheric and Oceanic Technology*, 14, 1513-1519, 1997.
- IPCC: *Climate change 2013: the physical science basis. Contribution of working group I to the fifth assessment report of the Intergovernmental Panel on Climate Change*, Cambridge University Press, Cambridge, United Kingdom and New York, NY, USA, 2013.
- IUSS: *World reference base for soil resources 2014. Update 2015. International soil classification system for naming soils and creating legends for soil maps. World Soil Resources Reports No. 106*, FAO, Rome, 2015.
- Jayawardena, A. W. and Rezaur, R. B.: Drop size distribution and kinetic energy load of rainstorms in Hong Kong, *Hydrological Processes*, 14, 1069-1082, 2000.
- Jobbágy, E. G. and Jackson, R. B.: The vertical distribution of soil organic carbon and its relation to climate and vegetation, *Ecological Applications*, 10, 423-436, 2000.
- John, B., Yamashita, T., Ludwig, B., and Flessa, H.: Storage of organic carbon in aggregate and density fractions of silty soils under different types of land use, *Geoderma*, 128, 63-79, 2005.
- Jordanova, D., Jordanova, N., Atanasova, A., Tsacheva, T., and Petrov, P.: Soil tillage erosion estimated by using magnetism of soils - A case study from Bulgaria, *Environmental Monitoring and Assessment*, 183, 381-394, 2011.
- Kätterer, T. and Andrén, O.: The ICBM family of analytically solved models of soil carbon, nitrogen and microbial biomass dynamics descriptions and application examples, *Ecological Modelling*, 136, 191-207, 2001.
- Kietzer, B.: *Soil translocation by tillage erosion in ground moraine landscapes of NE Germany*, 2007. Technical University Berlin, 147 pp., 2007.
- Kimaro, D. N., Deckers, J. A., Poesen, J., Kilasara, M., and Msanya, B. M.: Short and medium term assessment of tillage erosion in the Uluguru Mountains, Tanzania, *Soil & Tillage Research*, 81, 97-108, 2005.
- Kindler, R., Siemens, J., Kaiser, K., Walmsley, D. C., Bernhofer, C., Buchmann, N., Cellier, P., Eugster, W., Gleixner, G., Grunwald, T., Heim, A., Ibrom, A., Jones, S. K., Jones, M., Klumpp, K., Kutsch, W., Larsen, K. S., Lehuger, S., Loubet, B., McKenzie, R., Moors, E., Osborne, B., Pilegaard, K., Rebmann, C., Saunders, M., Schmidt, M. W. I., Schrupf, M.,

- Seyfferth, J., Skiba, U., Soussana, J. F., Sutton, M. A., Tefs, C., Vowinckel, B., Zeeman, M. J., and Kaupenjohann, M.: Dissolved carbon leaching from soil is a crucial component of the net ecosystem carbon balance, *Global Change Biology*, 17, 1167-1185, 2011.
- Kinnell, P. I. A.: Rainfall intensity-kinetic energy relationships for soil loss prediction, *Soil Science Society of America Journal*, 45, 153-155, 1981.
- Kirkels, F. M. S. A., Cammeraat, L. H., and Kuhn, N. J.: The fate of soil organic carbon upon erosion, transport and deposition in agricultural landscapes — A review of different concepts, *Geomorphology*, 226, 94-105, 2014.
- Kosmas, C., Gerontidis, S., Marathianou, M., Detsis, B., Zafiriou, T., Muysen, W. N., Govers, G., Quine, T. A., and Van Oost, K.: The effects of tillage displaced soil on soil properties and wheat biomass, *Soil & Tillage Research*, 58, 31-44, 2001.
- Kuhn, N. J., Armstrong, E. K., Ling, A. C., Connolly, K. L., and Heckrath, G.: Interrill erosion of carbon and phosphorus from conventionally and organically farmed Devon silt soils, *Catena*, 91, 94-103, 2010.
- Kuhn, N. J., Hoffmann, T., Schwanghart, W., and Dotterweich, M.: Agricultural soil erosion and global carbon cycle: controversy over?, *Earth Surface Processes and Landforms*, 34, 1033-1038, 2009.
- Lacoste, M., Viaud, V., Michot, D., and Walter, C.: Landscape-scale modelling of erosion processes and soil carbon dynamics under land-use and climate change in agroecosystems, *European Journal of Soil Science*, 66, 780-791, 2015.
- Lal, R.: Managing soils for food security and climate change, *Journal of Crop Improvement*, 19, 49-71, 2007.
- Lal, R.: Soil erosion and the global carbon budget, *Environment International*, 29, 437-450, 2003.
- Larsen, M. L., Kostinski, A. B., and Jameson, A. R.: Further evidence for superterminal raindrops, *Geophysical Research Letters*, 41, 6914-6918, 2014.
- Laws, J. O.: Measurements of the fall-velocity of water-drops and raindrops, *Transactions of the American Geophysical Union*, 22, 709-721, 1941.
- Laws, J. O. and Parsons, D. A.: The relation of raindrop-size to intensity, *Transactions of the American Geophysical Union*, 24, 452-459, 1943.
- Legout, C., Legu dois, S., and Le Bissonnais, Y.: Aggregate breakdown dynamics under rainfall compared with aggregate stability measurements, *European Journal of Soil Science*, 56, 225-237, 2005.
- Li, Y., Frielinghaus, M., Govers, G., Van Oost, K., Bork, H. R., Friedland, E. M., and Sch fer, H.: Spatial and temporal variations of tillage erosion at a moraine catena in NE Germany, *Leuven*, 1999, 1999, 42.
- Ligonja, P. J. and Shrestha, R. P.: Soil erosion assessment in Kondoa eroded area in Tanzania using universal soil loss equation, geographic information systems and socioeconomic approach, *Land Degradation & Development*, 26, 367-379, 2015.
- Lim, Y. S., Kim, J. K., Kim, J. W., Park, B. I., and Kim, M. S.: Analysis of the relationship between the kinetic energy and intensity of rainfall in Daejeon, Korea, *Quaternary International*, 384, 107-117, 2015.
- Lindstrom, M. J., Nelson, W. W., Schumacher, T. E., and Lemme, G. D.: Soil movement by tillage as affected by slope, *Soil and Tillage Research*, 17, 255-264, 1990.
- Liu, S., Bliss, N., Sundquist, E., and Huntington, T. G.: Modeling carbon dynamics in vegetation and soil under the impact of soil erosion and deposition, *Global Biogeochemical Cycles*, 17, 1074, 2003a.
- Liu, S. G., Bliss, N., Sundquist, E., and Huntington, T. G.: Modeling carbon dynamics in vegetation and soil under the impact of soil erosion and deposition, *Global Biogeochemical Cycles*, 17, 43-41-43-24, 2003b.
- Lobb, D. A., Kachanoski, R. G., and Miller, M. H.: Tillage translocation and tillage erosion in the complex upland landscapes of southwestern Ontario, Canada, *Soil and Tillage Research*, 51, 189-209, 1999.
- Lobb, D. A., Kachanoski, R. G., and Miller, M. H.: Tillage translocation and tillage erosion on shoulder slope landscape positions measured using CS-137 as a tracer, *Canadian Journal of Soil Science*, 75, 211-218, 1995.

- Logsdon, S. D.: Depth dependence of chisel plow tillage erosion, *Soil & Tillage Research*, 128, 119-124, 2013.
- Lopez-Vicente, M., Poesen, J., Navas, A., and Gaspar, L.: Predicting runoff and sediment connectivity and soil erosion by water for different land use scenarios in the Spanish Pre-Pyrenees, *Catena*, 102, 62-73, 2013.
- Lopez-Vicente, M., Quijano, L., Palazon, L., Gaspar, L., and Navas, A.: Assessment of soil redistribution at catchment scale by coupling a soil erosion model and a sediment connectivity index (Central Spanish Pre-Pyrenees), *Cuadernos De Investigacion Geografica*, 41, 127-147, 2015.
- Manies, K. L., Harden, J. W., Kramer, L., and Parton, W. J.: Carbon dynamics within agricultural and native sites in the loess region western Iowa, *Global Change Biology*, 7, 545-555, 2001.
- Marsalek, J.: Calibration of the tipping-bucket raingage, *Journal of Hydrology*, 53, 343-354, 1981.
- Marshall, J. S. and Palmer, W. M.: The distribution of raindrops with size, *Journal of Meteorology*, 5, 165-166, 1948.
- McGregor, K. C. and Mutchler, C. K.: Status of the R factor in the northern Mississippi. In: *Soil Erosion: Prediction Control*, Soil Conservation Society of America, Ankeny, Iowa, 1976.
- Menzel, R. G.: Enrichment ratios for water quality modeling. In: *CREAMS*, Knisel, W. G. (Ed.), USDA Cons. Res. Rep., 1980.
- Montanarella, L., Pennock, D. J., McKenzie, N., Badraoui, M., Chude, V., Baptista, I., Mamo, T., Yemefack, M., Singh Aulakh, M., Yagi, K., Young Hong, S., Vijarnsorn, P., Zhang, G. L., Arrouays, D., Black, H., Krasilnikov, P., Sobocká, J., Alegre, J., Henriquez, C. R., de Lourdes Mendonça-Santos, M., Taboada, M., Espinosa-Victoria, D., AlShankiti, A., AlaviPanah, S. K., Elsheikh, E. A. E. M., Hempel, J., Camps Arbestain, M., Nachtergaele, F., and Vargas, R.: World's soils are under threat, *SOIL*, 2, 79-82, 2016.
- Montero-Martinez, G. and Garcia-Garcia, F.: On the behaviour of raindrop fall speed due to wind, *Quarterly Journal of the Royal Meteorological Society*, 142, 2013-2020, 2016.
- Montgomery, D. R.: Soil erosion and agricultural sustainability, *Proceedings of the National Academy of Sciences of the United States of America*, 104, 13268-13272, 2007.
- Morgan, R. P. C.: *Soil erosion and conservation*, Blackwell Publishing, Oxford, 2005.
- Morgan, R. P. C., Quinton, J. N., Smith, R. E., Govers, G., Poesen, J. W. A., Auerswald, K., Chisci, G., Torri, D., and Styczen, M. E.: The European soil erosion model (EUROSEM): A dynamic approach for predicting sediment transport from fields and small catchments, *Earth Surface Processes and Landforms*, 23, 527-544, 1998.
- Myers, N.: *Gaia: An atlas of planet management*, Anchor Press, Garden City, 1993.
- Nadeu, E., Berhe, A. A., De Vente, J., and Boix-Fayos, C.: Erosion, deposition and replacement of soil organic carbon in Mediterranean catchments: a geomorphological, isotopic and land use change approach, *Biogeosciences*, 9, 1099-1111, 2012.
- Nadeu, E., Gobin, A., Fiener, P., Van Wesemael, B., and Van Oost, K.: Modelling the impact of agricultural management on soil carbon stocks at the regional scale: the role of lateral fluxes, *Global Change Biology*, 21, 3181-3192, 2015.
- Nash, J. E. and Sutcliffe, J. V.: River flow forecasting through conceptual models: Part I. A discussion of principles, *Journal of Hydrology*, 10, 282-290, 1970.
- Nearing, M. A., Foster, G. R., Lane, L. J., and Finkner, S. C.: A process-based soil erosion model for USDA-water erosion prediction project technology, *Transactions of the American Society of Agricultural Engineers*, 32, 1587-1593, 1989.
- Nearing, M. A., Govers, G., and Norton, D. L.: Variability in soil erosion data from replicated plots, *Soil Science Society of America Journal*, 63, 1829-1835, 1999.
- Nyssen, J., Vandenreyken, H., Poesen, J., Moeyersons, J., Deckers, J., Haile, M., Salles, C., and Govers, G.: Rainfall erosivity and variability in the Northern Ethiopian Highlands, *Journal of Hydrology*, 311, 172-187, 2005.
- Oades, J. M.: Soil organic matter and structural stability: mechanisms and implications for management, *Plant and Soil*, 76, 319-337, 1984.
- Oades, J. M. and Waters, A. G.: Aggregate hierarchy in soils, *Australian Journal of Soil Research*, 29, 815-828, 1991.

- Onaga, K., Shirai, K., and Yoshinaga, A.: Rainfall erosion and how to control its effects on farmland in Okinawa. In: Land conservation for future generation, Rimwanich, S. (Ed.), Department of Land Development, Bangkok, 1988.
- Park, S. W. and Mitchell, J. K.: An analysis of splash erosion mechanics, American Society of Agricultural Engineers Paper, 80-2502, 28, 1980.
- Parsons, A. J., Abrahams, A. D., and Luk, S.-H.: Hydraulics of interrill overland flow on a semi-arid hillslope, southern Arizona, *Journal of Hydrology*, 117, 255-273, 1990.
- Parton, W. J., Stewart, J. W. B., and Cole, C. V.: Dynamics of C, N, P and S in grassland soils: a model, *Biogeochemistry*, 5, 109-131, 1988.
- Petan, S., Rusjan, S., Vidmar, A., and Mikos, M.: The rainfall kinetic energy-intensity relationship for rainfall erosivity estimation in the mediterranean part of Slovenia, *Journal of Hydrology*, 391, 314-321, 2010.
- Peter, K. D., d'Oleire-Oltmanns, S., Ries, J. B., Marzolf, I., and Hssaine, A. A.: Soil erosion in gully catchments affected by land-levelling measures in the Souss Basin, Morocco, analysed by rainfall simulation and UAV remote sensing data, *Catena*, 113, 24-40, 2014.
- Pimentel, D.: Soil erosion: A food and environmental threat, *Environment, Development and Sustainability*, 8, 119-137, 2006.
- Pimentel, D. and Burgess, M.: Soil erosion threatens food production, *Agriculture*, 3, 443-463, 2013.
- Pimentel, D., Harvey, C., Resosudarmo, P., Sinclair, K., Kurz, D., McNair, M., Crist, S., Shpritz, L., Fitton, L., Saffouri, R., and Blair, R.: Environmental and economic costs of soil erosion and conservation benefits, *Science*, 267, 1117-1123, 1995.
- Pineux, N., Lisein, J., Swerts, G., Biielders, C. L., Lejeune, P., Colinet, G., and Degre, A.: Can DEM time series produced by UAV be used to quantify diffuse erosion in an agricultural watershed?, *Geomorphology*, 280, 122-136, 2017.
- Poesen, J.: An improved splash transport model, *Zeitschrift für Geomorphologie*, 29, 193-211, 1985.
- Poesen, J. and Savat, J.: Particle-size separation during erosion by splash and runoff. In: *Assessment of Erosion*, De Boodt, M. and Gabriels, D. (Eds.), Wiley, 1980.
- Polyakov, V. and Lal, R.: Modeling soil organic matter dynamics as affected by soil water erosion, *Environment International*, 30, 547-556, 2004a.
- Polyakov, V. O. and Lal, R.: Soil erosion and carbon dynamics under simulated rainfall, *Soil Science*, 169, 590-599, 2004b.
- Prechtel, A., von Lütow, M., Schneider, B. U., Bens, O., Bannick, C. G., Kögel-Knabner, I., and Hüttl, R. F.: Organic carbon in soils of Germany: Status quo and the need for new data to evaluate potentials and trends of soil carbon sequestration, *Journal of Plant Nutrition and Soil Science*, 172, 601-614, 2009.
- Quine, T. A., Desmet, P. J. J., Govers, G., Vandaele, K., and Walling, D. E.: A comparison of the roles of tillage and water erosion in landform development and sediment export on agricultural land near Leuven, Belgium, *IAHS Publications*, 224, 77-86, 1994.
- Quine, T. A. and Van Oost, K.: Quantifying carbon sequestration as a result of soil erosion and deposition: Restrospective assessment using caesium-137 and carbon inventories, *Global Change Biology*, 13, 2610-2625, 2007.
- Quine, T. A., Walling, D. E., and Govers, G.: Simulation of radiocaesium redistribution on cultivated hillslopes using a mass-balance model: An aid to process interpretation and erosion rate estimation. In: *Advances in hillslope processes*, Anderson, M. G. and Brooks, S. M. (Eds.), Wiley & Sons, Chichester, 1996.
- Quine, T. A. and Zhang, Y.: Re-defining tillage erosion: quantifying intensity-direction relationships for complex terrain. 2. Revised mouldboard erosion model, *Soil Use and Management*, 20, 124-132, 2004.
- Quinton, J. N., Catt, J. A., and Hess, T. M.: The selective removal of phosphorus from soil: is event size important?, *Journal of Environmental Quality*, 30, 538-545, 2001.
- Quinton, J. N., Govers, G., Van Oost, K., and Bardgett, R. D.: The impact of agricultural soil erosion on biogeochemical cycling, *Nature Geoscience*, 3, 311-314, 2010.
- Reichenau, T. G., Korres, W., Montzka, C., Fiener, P., Wilken, F., Stadler, A., Waldhoff, G., and Schneider, K.: Spatial heterogeneity of leaf area index (LAI) and its temporal course on arable

- land: Combining field measurements, remote sensing and simulation in a comprehensive data analysis approach (CDAA), *Plos One*, 11, 2016.
- Renard, K. G., Foster, G. R., Weesies, G. A., McCool, D. K., and Yoder, D. C.: Predicting soil erosion by water: A guide to conservation planning with the Revised Universal Soil Loss Equation (RUSLE), USDA-ARS, Washington DC, 1996.
- Renard, K. G., McCool, D. K., Cooley, K. R., Foster, G. R., Istok, J. D., and Mutchler, C. K.: Rainfall-runoff erosivity factor (R). In: Predicting soil erosion by water: A guide to conservation planning with the revised universal soil loss equation (RUSLE), Renard, K. G., Foster, G. R., Weesies, G. A., McCool, D. K., and Yoder, D. C. (Eds.), Agric. Handb. No. 703, U.S. Gov. Print Office, Washington D.C., 1997.
- Renwick, W. H., Smith, S. V., Sleezer, R. O., and Buddemeier, R. W.: Comment on "Managing soil carbon" (II), *Science*, 305, 2004.
- Römkens, M. J. M., Young, R. A., Poesen, J. W. A., McCool, D. K., El-Swaify, S. A., and Bradford, J. M.: Soil erodibility factor (K). In: Predicting soil erosion by water: A guide to conservation planning with the revised universal soil loss equation (RUSLE), Renard, K. G., Foster, G. R., Weesies, G. A., McCool, D. K., and Yoder, D. C. (Eds.), Agric. Handb. No. 703, U.S. Dep. Agric., Washington, 1997.
- Rosenbloom, N. A., Doney, S. C., and Schimel, D. S.: Geomorphic evolution of soil texture and organic matter in eroding landscapes, *Global Biogeochemical Cycles*, 15, 365-381, 2001.
- Rosewell, C. J.: Rainfall kinetic energy in Eastern Australia, *Journal of Applied Meteorology and Climatology*, 25, 1695-1701, 1986.
- Sadowski, H. and Sorge, B.: Der Normalhöhenpunkt von 1912 - Datumspunkt des DHHN 2012?, *Vermessung Brandenburg*, 2/2005, 31-39, 2005.
- Salles, C., Poesen, J., and Sempere-Torres, D.: Kinetic energy of rain and its functional relationship with intensity, *Journal of Hydrology*, 257, 256-270, 2002.
- Sanchez-Moreno, J. F., Mannaerts, C. M., Jetten, V., and Löffler-Mang, M.: Rainfall kinetic energy-intensity and rainfall momentum-intensity relationships for Cape Verde, *Journal of Hydrology*, 454, 131-140, 2012.
- Sanderman, J. and Berhe, A. A.: Biogeochemistry: The soil carbon erosion paradox, *Nature Clim. Change*, 7, 317-319, 2017.
- Scheinost, A. C., Sinowski, W., and Auerswald, K.: Regionalization of soil water retention curves in a highly variable soilscape, I. Developing a new pedotransfer function, *Geoderma*, 78, 129-143, 1997.
- Schiettecatte, W., Gabriels, D., Cornelis, W., and Hofman, G.: Impact of deposition on the enrichment of organic carbon in eroded sediment, *Catena*, 72, 340-347, 2008a.
- Schiettecatte, W., Gabriels, D., Cornelis, W. M., and Hofman, G.: Enrichment of organic carbon in sediment transport by interrill and rill erosion processes, *Soil Science Society of America Journal*, 72, 50-55, 2008b.
- Schlesinger, W. H.: Evidence from chronosequence studies for a low carbon-storage potential of soils, *Nature*, 354, 232-234, 1990.
- Schmidt, J.: A mathematical model to simulate rainfall erosion, *Catena Supplement*, 19, 101-109, 1991.
- Schwertmann, U., Vogl, W., and Kainz, M.: Bodenerosion durch Wasser - Vorhersage des Abtrags und Bewertung von Gegenmaßnahmen, Ulmer Verlag, Stuttgart, 1990.
- Sempere-Torres, D., Sanchez-Diezma, R., Zawadzki, I., and Creutin, J. D.: Identification of stratiform and convective areas using radar data with application to the improvement of DSD analysis and Z-R relations, *Physics and Chemistry of the Earth Part B-Hydrology Oceans and Atmosphere*, 25, 985-990, 2000.
- Sextstone, A. J., Revsbech, N. P., Parkin, T. B., and Tiedje, J. M.: Direct measurement of oxygen profiles and denitrification rates in soil aggregates, *Soil Science Society of America Journal*, 49, 645-651, 1985.
- Sharpley, A. N.: The selective erosion of plant nutrients in runoff, *Soil Science Society of America Journal*, 49, 1527-1534, 1985.
- Shedekar, V. S., King, K. W., Fausey, N. R., Soboyejo, A. B. O., Harmel, R. D., and Brown, L. C.: Assessment of measurement errors and dynamic calibration methods for three different tipping bucket rain gauges, *Atmospheric Research*, 178, 445-458, 2016.

- Sinowski, W. and Auerswald, K.: Using relief parameters in a discriminant analysis to stratify geological areas with different spatial variability of soil properties, *Geoderma*, 89, 113-128, 1999.
- Sinowski, W., Scheinost, A. C., and Auerswald, K.: Regionalization of soil water retention curves in a highly variable soilscape, II. Comparison of regionalization procedures using a pedotransfer function, *Geoderma*, 78, 145-159, 1997.
- Six, J., Bossuyt, H., Degryze, S., and Deneff, K.: A history of research on the link between (micro)aggregates, soil biota, and soil organic matter dynamics, *Soil & Tillage Research*, 79, 7-31, 2004.
- Six, J., Conant, R. T., Paul, E. A., and Paustian, K.: Stabilization mechanisms of soil organic matter: implications for C-saturation of soils, *Plant and Soil*, 241, 155-176, 2002.
- Smith, J. A. and De Veaux, R. D.: The temporal and spatial variability of rainfall power, *Environmetrics*, 3, 29-53, 1992.
- Smith, S. V., Renwick, W. H., Buddemeier, R. W., and Crossland, C. J.: Budgets of soil erosion and deposition for sediments and sedimentary organic carbon across the conterminous United States, *Global Biogeochemical Cycles*, 15, 697-707, 2001.
- Smith, S. V., Slezacek, R. O., Renwick, W. H., and Buddemeier, R. W.: Fates of eroded soil organic carbon: Mississippi basin case study, *Ecological Applications*, 15, 1929-1940, 2005.
- Sommer, M., Gerke, H. H., and Deumlich, D.: Modelling soil landscape genesis — A “time split” approach for hummocky agricultural landscapes, *Geoderma*, 145, 480-493, 2008.
- Stallard, R.: Terrestrial sedimentation and the carbon cycle: Coupling weathering and erosion to carbon burial, *Global Biogeochemical Cycles*, 12, 231-257, 1998.
- Steege, A., Govers, G., Nachtergaele, J., Takken, I., Beuselinck, L., and Poesen, J.: Sediment export by water from an agricultural catchment in the Loam Belt of central Belgium, *Geomorphology*, 33, 25-36, 2000.
- Steege, A., Govers, G., Takken, I., Nachtergaele, J., Poesen, J., and Merckx, R.: Factors controlling sediment and phosphorus export from two Belgian agricultural catchments, *Journal of Environmental Quality*, 30, 1249-1258, 2001.
- Steiner, M. and Smith, J. A.: Reflectivity, rain rate, and kinetic energy flux relationships based on raindrop spectra, *Journal of Applied Meteorology*, 39, 1923-1940, 2000.
- Thapa, B. B., Cassel, D. K., and Garrity, D. P.: Assessment of tillage erosion rates on steepland Oxisols in the humid tropics using granite rocks, *Soil & Tillage Research*, 51, 233-243, 1999.
- Thies-Clima: Laser Precipitation Monitor - Instructions for use, Thies-Clima, Göttingen, 2011.
- Tiessen, K. H. D., Mehuys, G. R., Lobb, D. A., and Rees, H. W.: Tillage erosion within potato production systems in Atlantic Canada - I. Measurement of tillage translocation by implements used in seedbed preparation, *Soil & Tillage Research*, 95, 308-319, 2007.
- Tisdall, J. M. and Oades, J. M.: Organic matter and water-stable aggregates in soils, *Journal of Soil Science*, 33, 141-163, 1982.
- Tranvik, L. J., Downing, J. A., Cotner, J. B., Loiselle, S. A., Striegl, R. G., Ballatore, T. J., Dillon, P., Finlay, K., Fortino, K., Knoll, L. B., Kortelainen, P. L., Kutser, T., Larsen, S., Laurion, I., Leech, D. M., McCallister, S. L., McKnight, D. M., Melack, J. M., Overholt, E., Porter, J. A., Prairie, Y., Renwick, W. H., Roland, F., Sherman, B. S., Schindler, D. W., Sobek, S., Tremblay, A., Vanni, M. J., Verschoor, A. M., Von Wachenfeldt, E., and Weyhenmeyer, G. A.: Lakes and reservoirs as regulators of carbon cycling and climate, *Limnology and Oceanography*, 54, 2298-2314, 2009.
- Turkelboom, F., Poesen, J., Ohler, I., VanKeer, K., Ongprasert, S., and Vlassak, K.: Assessment of tillage erosion rates on steep slopes in northern Thailand, *Catena*, 29, 29-44, 1997.
- Uijlenhoet, R. and Stricker, J. N. M.: A consistent rainfall parameterization based on the exponential raindrop size distribution, *Journal of Hydrology*, 218, 101-127, 1999a.
- Uijlenhoet, R. and Stricker, J. N. M.: Dependence of rainfall interception on drop size - a comment, *Journal of Hydrology*, 217, 157-163, 1999b.
- Usón, A. and Ramos, M. C.: An improved rainfall erosivity index obtained from experimental interrill soil losses in soils with a Mediterranean climate, *Catena*, 43, 293-305, 2001.
- Van Hemelryck, H., Fiener, P., Van Oost, K., Govers, G., and Merckx, R.: The effect of soil redistribution on soil organic carbon: an experimental study, *Biogeosciences*, 7, 3971-3986, 2010.

- Van Hemelryck, H., Govers, G., Van Oost, K., and Merckx, R.: Evaluating the impact of soil redistribution on the in situ mineralization of soil organic carbon, *Earth Surface Processes and Landforms*, 36, 427-438, 2011.
- Van Muysen, W. and Govers, G.: Soil displacement and tillage erosion during secondary tillage operations: the case of rotary harrow and seeding equipment, *Soil & Tillage Research*, 65, 185-191, 2002.
- Van Muysen, W., Govers, G., and Van Oost, K.: Identification of important factors in the process of tillage erosion: The case of mouldboard tillage, *Soil & Tillage Research*, 65, 77-93, 2002.
- Van Muysen, W., Govers, G., Van Oost, K., and Van Rompaey, A.: The effect of tillage depth, tillage speed, and soil condition on chisel tillage erosivity, *Journal of Soil and Water Conservation*, 55, 2-11, 2000.
- Van Oost, K., Beuselinck, L., Hairsine, P. B., and Govers, G.: Spatial evaluation of a multi-class sediment transport and deposition model, *Earth Surface Processes and Landforms*, 29, 1027-1044, 2004.
- Van Oost, K. and Govers, G.: Tillage erosion. In: *Soil erosion in Europe*, Boardman, J. and Poesen, J. (Eds.), Wiley, Chichester, 2006.
- Van Oost, K., Govers, G., Cerdan, O., Thauré, D., Van Rompaey, A., Steegen, A., Nachtergaele, J., Takken, I., and Poesen, J.: Spatially distributed data for erosion model calibration and validation: The Ganspoel and Kinderveld datasets, *Catena*, 61, 105-121, 2005a.
- Van Oost, K., Govers, G., De Alba, S., and Quine, T. A.: Tillage erosion: a review of controlling factors and implications for soil quality, *Progress in Physical Geography*, 30, 443-466, 2006.
- Van Oost, K., Govers, G., and Desmet, P.: Evaluating the effects of changes in landscape structure on soil erosion by water and tillage, *Landscape Ecology*, 15, 577-589, 2000a.
- Van Oost, K., Govers, G., Quine, T., Heckarth, G., Olesen, J. E., De Gryze, S., and Merckx, R.: Landscape-scale modeling of carbon cycling under the impact of soil redistribution: The role of tillage erosion, *Global Biogeochemical Cycles*, 19, 1-13, 2005b.
- Van Oost, K., Govers, G., and Van Muysen, W.: A process-based conversion model for caesium-137 derived erosion rates on agricultural land: An integrated spatial approach, *Earth Surface Processes and Landforms*, 28, 187-207, 2003.
- Van Oost, K., Govers, G., Van Muysen, W., and Quine, T. A.: Modelling translocation and dispersion of soil constituents by tillage on sloping land, *Soil Science Society of America Journal*, 64, 1733-1739, 2000b.
- Van Oost, K., Quine, T., Govers, G., and Heckrath, G.: Modeling soil erosion induced carbon fluxes between soil and atmosphere on agricultural land using SPEROS-C. In: *Advances in soil science. Soil erosion and carbon dynamics*, Roose, E. J., Lal, R., Feller, C., Barthes, B., and Stewart, B. A. (Eds.), CRC Press, Boca Raton, 2005c.
- Van Oost, K., Quine, T. A., Govers, G., De Gryze, S., Six, J., Harden, J. W., Ritchie, J. C., McCarty, G. W., Heckrath, G., Kosmas, C., Giraldez, J. V., Marques da Silva, J. R., and Merckx, R.: The impact of agricultural soil erosion on the global carbon cycle, *Science*, 318, 626-629, 2007.
- Van Rompaey, A., Bazzoffi, P., Jones, R. J. A., and Montanarella, L.: Modeling sediment yields in Italian catchments, *Geomorphology*, 65, 157-169, 2005.
- Van Rompaey, A. J. J., Verstraeten, G., Van Oost, K., Govers, G., and Poesen, J.: Modelling mean annual sediment yield using a distributed approach, *Earth Surface Processes and Landforms*, 26, 1221-1236, 2001.
- Vandaele, K., Vanommeslaeghe, J., Muylaert, R., and Govers, G.: Monitoring soil redistribution patterns using sequential aerial photographs, *Earth Surface Processes and Landforms*, 21, 353-364, 1996.
- VandenBygaart, A. J., Gregorich, E. G., and Helgason, B. L.: Cropland C erosion and burial: Is buried soil organic matter biodegradable?, *Geoderma*, 239, 240-249, 2015.
- Vanwalleghem, T., Jimenez-Hornero, F. J., Giraldez, J. V., and Laguna, A.: Simulation of long-term soil redistribution by tillage using a cellular automata model, *Earth Surface Processes and Landforms*, 35, 761-770, 2010.
- Verheijen, F. G. A., Jones, R. J. A., Rickson, R. J., and Smith, C. J.: Tolerable versus actual soil erosion rates in Europe, *Earth-Science Reviews*, 94, 23-38, 2009.

- Verstraeten, G., Poesen, J., Demarée, G., and Salles, C.: Long-term (105 years) variability in rain erosivity as derived from 10-min rainfall depth data for Ukkel (Brussels, Belgium): Implications for assessing soil erosion rates, *Journal of Geophysical Research*, 111, D22109, 2006.
- Verstraeten, G., Van Oost, K., Van Rompaey, A., Poesen, J., and Govers, G.: Evaluating an integrated approach to catchment management to reduce soil loss and sediment pollution through modelling, *Soil Use and Management*, 19, 386-394, 2002.
- Vieira, D. A. N. and Dabney, S. M.: Modeling edge effects of tillage erosion, *Soil & Tillage Research*, 111, 197-207, 2011.
- Vinci, A., Brigante, R., Todisco, F., Mannocchi, F., and Radicioni, F.: Measuring rill erosion by laser scanning, *Catena*, 124, 97-108, 2015.
- Vogel, E., Deumlich, D., and Kaupenjohann, M.: Bioenergy maize and soil erosion - Risk assessment and erosion control concepts, *Geoderma*, 261, 80-92, 2016.
- Von Lützw, M., Kögel-Knabner, I., Ekschmitt, K., Flessa, H., Guggenberger, G., Matzner, E., and Marschner, B.: SOM fractionation methods: Relevance to functional pools and to stabilization mechanisms, *Soil Biology & Biochemistry*, 39, 2183-2207, 2007.
- Walling, D. E. and Webb, B. W.: Erosion and sediment yield: a global overview. In: *Erosion and sediment yield: global and regional perspectives*, IAHS, 1996.
- Wang, X., Cammeraat, E. L., Romeijn, P., and Kalbitz, K.: Soil organic carbon redistribution by water erosion-the role of CO₂ emissions for the carbon budget, *Plos One*, 9, e96299, 2014a.
- Wang, X., Cammeraat, E. L. H., Cerli, C., and Kalbitz, K.: Soil aggregation and the stabilization of organic carbon as affected by erosion and deposition, *Soil Biology & Biochemistry*, 72, 55-65, 2014b.
- Wang, X., Cammeraat, L. H., Wang, Z., Zhou, J., Govers, G., and Kalbitz, K.: Stability of organic matter in soils of the belgian loess belt upon erosion and deposition, *European Journal of Soil Science*, 64, 219-228, 2013a.
- Wang, Z., Govers, G., Steegen, A., Clymans, W., Van den Putte, A., Langhans, C., Merckx, R., and Van Oost, K.: Catchment-scale carbon redistribution and delivery by water erosion in an intensively cultivated area, *Geomorphology*, 124, 65-74, 2010.
- Wang, Z., Govers, G., Van Oost, K., Clymans, W., Van den Putte, A., and Merckx, R.: Soil organic carbon mobilization by interrill erosion: Insights from size fractions, *Journal of Geophysical Research*, 118, 348-360, 2013b.
- Wang, Z. G., Hoffmann, T., Six, J., Kaplan, J. O., Govers, G., Doetterl, S., and Van Oost, K.: Human-induced erosion has offset one-third of carbon emissions from land cover change, *Nature Climate Change*, 7, 1-6, 2017.
- Wendt, R. C., Alberts, E. E., and Hjermfelt, A. T., Jr.: Variability of runoff and soil loss from fallow experimental plots, *Soil Science Society of America Journal*, 50, 730-736, 1986.
- Wiesner, J.: Beiträge zur Kenntnis des tropischen Regens, *Sitzungsber. Akad. Wiss. Wien*, 104, 1397-1434, 1895.
- Wilken, F., Fiener, P., and Van Oost, K.: Modelling a century of soil redistribution processes and carbon delivery from small watersheds using a multi-class sediment transport model, *Earth Surface Dynamics*, 5, 113-124, 2017a.
- Wilken, F., Sommer, M., Van Oost, K., Bens, O., and Fiener, P.: Process-oriented modelling to identify main drivers of erosion-induced carbon fluxes, *SOIL*, 3, 83-94, 2017b.
- Wilkinson, B. H. and McElroy, B. J.: The impact of humans on continental erosion and sedimentation, *Geological Society of America Bulletin*, 119, 140-156, 2007.
- Williams, J. R.: The EPIC model. In: *Computer models of watershed hydrology*, Singh, V. P. (Ed.), Water Resources Publications, Colorado, USA, 1995.
- Wischmeier, W. H. and Smith, D. D.: Predicting rainfall erosion losses - a guide to conservation planning, U.S. Gov. Print Office, Washington, DC, 1978.
- Wischmeier, W. H. and Smith, D. D.: Rainfall energy and its relationship to soil loss, *Transactions of the American Geophysical Union*, 39, 285-291, 1958.
- Wischmeier, W. H. and Smith, D. D.: A universal soil-loss equation to guide conservation farm planning, *Trans. Int. Congr. Soil Sci.*, 7th, 418-425, 1960.

- Yoo, K., Amundson, R., Heimsath, A. M., and Dietrich, W. E.: Erosion of upland hillslope soil organic carbon: Coupling field measurements with a sediment transport model, *Global Biogeochemical Cycles*, 19, GB 3003, 2005.
- Yu, B., Rose, C. W., Ciesiolka, C. A. A., Coughlan, K. J., and Fentie, B.: Toward a framework for runoff and soil loss prediction using GUEST technology, *Australian Journal of Soil Research*, 35, 1191-1212, 1997.
- Zanchi, C. and Torri, D.: Evaluation of rainfall energy in central Italy. John Wiley and Sons Ltd, Chichester, 1980.
- Zhang, J. H. and Li, F. C.: An appraisal of two tracer methods for estimating tillage erosion rates under hoeing tillage, *Environmental Engineering and Management Journal*, 10, 825-829, 2011.

List of tables

Article 1

2.1: Rainfall kinetic energy-intensity relations	13
2.2: Descriptive statistics of observed annual rainfall	14
2.3: Annual deviation of measured versus derived rainfall kinetic energy	20
2.4: Goodness of fit parameters of rainfall kinetic energy-intensity relations	22

Article 2

3.1: Parameter description and model setup	36
3.2: Study site and evaluation catchment description	39

Article 3

4.1: Parameter description and model setup	53
4.2: Experimental design of different model runs	56
4.3: Model validation	57

Article 4

5.1: Soil bulk density and stone content	71
5.2: Mean tracer translocation	78
5.3: Depth distribution of tracer translocation	79
5.4: Topographic changes	81

List of figures

1: Schematic TEROS project overview	3
-------------------------------------	---

Article 1

2.1: Rainfall kinetic energy-intensity relations	12
2.2: Topography and location of the study site	15
2.3: Measured drop size distribution	17
2.4: Measured proportions of individual drops and rainfall kinetic energies	18
2.5: Cumulative deviation of measured versus derived rainfall kinetic energy	19
2.6: Event based derived measured versus derived rainfall kinetic energy	21
2.7: Modelled uncertainty in annual sediment delivery	23
2.8: Cumulative spatial distribution of soil erosion and deposition	24

Article 2

3.1: Topography and location of the study site	35
3.2: Measured particle settling velocity distributions	38

3.3: Spatial erosion and deposition patterns _____	40
3.4: Event proportion of interrill erosion _____	41
3.5: Simulated and observed clay and carbon enrichment ratios _____	43
3.6: Cumulative erosion and delivery related to recurrence intervals _____	44

Article 3

4.1: Topography and location of the study site _____	49
4.2: Schematic overview of the MCST-C model _____	54
4.3: Topsoil grain size distribution _____	57
4.4: Spatial patterns of tillage and water erosion _____	58
4.5: Lateral and vertical carbon fluxes and carbon balance _____	59
4.6: Carbon enrichment in delivered sediments _____	60

Article 4

5.1: Test site and experimental setup _____	70
5.2: Applied cultivator and roller _____	71
5.3: Spatial translocation of the micro and macro tracers _____	76
5.4: Translocation of RFIDs _____	77
5.5: Tracer translocation _____	77
5.6: Soil depths-dependent translocation distance _____	78
5.7: Difference in topography from TLS and UAS/SfM _____	80
5.8: Soil translocation distance and rate _____	81
5.9: Scan angle related shadowing _____	84

Contribution of the author to the articles

Article I: The article was mainly written by Florian Wilken and Peter Fiener. The study was designed by Florian Wilken and Peter Fiener. All calculations were performed by Florian Wilken. The development of analysis tools was done by Florian Wilken with support from Martin Baur. Technical support and feedback to the article was provided by Michael Sommer, Detlef Deumlich and Oliver Bens.

Article II: The article was mainly written by Florian Wilken, Kristof van Oost and Peter Fiener. The study was designed by Kristof van Oost and Peter Fiener. Modelling was performed by Kristof van Oost. Analysis and data visualization was done by Florian Wilken and Kristof van Oost.

Article III: The article was mainly written by Florian Wilken and Peter Fiener. The study was designed by Florian Wilken and Peter Fiener. Model development of coupling the MCST and SPEROS-C model and further improvements were realized by Florian Wilken. Data analysis and visualization was done by Florian Wilken. Feedback to the article was provided by Michael Sommer, Kristof van Oost and Oliver Bens.

Article IV: The article was mainly written by Peter Fiener and Florian Wilken. The study design was developed by Peter Fiener, Florian Wilken and Michael Sommer. Tracer analysis was done by Peter Fiener. Topographical data analysis of terrestrial laser scanning and unmanned aerial system based structure from motion was done by Florian Wilken. Data visualization was done by Peter Fiener and Florian Wilken. Macro-tracer measurements were carried out by Florian Wilken and Peter Fiener. TLS measurements were carried out by Florian Wilken and Robert Wexler. TLS data post-processing was carried out by Robert Wexler. Flagstone measurements were done by Detlef Deumlich. UAS based SfM measurements were performed by Emilien Aldana Jaque and Kristof van Oost. Magnetite micro-tracer measurements were done by Gema Guzmán and José A. Gómez. Fluorescent micro-tracer measurements were applied by Robert Hardy and John Quinton. Infrastructure and feedback was given by Michael Sommer.